GENOTYPIC EXPRESSION OF TRAITS ON CRANIOFACIAL HARD TISSUE FOR POSITIVE IDENTIFICATION PURPOSES IN A MODERN EUROPEAN-AMERICAN SKELETAL COLLECTION

by

Kamar Afra, B.S.

A thesis submitted to the Graduate Council of
Texas State University in partial fulfillment
of the requirements for the degree of
Master of Arts
with a Major in Anthropology
August 2019

Committee Members:

Michelle D. Hamilton, Chair

Bridget FB Algee-Hewitt

M. Katherine Spradley

Nicholas P. Herrmann

DEDICATION

I dedicate this research project to Mohamad, Mom, Dad, Nour, Omar and Teta for the encouragement you provided from all the way in Lebanon.

I also want to dedicate it to all the missing persons and their families in Lebanon that made me want to pursue this field and the donors at Texas State University without whom I wouldn’t have had the resources to complete my project

ACKNOWLEDGEMENTS

I want to acknowledge all the people that trusted in my abilities and helped me along the way. I want to acknowledge the Graduate College and Dr. Grady Early for providing the necessary funding for completing this research. I want to acknowledge Fulbright program for offering the funding necessary to complete my master's studies. I want to acknowledge my advisor Dr. Michelle Hamilton for all the support she provided during those two years. I want to acknowledge all my committee members, Dr Herrmann, Dr. Spradley, and especially Dr. Algee-Hewitt for helping in the different methodologies necessary for this project. I want also to acknowledge Dr. Kang and his team Dr. Kim, Dami, Dinesh, and Ji-chul for all the help they provided during my DNA sequencing process. I want to thank Nathan for his inter-observer help, Grace for her illustrations, Marc and AUST for their protocol, Karen Taylor for her knowledge and workshops, and for all the support from Dr. Erhart, the Department, faculty, and all my friends that I gained during my two years in the United States.

TABLE OF CONTENTS

Page

LIST OF TABLES

Table **Page**

LIST OF FIGURES

LIST OF ABBREVIATIONS

Abbreviation	Description
DNA	Deoxyribonucleic Acid
CODIS	Combined DNA Index System
SNP	Single Nucleotide Polymorphism
RFLP	Restriction fragment length polymorphism
STR	Short Tandem Repeat
CHR	Chromosome
2D	Two dimensions
3D	Three dimensions
CT	Computed Tomography
ORPL	Osteological Research and Processing Laboratory
TMF	Mandibular body breadth at the Mental foramen
HMF	Mandibular body height at the Mental foramen
R	Right
L	Left
PCR	Polymerase Chain Reaction
AUST	American University of Science and Technology
NCBI	National Center for Biotechnology Information
GWAS	Genome-Wide Association Study
GC	Guanine-Cytosine
SOP	Standard Operation Procedure
qPCR	quantitative PCR
M1	Molar 1
Sup	Superior
Inf	Inferior
WRB	Minimum ramus breadth
Pt	Point
Zyg	Zygomatic
Mand	Mandible
FARF	Forensic Anthropology Research Facility
GEB	Grady Early Building
HCL	Hydrochloric acid
EDTA	Ethylenediaminetetraacetic acid
Tris	Hydroxymethyl aminomethane
TE	Tris/EDTA
SDS	Sodium Dodecyl Sulfate
SEB	Stain Extraction Buffer
PCI	Phenol Chloroform Isoamyl Alcohol

NaCl	Sodium chloride
EtOH	Ethanol
UV-vis	Ultraviolet-visible
TAE	Tris base/acetic acid/EDTA
PCA	Principal Component Analysis
GM	Geometric Morphometric
ILD	Inter-landmark distance

I. INTRODUCTION

Forensic science is the practice of science in a medicolegal context. As an area of study, it has many subdisciplines, and, in each one, researchers tend to focus on their field of expertise. Despite this wealth of specific knowledge, there are practical limitations that affect the process of establishing a positive identification. Human identification is a field that encompasses different subdisciplines found in forensic science. The process of identification discerns according to the data available. In the presence of biological samples such as blood, saliva, and hair follicles, DNA test is completed. If a body is decomposed or only human remains are found, forensic anthropologist and odontologist work on the identification of the body through the biological profile and dental identification respectively. For a last resort, forensic facial reconstruction is usually used.

However, this process is not always straight forward and it may require different approaches due to problems that may occur along the way within each discipline. Of particular concern to forensic anthropology is the problem of appropriate or adequate reference samples. There are several populations for which there are no skeletal collections available to study human variation or to use as comparative material for the development of the biological profile in forensic cases. This is true in both developed and developing countries but especially in the Arab world, including Lebanon. This absence of reference collections is of great importance because there are historic and modern wars that leave thousands of deceased and unidentified skeletons.

Another subdiscipline of forensic science that plays a critical role in human identification and encounters similar restrictions is forensic genetics. In the field of genetics, the identification of traces of DNA (deoxyribonucleic acid) occurs by a match between the unknown sample ("Q" or questioned) and a reference sample ("K" or known), with the latter, in a criminal case, often sourced from the national DNA Database, CODIS (Combined DNA Index System). However, this process can reach a dead-end if there is no potential match in the system. When both anthropology and genetics fail to produce evidence of positive identity for the unidentified skeleton, law enforcement agencies may refer to other reconstructive means as the last chance for possible recognition. This where forensic art steps in to attempt to establish identification. Forensic facial reconstruction is a facial approximation technique that derives its methods from anatomical knowledge and experiments, as it relies, for example, on tissue depth markers, and anthropological landmarks and measurements. Yet, this approach requires subjective artistic interpretations. There is a need, therefore, to reevaluate current facial reconstruction procedures.

The facial approximation is driven by a concern for recognition, however, with the incorporation of genetics, this focus could shift more towards identification. Currently, the study of the human face via genetic information only examines soft tissue data from living individuals, which are affected by their own unique set of variables that differ from those influencing the craniofacial skeleton (Claes et al. 2018). On the other hand, the relationships between skeletal remains and genetic information are traditionally studied to answer human variation questions on a population-based scale (Relethford 2016). Owing to the fact that the data from skeletal samples are commonly from different populations than the genetic population, this work is based on the study of the theory of biodistance and gene flow and its dispersion geographically within different populations (Relethford et al. 1997; Wright 1943). The different research questions on genetics pursued with soft-tissue and skeletal data result in different outcomes. Absent is, therefore, the link between these two kinds of data and genetics: this is needed for developing tools to improve the human identification process, especially in cases involving missing individuals.

The work presented here combines three areas of forensic science – anthropology, biology, and art – to address the gap in literature. One of the key factors that plays a role in the shape of a face is the skull. Yet, very few genetic researchers address the influence of the skull on the face. Importantly, none are asking the critical research question that I investigate in this thesis. Are SNP markers for craniofacial traits associated with craniofacial measurements?

This thesis project represents the first step towards a larger project investigating the role of the skull on the shape of the soft tissues of the face. For this study, I identified approaches used by current researchers, who are linking genotypic expression to soft tissue facial phenotypic features, in order to test whether there is an actual link between these previously identified genetic markers and their expression on the skull. Specifically, I examined a sample of 17 European American donated skeletal individuals' skulls and their blood cards. I extracted the DNA from those cards, amplified it, then sequenced it. I also recorded the facial landmark locations on each skull to obtain the inter-landmark distances and analyzed any possible associations through biostatistics. These findings from this research project may be of help in the facial reconstruction process in the future through the integration of genetic information into the process, which will increase the reliability of the facial reconstruction method.

II. LITERATURE REVIEW

Statement of the problem

Previous phenotype-genotype link studies were based on, and are still mainly focused on, the expression of mutations in the genome that can generate diseases or abnormalities (Buschang and Hinton 2005; Reijnders et al. 2018). After the human genome project was completed (Deloukas et al. 1998; Hudson et al. 1995; Stewart et al. 1997), researchers started observing the effects of genetic variations on the phenotypic expression of diseases or congenital conditions. Some of the conditions were related to the face such as a cleft lip or palate that can have either minimal or extreme effects and can be surgically fixed if discovered early (in utero), or during childhood. Those pathologies can render severe emotional and physiological problems in the child, which was a key reason for tackling those abnormalities (Kapp-Simon et al. 1992). In this research, scientists were able to study and track the mutation through inheritance by testing both the parents and their children (Mossey et al. 1998). After various research, they were also able to detect the gene responsible for the abnormality in craniofacial development. As facial development occurs in the embryological phase, mostly between 4^{th} to 7^{th} prenatal weeks (Chiego 2018), scientists would be able to test the normal development of an embryo and track it for any abnormalities by simply conducting a couple of genetic tests. This work also shed a light on the environmental factors that can play a role in healthy prenatal development and that could affect individuals even after birth. There are additional environmental factors that can play a role in the final outline of the face - factors influenced by epigenetics (Hallgrímsson et al. 2007). It is very important to take into considerations all the factors that play a role in the facial morphology.

Genetic information is one of the major avenues that can help in the determination of face shape. After establishing the elements needed in anthropometric facial measurements, and with the newly discovered technologies for DNA sequencing, researchers have started observing phenotypic expression of different genetic markers. These discoveries led geneticists to link anthropometric facial dimensions to genetic data (Little et al. 2006). This new interdisciplinary approach emerged all around the world (Cho et al. 2009) to tackle the subject of facial reconstruction through genetic information and soft tissue data on both the research and commercial levels (NanoLabs 2016). Once again, this work is only based on anthropometric data from living individuals and its translatability to the cranium is unknown, if at all appropriate. Anthropometric data on living people is quite different from the metric measurements on the skull; the data taken does not accurately depict the skeletal morphology of an individual, especially if the skull is the only available element. Currently, there are several data collection procedures to build a biological profile of a skeleton, that in turn can help in the determination of age, ancestry, sex, and stature of an individual through different statistical analysis and programs (Jantz and Ousley 2005; Langley et al. 2016; Ousley 2004). But those methods are still lacking the link to connect the morphology visualized on the skull with the genetic factors at the individual level. For this reason, biological anthropologists started tackling genetic information to implement an interdisciplinary approach to study variation of specific populations, using similar parameters as this current study (Algee-Hewitt 2017a).

However, despite of this new research, the study of the influence of specific genetic markers on specified parts of the skull is still minimal. Researchers have tried to study this influence through different anthropological questions such as quantitative evolutionary theory (Cheverud 1988), and phylogenetic associations to the cranium (Sherwood et al. 2008). This pilot study will answer a different anthropological question and aid future advances in forensic facial reconstruction methodologies by connecting these two areas of genotype-phenotype research together.

Genetic Approaches

The human genome is the whole set of the sequenced DNA that is unique for everyone except for identical twins, since they share the same genetic code from the same fertilized egg cell in the uterus. A gene is a small section of the genome that can be expressed to identify one or more traits within the human body (Mielke et al. 2011). Within this region, there are a different set of variables that have been tested over the years that can be tracked in each person such as Short Tandem Repeats (STR), indels, and Single Nucleotide Polymorphism (SNP). Furthermore, several techniques have been developed especially in forensic casework to use for identification methods, beginning with historic blood type determination to restriction fragment length polymorphism (RFLP), STR analysis, and next-generation sequencing (Alvarez-Cubero et al. 2017). These techniques were also used in developing medical research (Ulahannan et al. 2013).

Nevertheless, gene expression is a complex process with different variables. A researcher must be aware of this complexity while trying to identify the genotypic-phenotypic link in regard to the external environmental factors (Claes et al. 2014).

Genetic information is often related to specific populations. Previous research identified some genes responsible for specific phenotypic markers on the face (Shaffer et al. 2016). Early researchers tried to predict some direct phenotypic traits such as eye color (Liu et al. 2009) and other relatively connected features such as hair color, eventually integrating skin color as well to use for various forensic applications (Maroñas et al. 2015; Walsh et al. 2014).

But this research did not stop there; the same teams from different institutions developed their approaches and tested them through the years to obtain the latest set of variables within genes (Claes et al. 2018).

It is very important to acknowledge the different variations associated with human gene expression, and this variability is one of the points that renders this process such a complex one. In reviewing the literature, I found several researchers tried to identify gene expression for the phenotype using soft tissue measurements within different populations, acknowledging the importance of ancestry variability. In Peng et al.(Peng et al. 2013), the authors studied the genotypic-phenotypic link in a Far-East/Chinese population. Oher studies were conducted on the craniofacial features of Latin Americans by Adhikari et al. (Adhikari et al. 2016a), and Koreans (Cha et al. 2018), detecting different genes that may influence this phenotypic expression. However, in each of these populations, most of the identified genes were different from each other, which confirms that the population plays a large role as an independent variable in these studies.

Anthropological Approaches

Another major component in this project is related to biological anthropology. The study of human variation through craniometric data has been a very utilized approach, especially with the estimation of ancestry (Algee-Hewitt 2017b; Kranioti et al. 2018; Spradley 2016). However, there are different ways to obtain craniometric data. A researcher can either use standard or non-standard techniques to acquire this information but it all depends on the type of data and the population studied especially in estimating ancestry (Spradley and Jantz 2016). One of those methods is geometric morphometrics. Geometric morphometrics is the quantitative study of a set of data to analyze the variation of cranial shape obtained through measurements of lengths, angles, or points (Webster and Sheets 2010). The prevailing methodology is data obtained through points called landmarks. The study of those landmarks can help in the observations of the shape by itself or it can become the basis for the analysis of a different variable such as size (Slice 2005). On the other hand, there is another type of point that can be obtained through geometric morphometrics called semi-landmarks, and they are measured in a successive manner through the curve obtained from the data (Bookstein 1997).

Geometric morphometric can help in detecting any outliers and identification of distances between the landmarks by applying different settings in specialized programs such as Morpheus (Slice 2013) and MorphoJ (Klingenberg 2011). However, the landmarks indicated on a human skeleton can convey different information according to position and method of acquisition (Hessey 2014). While there are different descriptions of their positions and identifications, one of the most practical and abundantly used one is by Howells (Howells 1973). The program currently used at the Forensic Anthropology

Center at Texas State University is 3Skulls developed by Ousley, and it records the coordinates of the landmarks digitally from a Microscribe digitizer and input the data into a database observed through Advantage Data Architect 11.10 program (Ousley 2004). One of the positive aspects of this program is the ability to manipulate the number of landmarks in the template. These standardization of any type of template – the suite of landmarks chosen for digitization -- is quite difficult especially due to the creation of symmetric points of already existing landmarks or even completely new locations for some of the landmarks. Further, the kind of landmark determines how it is possible to collect their coordinate values. There are three types of landmarks according to Bookstein's (1997) definition:

Type I landmarks - associated with suture intersections (specifically three sutures) and the easiest ones to locate.

Type II landmarks - related to a structure found on the bone, so it can be defined morphologically according to a maxima curvature referenced by an adjacent bone feature.

Type III landmarks - the least accurate and usually obtained as extrema between distant bones (Hessey 2014; Slice 2005).

Even though you can apply a specific description of the location of the landmarks (such as the definitions from Howells), not everyone identifies the same landmarks equally or accurately. This is where the issue of inter and intra-observer error appears in morphometrics. However, a researcher can decrease error by repeating the measurements at different time lapses.

Facial Reconstruction Approaches

A forensic facial reconstruction is an approach adopted in human identification cases and criminal proceedings. It is part of the image identification category of forensic art (Taylor 2001). Each human face is unique, even between identical twins where epigenetics can play a role in the plasticity of the face (Wilkinson 2004a). There are several techniques that artists and anthropologists have developed throughout the years related to facial reconstruction: 2D facial superimposition, and 3D manual and computerized facial reconstruction (Gupta et al. 2015). Yet, the earliest forms of facial reconstruction involved sculpting by hand. Facial reconstruction applications were started by anatomists and medical doctors using stolen cadavers for the study of anatomy (Mitchell et al. 2011). One of the earliest facial reconstruction was in the Neolithic period by adding some of the facial features such as eyelids on plaster as part of funerary practices (Evison et al. 2016). However, one of the earliest historic forensic reconstruction was completed by His (1895), who adopted facial soft tissue from the German anatomist, - Welcker (His 1895; Welcker 1883). On the other hand, in the late 19th century, the Russian anatomist, Gerasimov, started developing more research-oriented experiments to test differences for facial reconstruction and the relationship between soft and hard tissue (Gerasimov 1971; Wilkinson and Rynn 2012). His technique is used even today, and is called the "Russian method," which relies on an anatomy-based approach for sculpting the muscles of the face. There is another technique created from measurements-based approaches developed by - Krogman, known as the "American method," which relies on compiled anthropometric measurements of the skull with the addition of soft tissue depth markers (Taylor 2001). A combination of these two approaches is the “Manchester method,” which uses both facial muscles and soft tissue depths for facial reconstructions in forensic cases and for missing persons (Gupta et al. 2015; Wilkinson 2004a).

As noted previously, facial reconstruction is a way to spark recognition. Problems in reconstructions can occur in forensic facial reconstructions when the mandible is missing. This can create an issue for the 2D superimposition and 3D facial reconstruction when depicting the face from the skull, even though there are several methods created to facilitate this process by estimating the proportion of the face (Sassoumi 1958; Taylor 2001). Unfortunately, the final depiction may hold inaccuracies, since it is still an estimate of facial proportions. This was tested in a study using skulls, where it was suggested that with further research, genetic information could help to obtain a more accurate approach for facial approximation in the absence of the mandible (Altes 2016). Researchers tried to develop new techniques to obtain more objective approaches for facial reconstruction, such as CT scan superimposition to estimate the cranial landmarks from deceased individuals (Sakuma et al. 2010) and to compare against living individuals (Guyomarc'h et al. 2014). Another technique found in the literature is the superimposition of 3D scans obtained through 3D laser technology (Sholts et al. 2010). Other 3D approaches have also been applied to different populations such as French (Guyomarc'h et al. 2014) and Korean (Lee et al. 2015) populations. While all these 3D facial reconstruction approaches work on landmark estimation, their associated landmarks are standardized to each population, and the research is focused mainly on soft tissue.

With the explosion of new genetic technologies and advances in SNP typing potential, DNA-driven forms of facial reconstruction are currently being developed and marketed commercially for law enforcement use. The Parabon NanoLabs company runs a project that uses machine learning-based mathematical algorithms to create models from genetic data to generate the template of a face (Steve Armentrout, personal communication, 2018), which a forensic artist uses to craft the final version and personalize it (Budowle and van Daal 2008; NanoLabs 2016). However, this approach's purpose is purely commercial, and not research/educational. For this reason, it is very important to continue studying effects of different genetic variants on the face. This can be achieved by incorporating research findings from biological anthropology – data from the skeleton and genetics – within the identification equation, by assessing genetic underpinnings of hard tissue expression, in the absence of soft tissues.

III. METHODOLOGY

Sample Selection

To test my hypotheses, I will use skulls from European-American individuals from the Texas State Donated Skeletal Collection (TXSTDSC), housed at the Grady Early Building (GEB) at Texas State University. This skeletal collection is from individuals who donated their body through the universal anatomical gift act. This willed body donation is completed by the donor themselves (before their death, and they are called living donors) or it can be performed by next of kin after death to honor the wishes of the individual. After donation, the bodies are placed at the Forensic Anthropology Research Facility (FARF) for decomposition purposes and forensic science research projects. Afterward, the remains are transported to the Osteology Research and Processing Laboratory (ORPL) for processing. Once the remains are skeletonized, they are permanently housed at GEB for research. The individuals chosen for my project were selected to meet the following criteria, which are based on the parameters defining the previously identified SNPs found in research literature and practical data considerations. The cases should be identified as European American. . Drawing upon prior findings of a non-trivial correlation between race and ancestry in the European American population from both cranial and DNA based analysis (Algee-Hewitt 2016; Bryc et al. 2015; Lao et al. 2014), White identity was used as a proxy for European ancestry. This identifier was self-reported by the donors or their kin and was retrieved here from the donation forms. Eligible donors needed to select White in the race section of the body donation form. The individuals also should be aged between 25 and 60 years old, with no fractures or trauma to the face, and not edentulous. Another major criterium is the presence of blood cards. Each individual had to have an associated blood card collected during the intake process by graduate students upon the arrival of the donor body at ORPL. Due to these requirements, my sample size was limited to 19. Of these, two samples were removed due to the unsuccessful extraction of DNA from their associated blood cards. My final sample size is 17 individuals as shown in Table 1.

Table 1. Table representing the individual's number at the Forensic Anthropology Center at Texas State (FACTS) along with their biological sex, social race, and nationality, ancestry they identify with. M: male; F:female; NA: Not Applicable; W: white; Trans: transgender.

TX State ID #	Sex	Race	Nationality/Ancestry
D38-2012	M	W	NA
D20-2012	M	W	NA
D39-2012	M	W	NA
D36-2012	F	W	NA
D27-2012	F	W	NA
D14-2013	M	W	NA
D22-2013	M	W	NA
D17-2013	F	W	NA
D55-2013	M/Trans	W	NA
D24-2013	F	W	NA
D57-2014	M	W	NA
D15-2014	M	W	NA
D49-2014	M	W	NA
D60-2014	M	W	NA
D60-2015	F	W	Western European
D31-2015	F	W	English/German/Redbourn/Lumbee
D41-2015	F	W	NA

Data collection

I collected data from the 17 aforementioned individuals from two main sources: craniometric data from their craniums, and DNA sequenced from their associated blood cards.

The skull

The morphology of the face is a critical component of this investigation. In order to test my project's hypothesis, I collected different landmarks to produce a final matrix of x,y,z coordinates and set of associated inter-landmark distances. I used a set of standard (type I, II, and III landmarks) and non-standard (e.g. symmetrical points to pre-existing landmarks, semi-landmarks) craniometric measurements, and followed several steps to accomplish a better outcome with lower errors. According to previous literature utilizing genetic data to understand the soft tissue phenotype of the face, the images obtained from the living individuals were a depiction of a picture that captured the entire face. In order to have a similar end-result using skulls, I needed to have a complete face, which means using the cranium and mandible in their anatomical position. I articulated the cranium of the individuals with their mandible using super glue in a method applied by forensic artists for sample preparations in forensic facial reconstruction methods (Taylor 2001). The next step was marking the landmarks. As there are different types of landmarks, some can be marked directly and others needed to be taken instrumentally using different kinds of calipers (Howells 1973; Langley et al. 2016). The set of landmarks used was modified from the original template found within the 3Skull program (Ousley 2004), a template adopted from Howells (Howells 1973). This revised version has 99 landmarks, as shown in Figure 1, 2, and Table 2. In addition to these landmarks, I included two major curves: frontal and nasal curves. Each one was recorded through a series of semi-landmarks taken 0.5 cm apart.

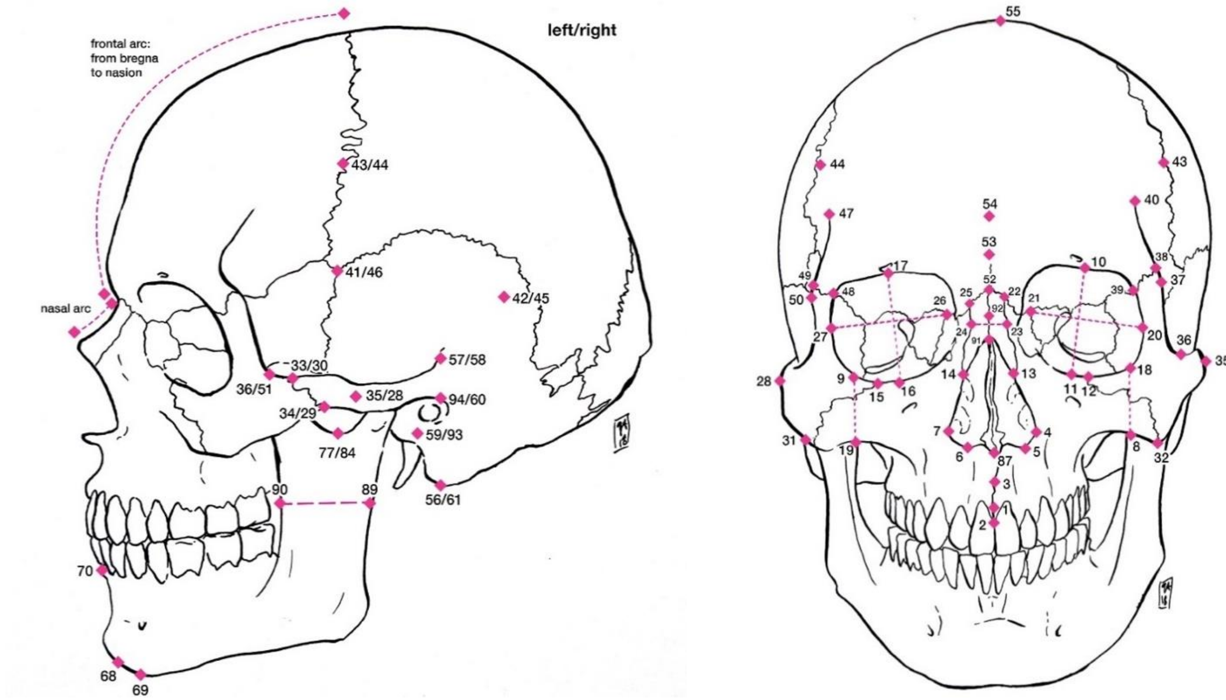

Figure 1. Frontal (on left) and lateral (on the right) view respectively of the skull with the corresponding landmarks (courtesy of Artist Grace Anderson).

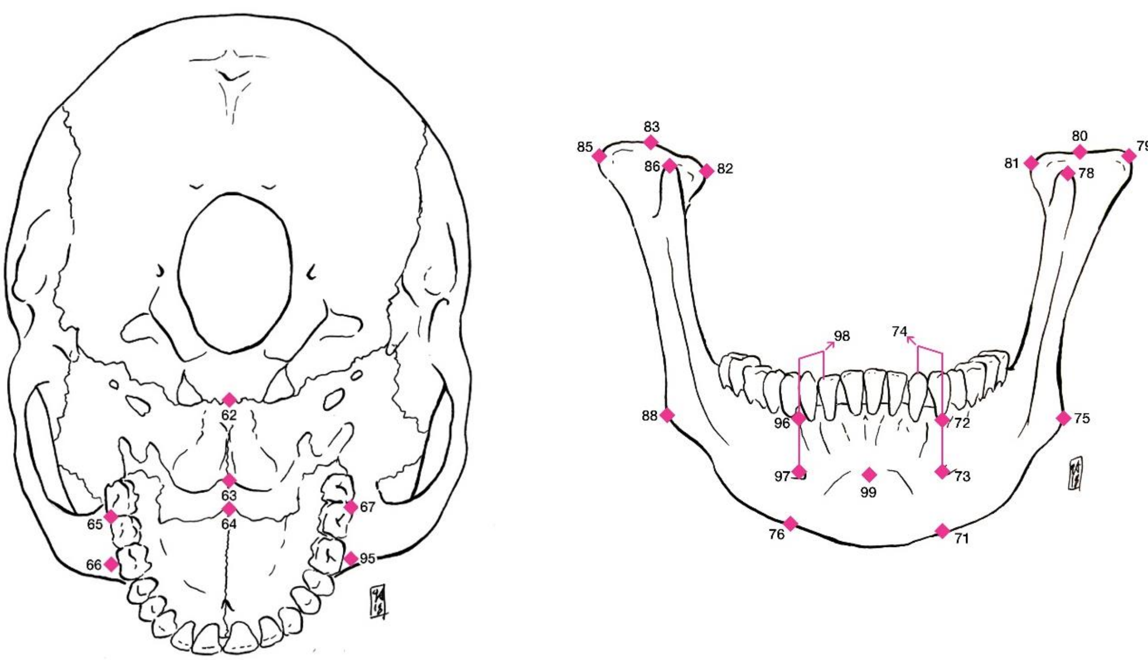

Figure 2. Inferior view of the skull (on left), and anterior view of the mandible (on right) (courtesy of Artist Grace Anderson).

Table 2. The 99 skull landmarks and their respective numbering shown in Figures 2 and 3.

#	Abrv	LANDMARK	#	Abrv	LANDMARK
1	prosH	Prosthion-Howells	50	mplr	Marginal Process Lateral R
2	prosM	Prosthion-Martin	51	jugr	Jugale R
3	ssp	Subspinale	52	nas	Nasion
4	alarl	Alare L	53	glb	Glabella
5	nlhil	Most Inferior Nasal Border L	54	spglb	Supraglabellare
6	nlhir	Most Inferior Nasal Border R	55	brg	Bregma
7	alarr	Alare R	56	mastl	Mastoideale L
8	wmhil	Cheek Height Inf Point L	57	aubl	Radiculare L (Zyg Root)
9	wmhsl	Cheek Height Sup Point R	58	aubr	Radiculare R (Zyg Root)
10	obhsl	Upper Orbital Border L	59	radptl	Radiometer Point L
11	obhil	Lower Orbital Border L	60	porr	Porion R
12	zygool	Zygoorbitale L	61	mastr	Mastoideale R
13	nasil	Nasale Inferius L	62	hor	Hormion
14	nasir	Nasale Inferius R	63	alv	Alveolon (Rubber Band)
15	zygoor	Zygoorbitale R	64	staur	Staurion
16	obhir	Lower Orbital Border R	65	ecml	Ectomolare L
17	obhsr	Upper Orbital Border R	66	avrptl	M1 Anterior Point L
18	wmhsr	Cheek Height Sup Point L	67	ecmr	Ectomolare R
19	wmhir	Cheek Height Inf Point R	68	malapt	Pogonion (Mand Length)
20	ectl	Ectoconchion L	69	gniipt	Gnathion
21	dacl	Dacryon L	70	gnispt	Infradentale
22	nassl	Nasale Superius L	71	hmfiptl	HMF Inf Pt L
23	wnbl	Nasomaxillary Suture Pinch L	72	hmfsptl	HMF Sup Pt L
24	wnbr	Nasomaxillary Suture Pinch R	73	tmfbptl	TMF Buccal Pt L
25	nassr	Nasale Superius R	74	tmflptl	TMF Lingual Pt L
26	dacr	Dacryon R	75	gonl	Gonion L
27	ectr	Ectoconchion R	76	hmfiptr	HMF Inf Pt R
28	zygr	Zygion R	77	imnptl	Inferior Mandibular Notch L
29	zytil	Zygotemporale Inferior R	78	coronl	Coronion L
30	zytsl	Zygotemporale Superior R	79	latcndl	Condylion Laterale L
31	zygomr	Zygomaxilare R	80	supcndlP	L Sup Condyle Post
32	zygoml	Zygomaxilare L	81	medcndl	Condylion Mediale L
33	zytsr	Zygotemporale Superior L	82	medcndr	Condylion Mediale R
34	zytir	Zygotemporale Inferior L	83	supcndrP	R Sup Condyle Post
35	zygl	Zygion L	84	imnptr	Inferior Mandibular Notch R
36	jugl	Jugale L	85	latcndr	Condylion Laterale R
37	mpll	Marginal Process Lateral L	86	coronr	Coronion R
38	fmtl	Frontomalare Temporale L	87	ans	Anterior Nasal Spine
39	fmal	Frontomalare Anterior L	88	gonr	Gonion R
40	wfbl	Frontotemporale L	89	wrbapt	WRB Posterior Pt
41	krol	Krotaphion L	90	wrbppt	WRB Anterior Pt
42	xfbl	Maximum Frontal Point L	91	sispt	Nasal Bone Elevation
43	stpl	Stephanion L	92	ndspt	Deepest Point On Nasal
44	stpr	Stephanion R	93	radptr	Radiometer Point R
45	xfbr	Maximum Frontal Point R	94	porl	Porion L
46	kror	Krotaphion R	95	avrptr	M1 Anterior Point R
47	wfbr	Frontotemporale R	96	hmfsptr	HMF Sup Pt R
48	fmar	Frontomalare Anterior R	97	tmfbptr	TMF Buccal Pt R
49	fmtr	Frontomalare Temporale R	98	tmflptr	TMF Lingual Pt R
			99	chpp	Chin Protrusion Point

Individual landmarks. After marking the landmarks' positions with a pencil, I placed the skulls in an inverted position so that the skull is observed from its inferior side as shown in Figures 3 and 4. The superior side is held by three columns of oil-based clay to maintain stability while digitizing with no damage to the skull. I started recording each landmark point using the Microscribe Digitizer which saved the 3D coordinates (x, y, z) in the 3Skull program (Ousley 2004). This data was extracted through the Advantage Data Architect v11.1 as an excel sheet for further data processing. Then, I was able to separate the two major type of data: curves and non-curves. The non-curves landmarks were inputted in the geometric morphometrics (GM) program, MorphoJ (Klingenberg 2011), after standardizing it to the Morphologika format (O'Higgins and Jones 2006). The first goal was to detect any visible outliers by plotting the data in reduced dimensional space. I performed in a Principal Component Analysis (PCA) and selected the PCs by the percentage of explained variation, using their eigenvalues. Second, it was important to visualize only the "shape," instead of the whole "form," of the skull, and, so, I removed size by implementing a Procrustes analysis. To visualize the landmarks and the associated wireframes (based on inter-distance landmarks) for each phenotypic trait, I input the same data set, in Morphologika format, into the GM program Morpheus (Slice

Figure 3. The MicroScribe G2 Digitizer in resting position and positioning of the skull during data collection (skull held by oil-based clay columns).

Figure 4. The positioning of the skull of an individual for data collection through the MicroScribe digitizer. A: Anterior view; L: Lateral view; S: Superior view.

2013). In this program, I connected two different points to obtain a linear measurement. Those lines characterize the distance between two landmarks within one target area of the face. A specific set of linear measurements will be used eventually to test their association with the presence/absence of the correlated SNP. The inter-landmark distances were calculated manually, through the Microsoft Excel package, according to the Pythagorean Theorem in space for 3D shapes (Veljan 2000) and I verified the results by comparing these with some of the existing distances already obtained from 3Skulls.

Curves. Another program was used for this type of data called Resample (Raaum 2006). This program standardizes the number of semi-landmarks in each curve obtained from the different individuals in order to have a common number of semi-landmarks. This standardization enabled me to run it through Morpheus and detect the shape among the different samples to later plot the data into a Procrustes test for further analysis.

The DNA

For my thesis project, I will focus on individuals of European American ancestry, since researchers that studied European ancestry have already identified a number of specific genes (Table 3) with single-nucleotide polymorphisms (SNPs); the variables that may influence the phenotype associated with the soft tissue of the individual. The SNP is a single mutation that occurs randomly at the allele level in different sites of the genome. I was also able to locate specific SNPs of interest and their associated traits described in the various literature (Claes et al. 2018; Liu et al. 2012; Paternoster et al. 2012a; Shaffer et al. 2016). Please note, while many of these genes are related specifically to European ancestry, some may also apply to other ancestries. I have also specifically chosen SNPs related to Latin America (Adhikari et al. 2016a) with the assumption that they won't show expression on the European population. This will be used as a control-based sample for comparison.

Table 3. Selected SNPs used for this pilot study with their chromosome location and their associated trait as found in previous literature. SNP: Single nucleotide polymorphism; Chr: Chromosome.

SNP	Chr	Associated Trait	Reference Article
rs17447439	chr3	Left Eye To Right Eye	(Liu et al. 2012) (Shaffer et al. 2016) (Claes et al. 2018)
rs72691108	chr1	Right /Left Eye To Nasion-Upper facial quadrant	(Claes et al. 2018)
rs7559271	chr2	Nasion To Mid-Endocanthion Point/Nasion Position	(Shaffer et al. 2016) (Paternoster et al. 2012) (Claes et al. 2018) (Adhikari et al)
rs11738462	chr5	Pronasale To Left Alare	(Shaffer et al. 2016) (Paternoster et al. 2012) (Claes et al. 2018)
rs8007643	chr14	Nasal Ala Length	(Claes et al. 2018) (Shaffer et al. 2016)

Table 3 Continued

rs1982862	chr3	Pronasale To Left Alare	(Shaffer et al. 2016) (Paternoster et al. 2012) (Claes et al. 2018)
rs4648379	chr1	Pronasale To Left/Right Alare// Nasal Ala Length	(Liu et al. 2012) (Shaffer et al. 2016) (Claes et al. 2018)
rs6555969	chr5	Left/Right Zygion To Nasion// Right /Left Eye To Nasion	(Liu et al. 2012) (Shaffer et al. 2016) (Claes et al. 2018)
rs12786942	chr11	Upper facial depth	(Shaffer et al. 2016)
rs10862567	chr12	Right Endocanthion In Yz Direction	(Shaffer et al. 2016) (Paternoster et al. 2012) (Claes et al. 2018)
rs17106852	chr14	Cranial base width	(Claes et al. 2018) (Shaffer et al. 2016)
rs6129564	chr20	Cranial Base Width	(Claes et al. 2018) (Shaffer et al. 2016)
rs3827760	chr2	Chin Protrusion	(Adhikari et al. 2016; Claes et al. 2018)
rs6740960	chr2	mandible/chin	(Claes et al. 2018)
rs927833	chr20	Nose Wing Breadth	(Adhikari et al. 2016; Claes et al. 2018)
rs17640804	chr7	Nose Wing Breadth	(Adhikari et al. 2016; Claes et al. 2018)
rs2977562	chr3	Nose Wing Breadth/ philtrum	(Claes et al. 2018)
rs5880172	chr6	Forehead	(Claes et al. 2018)
rs9995821	chr4	Columella/Nose Tip-- columella inclination	(Claes et al. 2018)
rs10238953	chr7	mandible and chin	(Claes et al. 2018)

I obtained the archived blood samples from the 17 individuals in the Texas State Donated Skeletal Collection. Each donated body has a blood card, and I was able to take a section of the dried blood, extract the deoxyribonucleic acid (DNA) according to an adjusted protocol, and amplify it according to an optimized method. Once I received those results, I was able to prepare my library by attaching barcode adapters to identify each sample, quantify the amount of DNA necessary for my sequencing according to a reference library, and finally, conduct next-generation sequencing as shown in Figure 5. Then, I analyzed the data through a bioinformatic pipeline to obtain a list of the targeted single nucleotide polymorphism (SNP) available within each sample genome. All the chemical solutions were prepared according to the laboratory manual (Sambrook and Russell 2001).

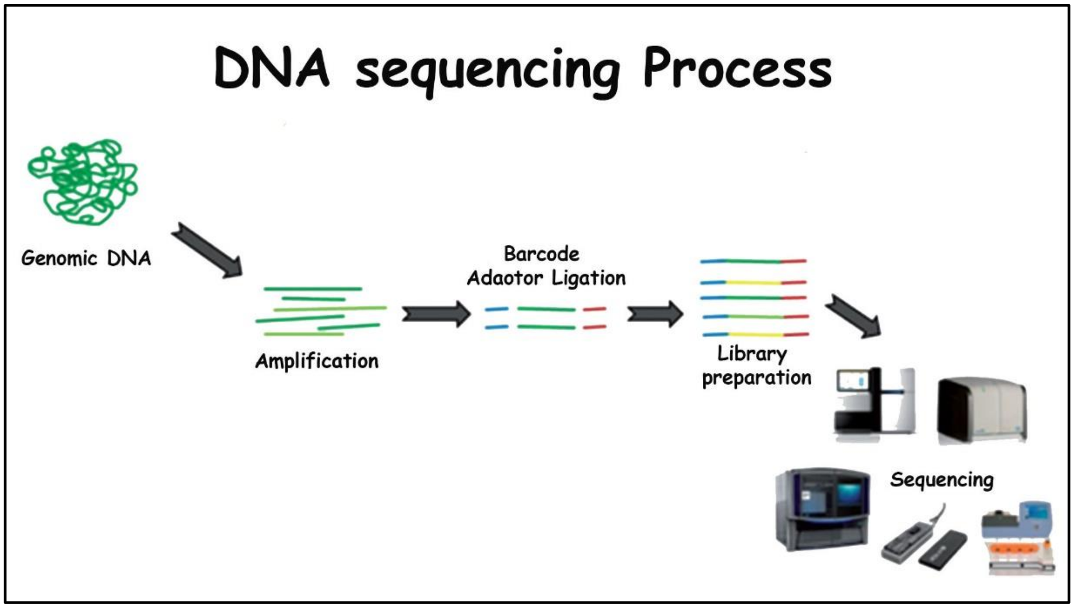

Figure 5. A basic flow chart representing the different mechanisms performed in next-generation sequencing. Adapted from an original image found in (Alvarez-Cubero et al. 2017)(used with the permission of the author).

DNA extraction. All genetic sequencing work was performed at the Kang Laboratory at Texas State University, under the direction of Dr. Hong Gu Kang, Associate Professor in the Department of Biology at Texas State University. I applied organic DNA extraction or phenol-chloroform extraction. I used a protocol developed by the molecular genetic laboratory at the American University of Science and Technology (AUST), Beirut, Lebanon (SOP-FS12014). I tested my own blood as a pilot study to start modifying the protocol for optimum results with the help of other sources (Healthcare 2010). Most of those modifications were related to the stain extraction buffer (SEB) buffer. I initially prepared the SEB buffer containing Tris-HCl (1M; pH=8), EDTA (0.5M; pH=8), 10% SDS, and the rest is ddH_2O. After preparing the SEB, I cut around 1cm^2 of the dried blood from the blood cut using an autoclaved surgical scissor and placed it in a 1.5ml microcentrifuge tube containing 500 µl of SEB. Then, I added 20 µl of Proteinase K from the stock solution (20mg/ml). After Inverting several times, I incubated the tube overnight, at 56°C for the activation of the proteinase K enzyme. The next day, I transferred the resulting liquid to a new 1.5ml microcentrifuge. I added on top of it 500 µl of phenol chloroform isoamyl alcohol (PCI) and vortexed the tube well for 10 minutes, then centrifuged it at 8000 rpm speed for 10 minutes at 23°C using compact Benchtop Centrifuges (Thermo Fisher Scientific). After this step, there are two different phases: the organic and aqueous phase. I transferred the aqueous phase that is less dense (upper phase) into a new 1.5ml microcentrifuge, then added 5M NaCl with a double volume of 99% EtOH, then I inverted the tube several times to precipitate DNA from the supernatant. This tube was left at -20°C for 60 minutes then centrifuged for 25 minutes at 23°C then another 20 minutes centrifugation at 4°C to enhance the quantity of DNA. The supernatant was gently poured off, then 70% Ethanol was added to the formed DNA pellet with a brief vortex for homogeneity. Another centrifuge was conducted at maximum speed for 10 minutes at 23°C to facilitate the remove of the supernatant, and then another quick spin to remove all trace of ethanol. Finally, I let the pellet dry for 5 minutes and then resuspended it in TE. The samples were left on ice for 15 minutes, then each tube was flicked by my fingers 10 times with a 1-minute break between each flick. The samples were stored at -20°C for a short period of time, the transferred at -80°C.

Quality control. After the DNA extraction, I wanted to test the quality and quantity of the final product through Thermo Scientific™ NanoDrop ND-1000 (Desjardins and Conklin 2010). This instrument is a spectrophotometer. This means that it measures the purity and quantity of DNA fragments through an Ultraviolet-visible (UV-vis) spectrum of light in which the sample is absorbed in 230, 260, and 280 nm. The ratios of 230/260 and 260/280 are calculated to determine and asses the quality of DNA and contaminants found in the sample. In addition, the NanoDrop detects the quantity of all the available DNA whether it is single or double-stranded. All my DNA samples were tested through the NanoDrop by first applying 1µlof water for initialization of the instrument. Then I added 1µlof the elution buffer used which was, in this case TE, and finally I started testing each sample by adding 1µl volume and wiping the NanoDrop between each sample using KimTech wipes.

Primer design. Once the DNA samples were ready, I needed to design the primers for Polymerase Chain Reaction (PCR) amplification. I used the National Center for Biotechnology Information (NCBI) database and the Genome-Wide Association Study (GWAS) database to build my genetic library. I was able to detect the DNA strands that I needed to amplify through the different primers. The primers are a different set of nucleotides that attach to the new copy of amplified DNA strands. The creation of the primers depends on several factors such as the length of each one, temperature, and Guanine-Cytosine (GC) percentage contents. This can be achieved by using Primer3Plus software that can create primers according to the settings that the researcher chooses (Untergasser et al. 2012). After designing the primers digitally, I ordered them from Thermo Fisher as dried primer strands and then diluted them from a stock solution of 100µM concentration to a 10µM working concentration that can be used in a PCR reaction.

Cycle determination of designed and barcode primers. After acquiring the designed primers, I wanted to obtain the amplification cycles in which each primer pair needs to amplify the targeted DNA segment. I used a real-time polymerase reaction also known as quantitative PCR (qPCR). At first, I started by testing the 20 selected primers, Then I conducted another experiment for the barcoded primers (P5/P7) provided from the Plant Immunology Laboratory at Texas State University as compatible vehicles for library sequencing. The protocol of this experiment started by preparing a master mix of 5x HOT FIREPol® SolisGreen qPCR Mix, DNA template (5x dilution), primers (10µM) that was added to each individual well separately, and the rest was water to generate for each qPCR well a total volume of 10µl. The qPCR wells are part ofa 96 plate wells where, after adding the solutions, the plate was sealed firmly by an optical covered. Then, I vortexed it gently using a Scientific Industries SI™ Vortex-Genie™ (Thermo Fisher Scientific), then centrifuged it with a Benchtop centrifuge (Thermo Fisher Scientific). The plate was ready for qPCR. I inserted the plate and ran the samples with a Solis-RT set-up through the Bio-Rad CFX Manager. The common amplification cycles determined the preferable cycles for each pair of primers.

Amplification (PCR1). The polymerase chain reaction (PCR) as mentioned previously will amplify specific strands of DNA according to the primers adopted. The protocol consists of a master mix that contains 5X Herculase II Reaction Buffer, dNTP (2.5 µM), combined primers with a concentration of 2.5 µM, Herculase II Fusion DNA Polymerases, DNA template (50ng/µl) added to individual tubes, with the rest being water.

The combined volume of all the solutions in a single tube was 20µl. The PCR reaction was run through the Bio-RadT100 Thermal Cycler for PCR - Compact Thermal Cycler PCR machine under the following conditions: 95°C for 2 minutes, followed by 30 cycles of 95°C for 10 seconds, 60°C for 20 seconds, and 72°C for 20 seconds. After the termination of those cycles, the samples went through 3 minutes at 72 °C, to run for infinity at 12°C until I stopped the run. After this process was finalized, I added 22.5% of BioLabs gel loading dye, Purple (6X) to the total volume of each sample product to prepare them for gel electrophoresis. The gel was made through agar powder and 1X TAE at 2% concentration, in a medium size mold, using 12-wells combs, on the thin side. The samples were run along a GeneRuler 1 kb Plus DNA Ladder on gel electrophoresis at an electric current of 150V. This process allowed me to check for the quantity and quality of the amplified strands and isolate the bands of interest.

Band isolation of amplicon. This experiment was done after the gel electrophoresis ran for over 40 minutes for complete separation. The gel with the final product was photographed under UV light with an Azure c600 biosystems imaging system. In order to be able to determine the size of the correct band, I added the size of the amplicon to the size of the attached adapter from the PCR reaction for each primer pair, then averaged it. The results are shown in Table 4. After determining the correct size, I was able to cut the gel electrophoresis on a UV-transilluminators using a metal blade. Each band's sample was cut carefully and inserted in a new 2ml microcentrifuge tube. After finishing

Table 4. The size of the generated amplicon from each primer pair, the value after adding the adapter with the first PCR reaction, and the final band size after adding the barcode adapter by the second PCR reaction.

SNP	**Amplification size**	**(+) Adapter**	**(+) Barcode**
rs17447439	109	176	245
rs72691108	98	165	234
rs7559271	97	164	233
rs11738462	99	166	235
rs8007643	100	167	236
rs1982862	100	167	236
rs4648379	109	176	245

Table 4 Continued

rs6555969	97	164	233
rs12786942	100	167	236
rs10862567	100	167	236
rs17106852	107	174	243
rs6129564	100	167	236
rs3827760	100	167	236
rs6740960	110	177	246
rs927833	110	177	246
rs17640804	100	167	236
rs2977562	100	167	236
rs5880172	99	166	235
rs9995821	108	175	244
rs10238953	105	172	241
Average	**102.40**	**169.40**	**238.40**

this step, the band isolation was completed through an Invitrogen DNA PureLink quick gel extraction kit. First, I weighted the different gel and recorded their masses, then I added a triple volume of the gel of solubilization buffer (L3), incubated it for 10 minutes at 50°C water bath, inverting the tubes every 3 minutes. Once the gel was melted and the liquid was homogenized, the tubes were transported at 4°C on ice for heat shock for 5 minutes. Afterward, an equal volume of Isopropanol (equal in volume to the gel) was added to each tube. For the next step, a gel extraction column labeled for each sample was attached to a Promega™ Vac-Man™ Vacuum Manifold. Then, the mixture of each sample was loaded in the vacuum, at that point, the vacuum was opened to let the liquid pass through the column where the DNA will bind to the silica-based membrane. After I loaded and vacuumed the liquid through the column, a washing step was required. This washing step was applied by loading the washing buffer (W1 with ethanol) found in the gel extraction kit. After applying a second vacuum step for removing all the liquid, the column was transported to a sample collection tube, then centrifuged to remove any liquid excess. After drying it for 5 minutes with all the ethanol evaporated, the columns were transported to a new 1.5ml microcentrifuge tube. An elution buffer was added to the center of the silica membrane and was left to rest. Eventually the column inside the elution tubes were centrifuged and the final liquid contained the DNA sample. In order to confirm the success of this experiment, the new DNA template was tested with 10% of its volume running through gel electrophoresis (2%).

Barcode amplification (PCR2). After completing the first band isolation, I obtained a new DNA template containing an adapter that will get attached to other segments found on the barcode primers. In the end, I obtained an amplified DNA fragment with the amplicon, adapter and barcode segments as shown in Figure 6. In order to complete this quest, I quantified the gel extracted DNA samples from PCR 1 through NanoDrop spectrophotometry. Then, I was able to prepare a master mix that contains 5X Herculase II Reaction Buffer, dNTP (2.5 µM), Forward primer P5 (10 µM), Reverse primer P7 (10 µM), Herculase II Fusion DNA Polymerases, and DNA template (10ng/µl) added to individual tubes, with the rest being water. The combined volume of all the solutions in a single tube was 20µl. The PCR reaction was run through the Bio-RadT100 Thermal Cycler for PCR - Compact Thermal Cycler PCR machine under the following conditions: 95°C for 2 minutes, followed by 20 cycles of 95°C for 10 seconds, 60°C for 20 seconds, and 72°C for 20 seconds. After the termination of those cycles, the samples went through 2 minutes at 72 °C, to run for infinity at 12°C until I stopped the run. After this process was finalized, I added 22.5% of BioLabs gel loading dye, Purple (6X), to the total volume of each sample product to prepare them for gel electrophoresis.

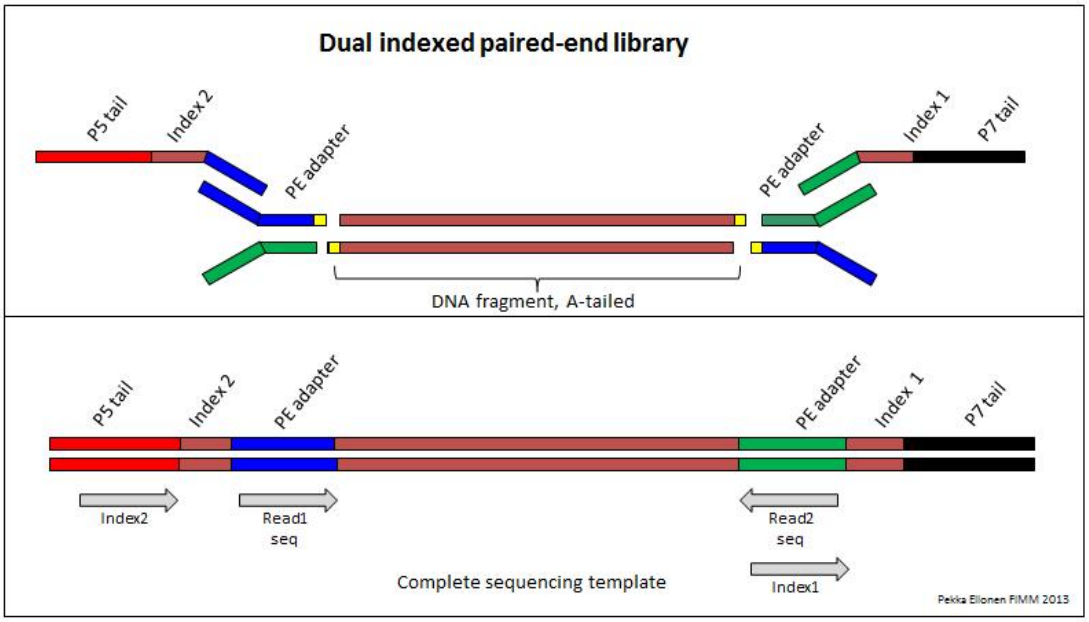

Figure 6. A representation of the library preparation for next-generation sequencing in a Multiplex setting, from (Ellonen 2013) (used with permission of the author).

The gel electrophoresis was made with agar powder and 1X TAE at 2% concentration, in a medium size mold, using 12-wells combs, on the thin side. The samples were run along a GeneRuler 1 kb Plus DNA Ladder on gel electrophoresis with an electric current of 150V. Each sample had a different barcode primer combination. This will give a unique tag to each sample to help in bioinformatics analysis. The different combinations of barcode primers are found in Appendix I.

Band isolation of barcoded amplicon. This step is very similar to the previous band isolation. The gel extraction was performed after running the samples on the gel electrophoresis for 50 min, then the correct band size was determined according to the values found in Table 4. The final product obtained from the Invitrogen DNA PureLink quick gel extraction kit was the new DNA template product, having all the different adapters connected to the amplicon for Illumina sequencing. After running the new DNA template, there were two bands instead of one. In order to test the appearance of the band, a Denaturing Urea Polyacrylamide Gel Electrophoresis (Urea PAGE) was done, where the second higher band was eliminated, suggesting that this second band was a secondary structure and would not interfere with the DNA sequencing.

Quantification via Qubit. The quantification was initially completed through Qubit® 3.0 Fluorometer using the Qubit® dsDNA HS Assay Kit protocol. Any double-stranded DNA found within the sample can be detected by this fluorescence-based technique. The samples were prepared via two major steps. First, a working solution was prepared by mixing the 0.5% of Qubit reagent volume and 99.5% volume of Qubit buffer for a total volume of 200µl. Then specialized Qubit tubes in which the samples will be kept in for the measurement through the fluorometer machine were prepared. There were also two standards, sample I and II, from the Qubit dsDNA HS Assay Kit. Those two samples contained 95% of the working solution and 5% of the standard sample in each tube for a volume of 200µl. The reference library along with the 17 different samples contained 99.5% of the working solution and 0.5% of the actual DNA sample. The Qubit fluorometer was set up as shown in the manual from Thermo Fisher Scientific Inc. After quantifying the two standards, a standard curve was created for quality assurance. The rest of the samples were tested and quantified, and the data was exported into a table.

Quantification via qPCR. Another method was applied to quantify the DNA in each sample. This method relied on qPCR, or real-time PCR. It is the same machine used in cycle determination for both sets of primers, but a different kit was used for quantification. The first step of this process was combining all the samples together in one 1.5ml microcentrifuge tube.. Afterward, there was a set of calculations performed for both the reference sample (which is the previously tested sample obtained from the Plant Immunology Laboratory) and the multiplex library (which represents all the samples combined together). The first step of calculations is related to attaining a desired starting concentration for the dilution as shown in the KAPA Library Quantification Kit Illumina®-KR0405 – v8.17. In order to accomplish this step, both samples' concentrations were converted to pM from ng/µl by applying the formula below, where average library size in bp is found in Table 4 :

$$\text{Concentration in } pM = \frac{Concentration\ in\ \ ng/\mu l}{(660\,\frac{g}{mol}\ \text{x}\ average\ library\ size\ in\ bp)}\ \text{x}\ 10^9$$

Then, for the reference library, a series of dilutions were calculated and completed to be tested in order to create a standard curve equation and compare it to my multiplex library, as shown in Table 5. As for the multiplex library, further dilutions were performed to attain different concentration values that should appear within the borders of the standard curve. Those calculations are shown in Table 6. After preparing the different sample, a master mix was prepared using adapters of P5/P7 primers (10 µM), 5X SYBR buffer from KAPPA kit, DNA template, with the rest being water to attain a total volume of 10 µl for each sample. The DNA templates were added to each well first, then 5 µl was added from the master mix. The plate was sealed, mixed and centrifuged for the qPCR. Each sample had three replicates to test the accuracy of the pipetting. The plate was ready for qPCR. I inserted it in qPCR and ran the samples with a Solis-RT set-up through the Bio-Rad CFX Manager. The results obtained showed Cp values which represents the amount of time it took for the DNA sample to absorb the emitted light from qPCR. This helped me develop a standard curve to be used to test the multiplex library.

Table 5. Reference library preparation for quantification and creation of a standard curve according to the series dilutions via qPCR. DNA: Deoxyribonucleic Acid; ddH_2O: double distilled water; C_i: Initial concentration; C_f: Final concentration; V_i: Initial volume; V_f: Final volume.

Reference Library				
	DNA (µL)	**ddH_2O (µL)**		
Primary *dilution*	5 µL	450 µL	91 times	
V_i for 20 pM	10.76 µL	39.24 µL	C_i pM	102.1705 pM
V_t for 20 pM	50 µL		C_f pM	21.9871 pM
Ready for dilution				
***Dilution* series**	**DNA (µL)**	**ddH2O (µL)**	**Dilution by**	**[pM]**
1st dilution	2 µL	18 µL	10	2.19871 pM
2nd dilution	2 µL	18 µL	100	0.219871 pM
3rd dilution	2 µL	18 µL	1000	0.021987 pM
4th dilution	2 µL	18 µL	10000	0.002199 pM

Table 6. Multiplex samples library preparation for quantification through qPCR.
C: concentration; m: mass; V: volume.

Multiplex Library				
Mass of DNA (ng):	m = 5.28 x17= 89.76 ng			
Total Volume (µL) :	V= 25.08 µL			
[C] $_{ng/\mu l}$= m/V =>	C= 3.58 ng/µL			
[C]=3.58/ (660X238.4) x10^9 =		22746 pM		
Ready for dilution				
Dilution series	**DNA (µL)**	**ddH_2O (µL)**	**Dilution by**	**[C]**
1st dilution	5 µL	450 µL	91 times	249.956 pM
2nd dilution	5 µL	450 µL	8281 times	2.74677 pM
3rd dilution	5 µL	450 µL	753571 times	0.030184 pM

Sequencing. Library preparation for sequencing was done through the MiSeq Reagent Nano Kit v2 (300-cycles). According to the kit protocol, the kit, stored at -20°C, was removed to defrost at 4°C, then at room temperature while incubating in a water bath on a Thermo Scientific Plate Shaker. During this time, I also prepared a fresh solution of NaOH (0.2M) using water and NaOH tablet. Then, I prepared the custom primer (0.5µM) from the stock solution (100 µM) and the Hybridization buffer (HT1) obtained from the reagents kit with a final volume of 600 µl. This custom primer represents the read 1 primer from Figure 6. As for read 1 and index 1 primers, these are already present by default in the kit. Afterward, I prepared a multiplex library mix with a concentration of 20 pM. This mixture contained the original multiplex library without any dilution, NaOH (0.2M), and water. After mixing, centrifugation, and resting the mixture at room temperature for 5 minutes, the HT1 buffer is added to complete the volume of 1 ml. In order to attain the desired concentration of 6 pM, I diluted my sample with a final volume of 600 µl. A sample sheet was prepared with different information for the Illumina MiSeq™ System including the different primer combinations and the number of reads. After the solutions in the kit were defrosted, the multiplex library sample was loaded on the 17th position, and the custom primer sample was loaded in the 18th position. Then the kit was transported to the MiSeq™ System where all the necessary information was entered and the sequence by synthesis started for 12 hours. After the run finished and passed the Illumina quality control, the results were downloaded for bioinformatic analysis.

Bioinformatic analysis. The reads generated by MiSeq Illumina sequencer were assessed through FASTQC. The online system from Illumine trimmed the P5 and P7 tails, indexes, and PE adapter according to the unique index values provided for each sample. The trimming of those barcode adapters generated 17 different files, with each file representing one sample. For each sample, I had all the reads that corresponded to the associated sample. I used Jupyter (Toomey 2016), an IPython notebook, along with MobaXterm, a user interface for remote computing by Mobatek®. Those programs facilitated processing my command lines for further analysis. After setting up my files, I was able to use the “cutadapt” function in python (Martin 2011) to select my previously known amplicons for the 20 single nucleotide polymorphism (SNPs) from the different reads 1 and 2 segments. After completing this step, for each sample I obtained a folder with 20 files representing the amplicon generated by the 20 primers set. Those segments represent the different chromosome positions containing the targeted SNPs. These raw data files were ready for alignment. For that step, I needed to create a reference index using Bowtie2 with build -f function. I was then able to align each single-ended file, then merged them together as double-ended files through a pair end alignment in Bowtie2 (Langmead and Salzberg 2012) for each SNP of each sample using different loops in python (McKinney 2012). The aligned data compromised of both read 1 and read 2 in one single file. At this stage, I had to look for the desired SNPs using the best SNP calling software appropriate to my file type: Samtools and Bcftools (Li 2011; Liu et al. 2013). This generated information regarding each nucleotide position and allele at this position, if the minor allele was present, then I had a targeted SNP. Finally, to obtain the targeted SNPs from the known location in each amplicon, basic Unix command and AWK were applied (Dougherty and Robbins 1997). At the end, I generated a matrix compromising of the presence or absence of the targeted SNPs for each sample. This process was performed via the data acquired from Illumina MiSeq and was analyzed through an optimized bioinformatic pipeline code. This script is available upon request.

Genotype-Phenotype assessment

Statistical analysis depends on the sample size. Because my sample size was not considered as a population, my chosen statistical tests were related to a sample, not a population. The data sets were obtained from the inter-landmark distances of the skull and the DNA sequencing results. The different functional groups with their associated single nucleotide polymorphisms (SNP) had different landmarks related to them as shown in Figure 7. Each SNP had their own set of inter-landmark distances (ILDs) that represents the associated phenotype area/functional group of the face. A large table with figures containing the different SNPs with the representation of ILDs, their name, and their associated functional group are found in Appendix II. I performed several analyses:

1. *Spearman's rank-order Correlation between all the SNPs and ILDs.*

I performed this test with JMP (Sall et al. 2012) by using the continuous data obtained from the calculated ILDs and the categorial data obtained from SNPs (0 being absent and 1 being present). I joined ILD and SNP tables together with the samples from both tables as matching columns. Then, I selected the multivariate option in multivariate methods. I selected all the SNPs and ILDs and assigned their role as columns. After obtaining the correlations, I selected the non-parametric Spearman's ρ and all the values of the bilateral correlations were present. The Spearman's correlation is a non-parametric test that employs the same statistical approach to Pearson's product-moment correlation. The correlation coefficient (ρ) or rs shows the direction and the strength of association between two sets of values by providing a range between 1 and -1. The extremes (1, -1) show perfect correlation and the correlation decreases as the values navigate toward 0. On the other hand, the p-value shows the significance of the correlation according to the value obtained. A very weak correlation is any value higher than 0.1, a weak correlation is between 0.1 and 0.05, and a strong correlation is between 0.05 and 0.01 (Fowler et al. 2013). For this reason, I eliminated any raw values that had a p-value of more than 0.05

and created a new table with only the significant correlations. The final outcome, found in the Results chapter, was used for further analysis.

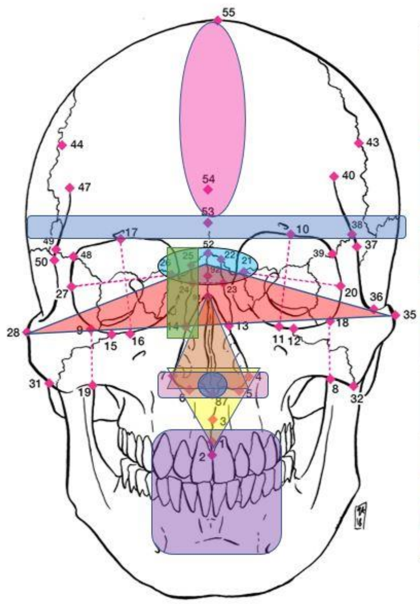

Section	Function group	SNP
Section 1	Eye-Nasion- Eye	rs72691108 rs6555969 rs7559271 rs17447439
Section 2	Nasal Ala length (L &R)	rs4648379 rs8007643 rs1982862 rs11738462
Section 3	Zygion-Nasion-Zygion	rs12786942 rs6555969
Section 4	R endocation in space	rs10862567
Section 5	Cranial width	rs17106852 rs6129564
Section 6	Chin protrusion	rs3827760 rs6740960 rs10238953
Section 7	Nose wing breadth	rs927833 rs17640804
Section 8	Philitrum width	rs2977562
Section 9	Forehead	rs5880172
Section 10	Nose tip	rs9995821

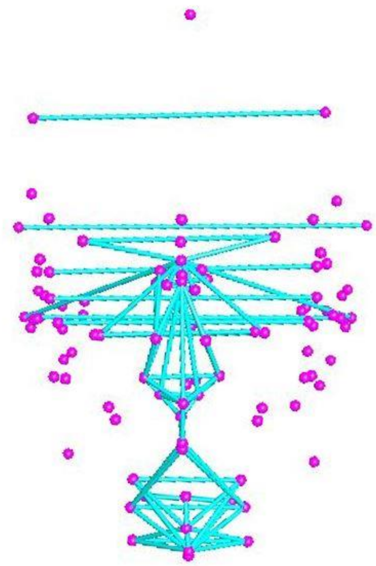

Figure 7. The different sections showing the functional group along with their associated SNPs. On the left, illustrated skeleton with the different morphological functional groups colored according to their section number. The table represents the different sections with their associated function group and SNP. The figure on the right represents the 99 landmarks and all the inter-landmark distances used.

2. Two-way Hierarchical Clustering of the significant correlations obtained.

The results from the previous test were tested through a two-way hierarchical clustering test with JMP in order to visualize any direct relatedness or similarity between the different variables that were shown as significant previously (Phips and Larry 1996). After only selecting the significant correlations, I selected the hierarchical cluster option in clustering and added only the columns with the SNPs and their associated ILD with significance association. Then, I selected the two-way clustering and presented it as a heat map as shown in the Results chapter.

3. *Bootstrap Forest model for the significant correlations obtained.*

The Bootstrap Forest model is a machine learning approach that resamples the samples and then creates decisions trees (100 in this case) that will be averaged, and then splits randomly to create a simulated final random predictive data. The R-square range is between 0 and 1. The model represents a better fit if the R-square value is closer to 1 and the Root-Mean-Square Error (RMSE) is a low value. Those values are represented in the Results chapter. I performed the test using JMP by employing the Bootstrap model option in predictive modeling. I set the factor (X) as the significant ILDs and the response (Y) as their associated SNP. I performed each individual SNP correlation separately while selecting the default settings for the Bootstrap specifications. This method provided discrete R-square and RMSE values for each correlation.

4. *Prediction profiler from the Bootstrap forest model results.*

The prediction profiler is a subsection of the Bootstrap Forest model. It provides the probability in which a certain value of the variables can have an effect on predicting the values of the response. In this case, I was able to obtain this profiler by using the results obtained from the Bootstrap model and applying the profiler option through JMP, keeping the default value chosen as predictive value of the response (SNP), according to the presented factor (ILDs) values.

5. *Principal Component Analysis (PCA) to SNPs and ILDs separately*.

Principal component analysis is a multivariate statistical analysis that extrapolates the variations present in a set of variables and reduces them into multidimensional representations (Anderson and Willis 2003). I performed two main principal component analyses using JMP. First for the SNP data obtained from the bioinformatic analysis, and second for the ILDs of interest. The analysis was performed through the principal component option in the multivariate analysis section. The column with the variables were selected as roles (Y). The analysis is comprised of table of Eigenvalues that represents the distribution of variation within these samples. I represented all the Eigenvalues in the Results chapter, and I highlighted the threshold of around 70% representation of variance. However, I have only denoted the first two principal components as they represent the highest representation of variance (Jolliffe 2011). The loading matrixes showing the highest correlations between variables in each principal component for every test performed are present in Appendix III.

6. Procrustes analysis through pair-wise comparison between SNPs and ILDs. Procrustes analysis relies on the PCA results and performs a pair-wise comparison between two sets of variables (Wang et al. 2010), in this case ILDs and SNPs. The pair-wise comparison relies on bringing the set that shows a higher relative importance among the different groups. This was performed through an R script developed and provided by Dr. Bridget FB Algee-Hewitt. The script provided a pair-wise analysis with the sum of squares deviation between rotations, ordination diagrams, and plots of pair-wise residuals. After receiving the data from the symmetric Procrustes analysis, different statistical calculations were performed to generate m-squares, sum of squares (ss), and the correlation-like (t) statistic. Finally, a permutation was applied for all individuals' Procrustes analysis to check the difference between the fit value and the randomness.

This eventually can provide a p-value that can show the absence or present of a non-random significance.

IV. RESULTS

The results of this analyses were confined to the findings from each section, and their relevance to the research question regarding whether SNP markers for craniofacial traits are associated with craniofacial measurements.

The skull

Landmark coordinates. After completing data collection of the ILD craniometrics, I performed Procrustes and principal component analysis as shown in Figures 8, 9, and 10. The highest representation of variability is shown in the principal component 1 and 2 with a cumulative value of around 40%, as shown in Figure 9. The distribution of the samples is homogeneous and there is no distinction between females and males according to the shape of the skull, as shown in Figure 10. There are 10 males and 7 female samples, and most of the females are clustered, i.e., between 0.02 and -0.04 in PC1 . As for the males, variation is greater, ranging from -0.04 to 0.08 in PC1. The Procrustes coordinates are shown in Figure 8 along with the sum of squares. The 0.079

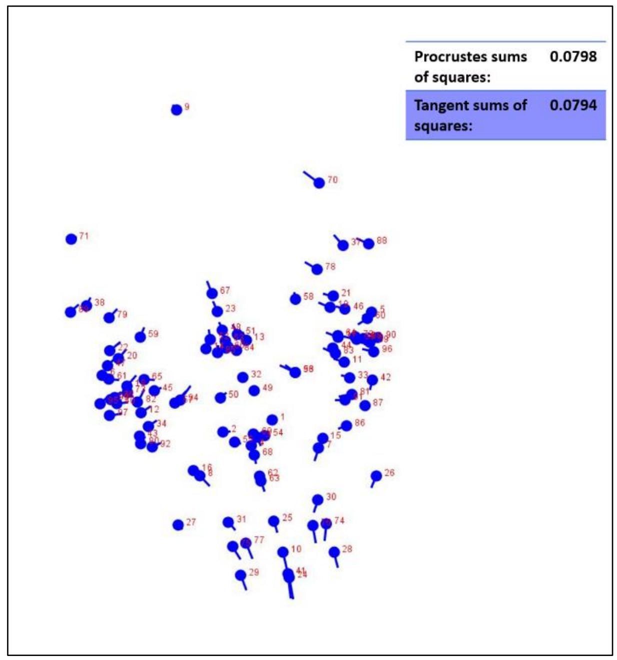

Figure 8. An example of the Procrustes coordinates with the sum of squares and its tangent from all the coordinates.

value of the sum of squares shows the lowest distance between the landmarks of the samples after superimposition (Klingenberg 2011).

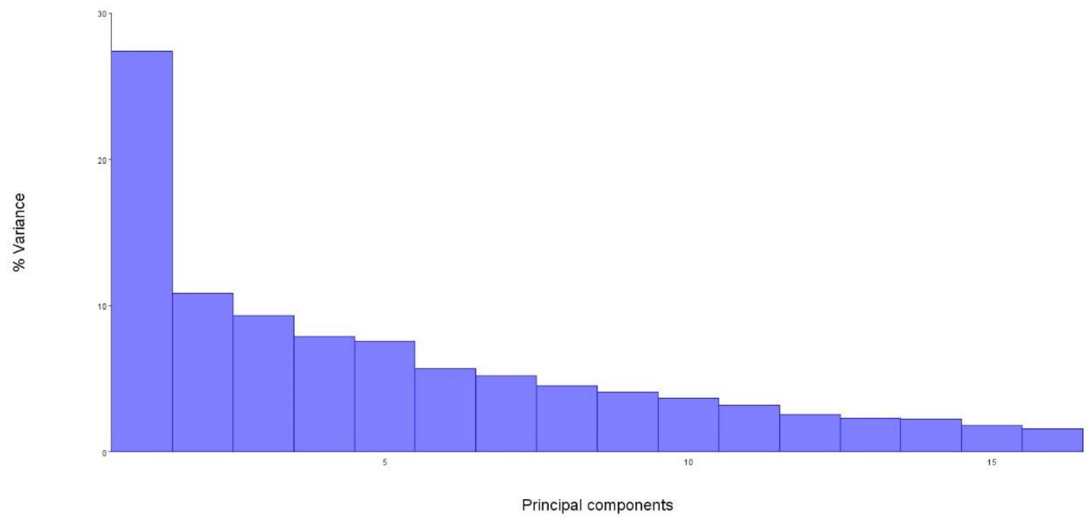

Figure 9. Eigenvalues of the principal components gained from the analysis of the coordinates of the 99 landmarks obtained with the MicroScribe digitizer.

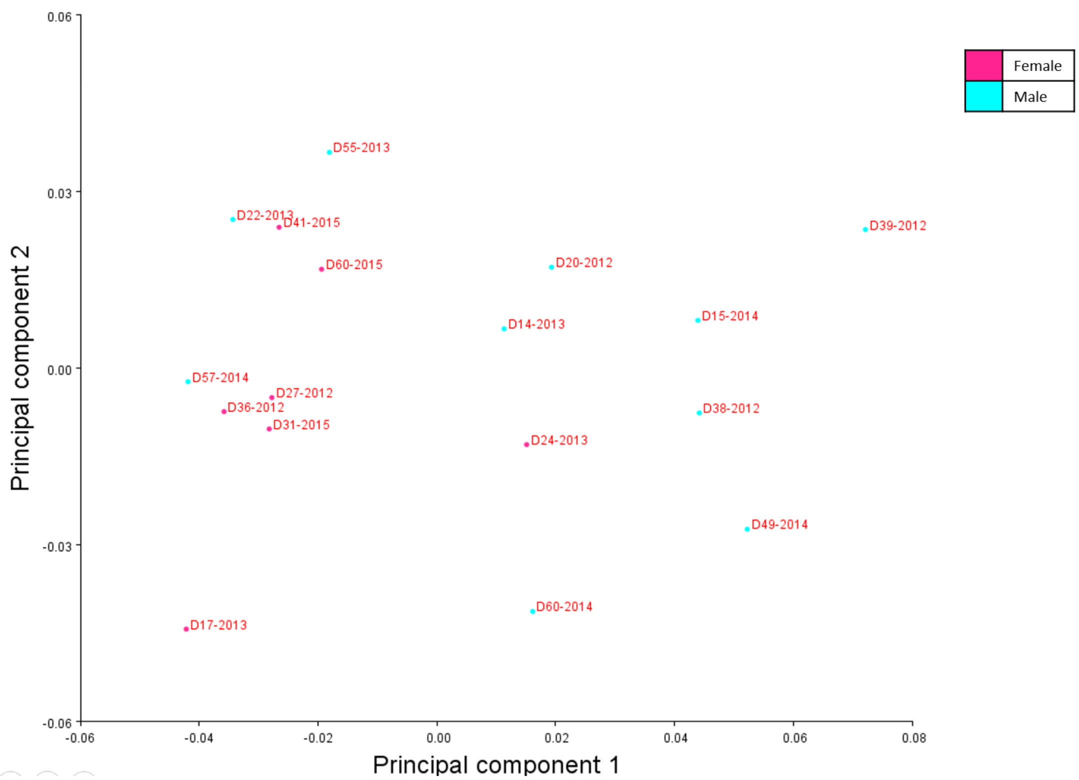

Figure 10. The distribution of variation among the samples in a 2D representation of principal component analysis.

Frontal arc. The coordinates obtained through 3Skull and the Microscribe digitizer were analyzed through MorphoJ. The Eigenvalues in Figure 11 represents the variations of

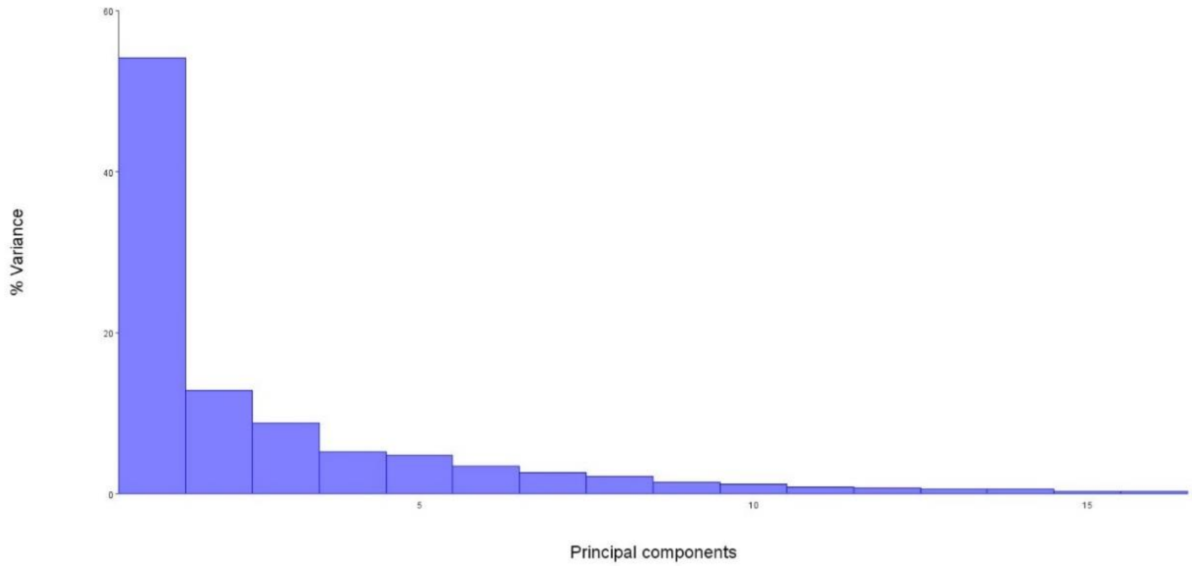

Figure 11. Eigenvalues of the principal components gained from the analysis of the coordinates of the frontal arc semi-landmarks obtained with the MicroScribe digitizer.

each principal component (PC). The first two PCs represent around 60% of the variation. The plot of those two PCs is represented in Figure 12, where the individuals are separated according to sex (red dot=female, blue dot=male). The variations among the samples had the same pattern as the coordinates of the landmarks, where the distribution of variation within females was smaller than the variation within males, with a range between around

-0.04 and 0. However, the variation within males was between -0.04 and 0.06 in PC1.

The Procrustes coordinates in Figure 13 were split and plotted according to sex.

The different shapes, especially around the last 10 semi-landmarks, are different between sexes. This morphology coincides with the presence of the glabella projection on the frontal bone.

The low value of the sum of squares of 0.03 among all the samples shows the small distance needed to superimpose the different shapes of the frontal arcs of the individuals.

Figure 12. The distribution of variation among the samples in a 2D representation, using the first two principal components.

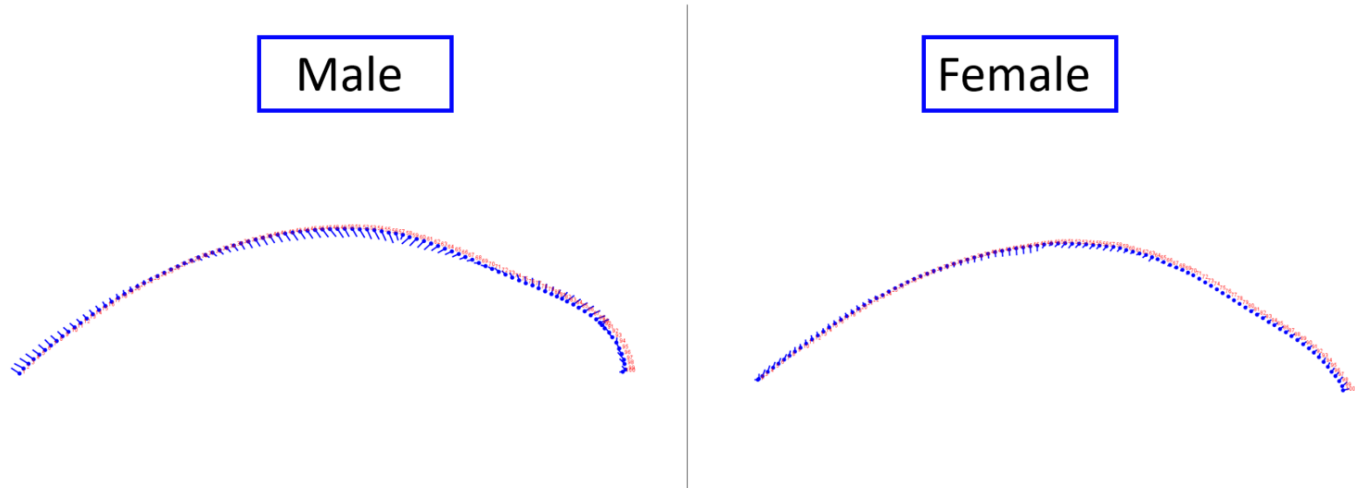

Procrustes sums of squares:	0.03
Tangent sums of squares:	0.03

Figure 13. An example of the Procrustes coordinates with the sum of squares and its tangent from all the coordinates of the frontal arc divided according to the sex of the individuals. The red represents the numbers of landmarks forming the frontal arc (100), and the blue represents the landmark points and the direction of deviation from the total mean.

The DNA

The process of DNA sequencing required multiple steps, as mentioned in the Materials and Methods chapter. The final outcome of the DNA sequencing was the presence and absence of the desired minor allele that represent the single nucleotide polymorphisms (SNP). In bioinformatics, the alleles were differentiated according to their haplotype, and the presence of the minor alleles was coded as 1 and the absence of this allele was coded as 0, as shown in Table 6. SNPs rs2977562, rs72691108, and rs9995821 had the highest presence within the sample with 10, 9, and 8 occurrences respectively. However, there was several SNPs that did not have any occurrence among the individuals. Those SNPs were: rs10862567, rs7559271, rs3827760, rs6740960, rs17447439, rs6555969, rs5880172, rs17640804, rs10238953.

Table 7. Presence/absence of SNPs in each sample, according to the bioinformatic analysis (1=present, 0=absent). Willed body donor numbers are along the top, target SNPs are to the left.

	D36-2012	D17-2013	D60-2015	D24-2013	D31-2015	D41-2015	D27-2012	D20-2012	D38-2012	D15-2014	D22-2013	D49-2014	D39-2012	D55-2013	D14-2013	D57-2014	D60-2014	**Total**
rs72691108	1	1	1	1	1	1	0	1	0	0	0	0	1	0	0	1	0	**9**
rs4648379	0	0	0	0	0	0	1	0	1	0	0	1	1	0	0	0	0	**4**
rs12786942	0	0	1	0	0	0	0	0	0	0	1	0	0	0	1	0	0	**3**
rs10862567	0	0	0	0	0	0	0	0	0	0	0	0	0	0	0	0	0	**0**
rs8007643	0	0	0	0	0	0	0	0	0	0	0	1	0	1	0	0	0	**2**
rs17106852	0	0	0	0	1	0	1	1	0	0	0	0	0	1	0	0	0	**4**
rs7559271	0	0	0	0	0	0	0	0	0	0	0	0	0	0	0	0	0	**0**
rs3827760	0	0	0	0	0	0	0	0	0	0	0	0	0	0	0	0	0	**0**
rs6740960	0	0	0	0	0	0	0	0	0	0	0	0	0	0	0	0	0	**0**
rs6129564	0	0	1	0	0	0	0	0	0	1	0	0	0	0	0	0	0	**2**
rs927833	0	0	0	0	1	0	0	0	0	0	0	0	0	1	0	0	0	**2**
rs17447439	0	0	0	0	0	0	0	0	0	0	0	0	0	0	0	0	0	**0**
rs1982862	0	0	0	0	0	0	0	0	0	0	0	0	0	0	1	1	0	**2**
rs2977562	1	0	0	0	1	1	0	1	0	1	1	1	1	1	0	1	0	**10**
rs9995821	1	0	1	0	0	0	0	0	0	1	1	1	0	1	0	1	1	**8**
rs11738462	1	0	0	1	0	1	0	0	0	0	0	0	1	0	1	0	1	**6**
rs6555969	0	0	0	0	0	0	0	0	0	0	0	0	0	0	0	0	0	**0**
rs5880172	0	0	0	0	0	0	0	0	0	0	0	0	0	0	0	0	0	**0**
rs17640804	0	0	0	0	0	0	0	0	0	0	0	0	0	0	0	0	0	**0**
rs10238953	0	0	0	0	0	0	0	0	0	0	0	0	0	0	0	0	0	**0**

Genotype-Phenotype correlation

Spearman's rank-order correlation between all the SNPs and ILDs. The Spearman's correlation against both large SNP and ILD data sets showed different patterns (Figure 14). There are three distinct patterns visible in the heat map. The first one is the absence of correlation, which is represented by 0 (in white). The second pattern is positive

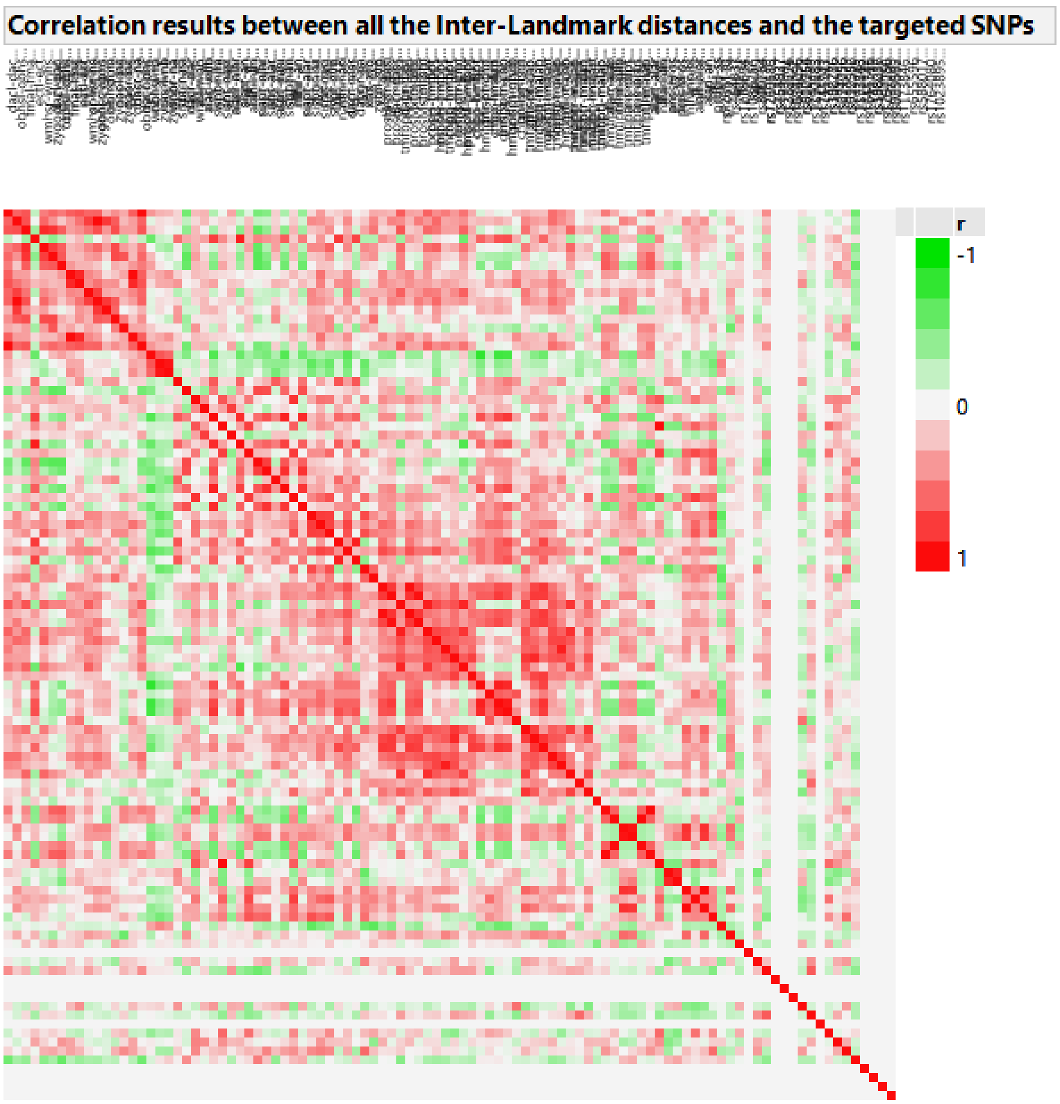

Figure 14. Heat map with the correlation between all the inter-landmark distances and the targeted SNPs. The green hues represent a negative correlation (-1 to -0.01), the white represents no correlation (0), and the red hues represents positive correlations (0.01 to 1).

correlation characterized by the red; and the third pattern is the negative correlation, presented in green. However, in order to check relevant and significant correlations in this large pool, I only selected significant correlations with p-values lower than 0.05, as shown in Table 8. The blue spectrum color shows the correlation coefficient (r), and the pink spectrum color shows the p-value for each correlation. The correlation coefficient was within 0.65 and 0.48 on both spectra (negative and positive).

There was not a perfect correlation, however, the distribution of those values is shown with the corresponding ILDs in Figure 15. The different sizes correspond to the actual numerical value of the ILDs. There is a visible linear correlation on the negative side, and another similar representation on the positive side. In Table 8, there are very strong

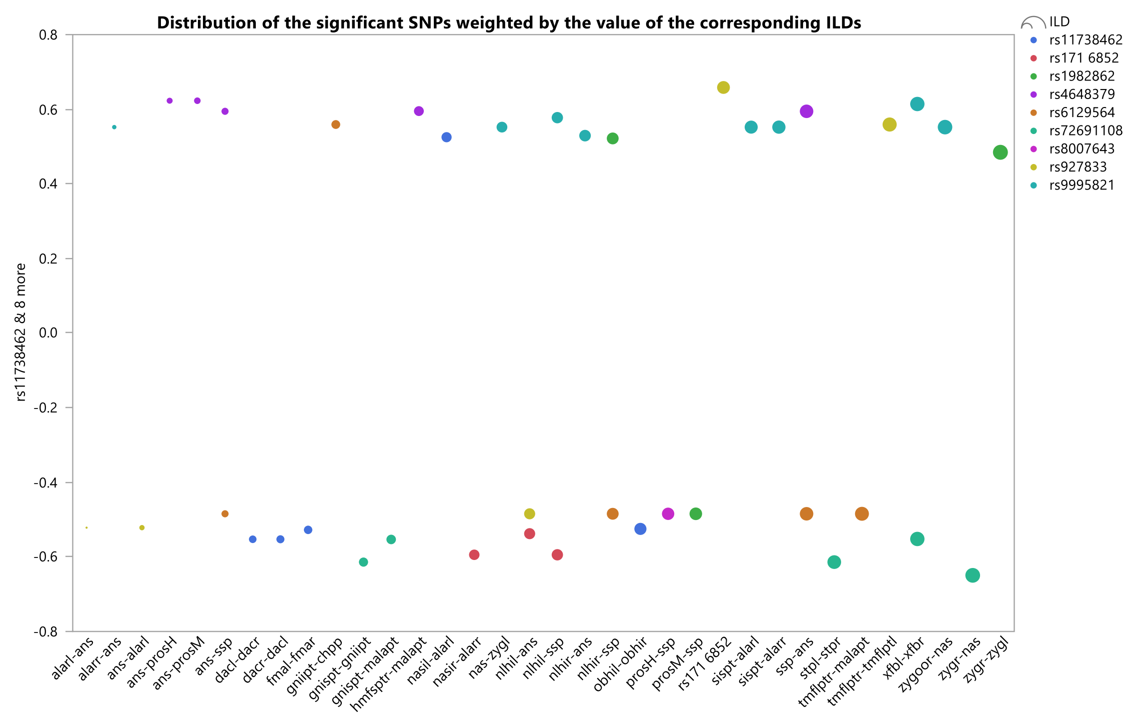

Figure 15. Distribution of the correlation between the SNPs and ILDs showing significant associations.

positive correlations with a p-value of 0.0076 between Ans-prosH (Anterior Nasion spine and prosthion-Howells), and Ans-prosM (Anterior Nasion spine and prosthion-Martin) and SNP rs46483792. This correlation is also shown between ILDs and SNPs from a different but related functional group: Nasal Ala length and philtrum length.

Another strong negative correlation, with a p-value of 0.0048, occurs between zygr-nas (zygion-R and nasion) and SNP rs72691108. Those two elements are also from different groups: zygion-nasion-zygion and eye-nasion-eye respectively. This correlation shows that increasing the value of zygion-R to nasion can affect the presence of SNP rs72691108. Another significant positive correlation with a p-value lower than 0.01 is between two different SNPs: rs1716852 and rs9278332. Those two SNPs are related to two different functional groups; cranial width and nose wing breadth, respectively. In Figure 16, I performed a principal component analysis showing a correlation between both the SNPs described above, and the common ILDs that are also scientifically correlated with them, as provided in Table 7. The inter-landmark distance is the most inferior nasal border on the left side to anterior Nasal spine (nlhlil-ans). As shown in Figure 16, there were three variables which provided three transformation vectors or Eigenvectors distributed with a 2.0247 for PC1 (67.5%), 0.6358 for PC2 (21.2%), and 0.3395 for PC3 (11.3 %) .

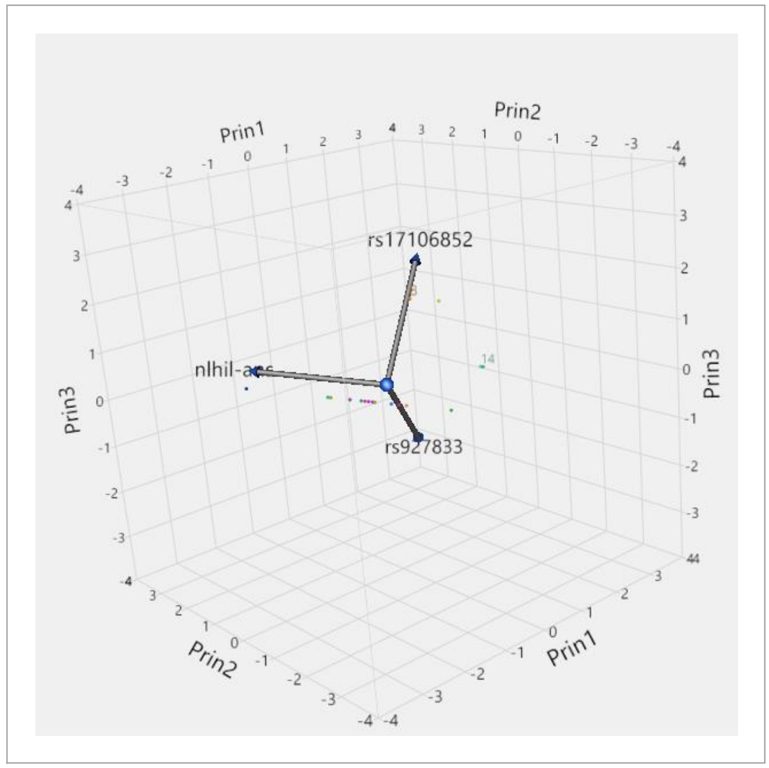

Figure 16. Principal component analysis with eigenvectors related to the correlation of rs1716852 and rs9278332, and the measurement of nasal spine.

Table 8. Spearman's correlation between the SNPs and ILDs, with a p-value < 0.05.

		Nasal Ala length (L &R)		Cranial width		Nasal Ala length (L &R)		Nasal Ala length (L &R)		Cranial width		Eye-Nasion- Eye		Nasal Ala length (L &R)		Nose wing breadth		Nose tip	
	SNP / ILD	rs11738462		rs171 68522		rs19828623		rs46483792		rs61295642		rs72691108		rs80076432		rs9278332		rs9995829	
philtrum width	alarl-ans															-0.5217	0.0317		
philtrum width,Nasal Ala length (L &R)	alarr-ans																	0.5052	0.0386
Nasal Ala length (L &R)	ans-alarl															-0.5217	0.0317		
philtrum width	ans-prosH							0.6228	0.0076										
philtrum width	ans-prosM							0.6228	0.0076										
philtrum width	ans-ssp							0.5944	0.0118	-0.4845	0.0487								
Eye-Nasion- Eye	dacl-dacr	-0.5528	0.0214																
Eye-Nasion- Eye	dacr-dacl	-0.5528	0.0214																
Eye-Nasion- Eye	fmal-fmar	-0.5276	0.0295																
Chin protrusion	gniipt-chpp									0.559	0.0197								
Chin protrusion	gnispt-gniipt											-0.6014	0.0107						
Chin protrusion	gnispt-malapt											-0.5533	0.0212						
Chin protrusion	hmfsptr-malapt							0.5095	0.0367										
Nasal Ala length (L &R)	nasil-alarl	0.5025	0.0398																
Nasal Ala length (L &R)	nasir-alarr			-0.5944	0.0118														
Zygion-Nasion-Zygion	nas-zygl																	0.5052	0.0386
Nose tip,philtrum width,Nasal Ala length (L &R)	nlhil-ans			-0.5378	0.026											-0.4845	0.0487		
Nose tip	nlhil-ssp			-0.5944	0.0118													0.5774	0.0152
Nose tip,philtrum width,Nasal Ala length (L &R)	nlhir-ans																	0.5292	0.0289
Nose tip	nlhir-ssp					0.5217	0.0317			-0.4845	0.0487								
Eye-Nasion- Eye	obhil-obhir	-0.5025	0.0398																
philtrum width	prosH-ssp													-0.4845	0.0487				
philtrum width	prosM-ssp					-0.4845	0.0487												
Cranial width	rs171 6852															0.6583	0.0041		
Nasal Ala length (L &R)	sispt-alarl																	0.5052	0.0386
Nasal Ala length (L &R)	sispt-alarr																	0.5052	0.0386
Nose tip	ssp-ans							0.5944	0.0118	-0.4845	0.0487								
Cranial width	stpl-stpr											-0.6014	0.0107						
Chin protrusion	tmflptr-malapt									-0.4845	0.0487								
Chin protrusion	tmflptr-tmflptl															0.559	0.0197		
Cranial width	xfbl-xfbr											-0.5052	0.0386					0.6014	0.0107
Eye-Nasion- Eye	zygoor-nas																	0.5052	0.0386
Zygion-Nasion-Zygion	zygr-nas											-0.6495	0.0048						
Zygion-Nasion-Zygion	zygr-zygl					0.4845	0.0487												

Two-way hierarchical clustering of the significant correlations. I performed the two-way hierarchical clustering, showing the dendrograms according to the distribution of the clusters, and according to the extent of distance between each (Figure 17). Individuals D22-2013 and D57-2014 and D20-2012 and D36-2012 are clustered together showing similarity to each other . Those clusters are applied only to the values of the SNPs and ILDs selected. There are several clusters that are composed of two variables showing high values such as ans-prosH and ans-prosM, or gnispt-malapt (Infradentale-gnathion).

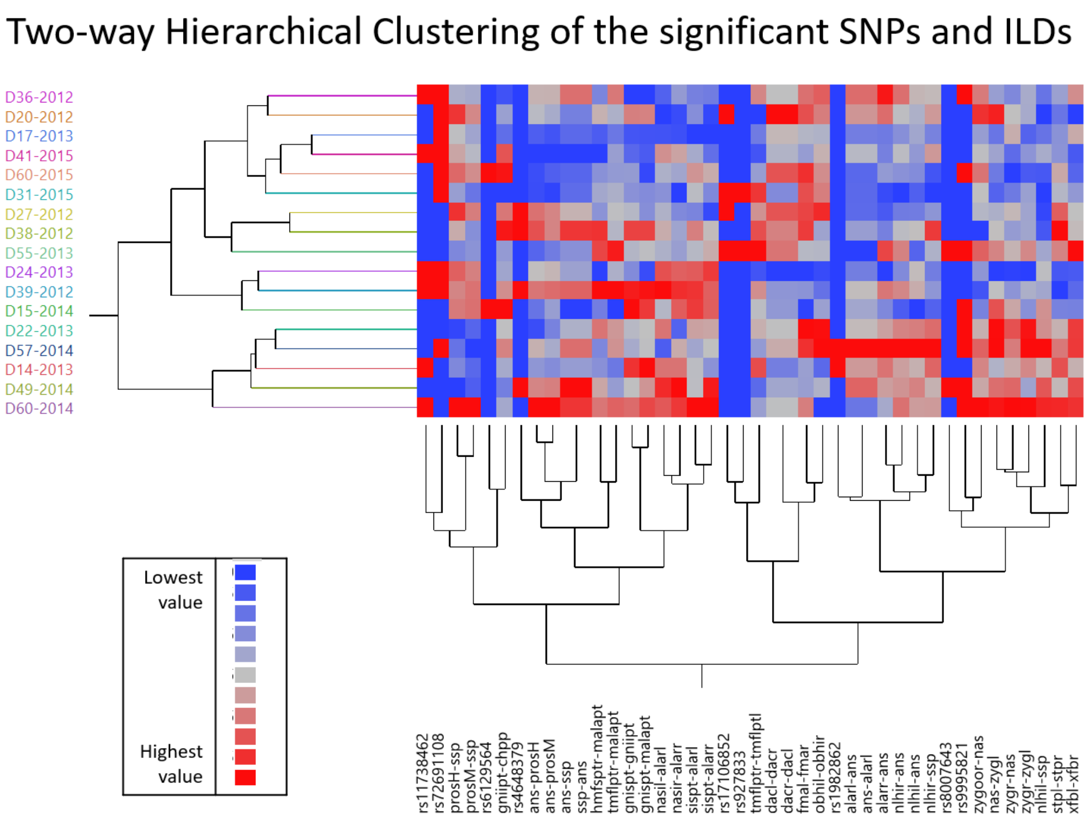

Figure 17. Two-way hierarchical clustering of the significant SNPs and ILDs against the clustering among the donated individuals used in this study.

However, there were clusters with lower values formed by two variables, such as rs1716852 and rs9278332. Another set of close neighbors is rs1982862 and alarl-ans (nasal ala breadth left side-Anterior nasal spine). The difference in values are visualized with a heat map showing the lowest value in blue and the highest value in red (Figure 17).

Bootstrap Forest model for the significant correlations obtained. After establishing which single nucleotide and inter-landmark distances show any type of significant correlations, I performed a Bootstrap Forest model to determine if or how those correlations could be useful for future predictions. In Table 9, the yellow coloration spectrum shows the different values of R-square obtained from the analysis. The values range between 0.35 for rs8007643 and 0.63 for rs9995821. The ones closest to rs9995821 show the highest likelihood for a perfect model. this trend is correlated with the root mean square error, as shown in the pink spectrum of colors. The lowest RMSE is 0.23 and it is related to rs927833. The RMSE does exceed 0.32.

Table 9. Bootstrap analysis results according to individually correlated variables.

Single nucleotide polymorphism (SNP)	Inter-Landmark distances (ILD) used	RSquare	Root mean square error (RMSE)
rs11738462	dacl-dacr dacr-dacl fmal-fmar nasil-alarl obhil-obhir	0.49	0.34
rs17106852	nasir-alarr nlhil-ans nlhil-ssp	0.43	0.32
rs1982862	nlhir-ssp prosM-ssp zygr-zygl	0.45	0.24
rs4648379	ans-prosH ans-prosM ans-ssp hmfsptr-malapt ssp-ans	0.57	0.28
rs6129564	ans-ssp gniipt-chpp	0.41	0.25

Table 9 Continued

	nlhir-ssp ssp-ans tmflptr-malapt		
rs72691108	gnispt-gniipt gnispt-malapt stpl-stpr xfbl-xfbr zygr-nas	0.59	0.32
rs8007643	prosH-ssp	0.35	0.26
rs927833	alarl-ans ans-alarl nlhil-ans tmflptr-tmflptl	0.47	0.23
rs9995821	alarr-ans nas-zygl nlhil-ssp nlhir-ans sispt-alarl sispt-alarr xfbl-xfbr zygoor-nas	0.63	0.30

Prediction profiler from the Bootstrap Forest model results. Evaluation of the random forest model was performed by producing a prediction profile of the SNPaccording to a certain value of the associated variable corresponding to it (as shown in Table 10). For example, if the following inter-landmark distances have these values: Anterior nasal spine- Subspinale (ans-ssp) is 6.9281 mm, gnathion- chin protrusion point (gniipt-chpp) is 13.3347 mm, most inferior nasal border R – Subspinale (nlhir-ssp) 11.332 mm, Subspinale- Anterior nasal spine (ssp-ans) is 6.9281 mm, and TMF lingual point R-pogonion (tmflptr-malapt) is 28.4267mm, then the SNP rs6129564 is not present and thus the major allele is present which means that this individual has the common allele in this position. These data are interpreted in further depth in the discussion.

Table 10. Prediction profiles of the different significant single nucleotide polymorphisms and their associated inter-landmark distances.

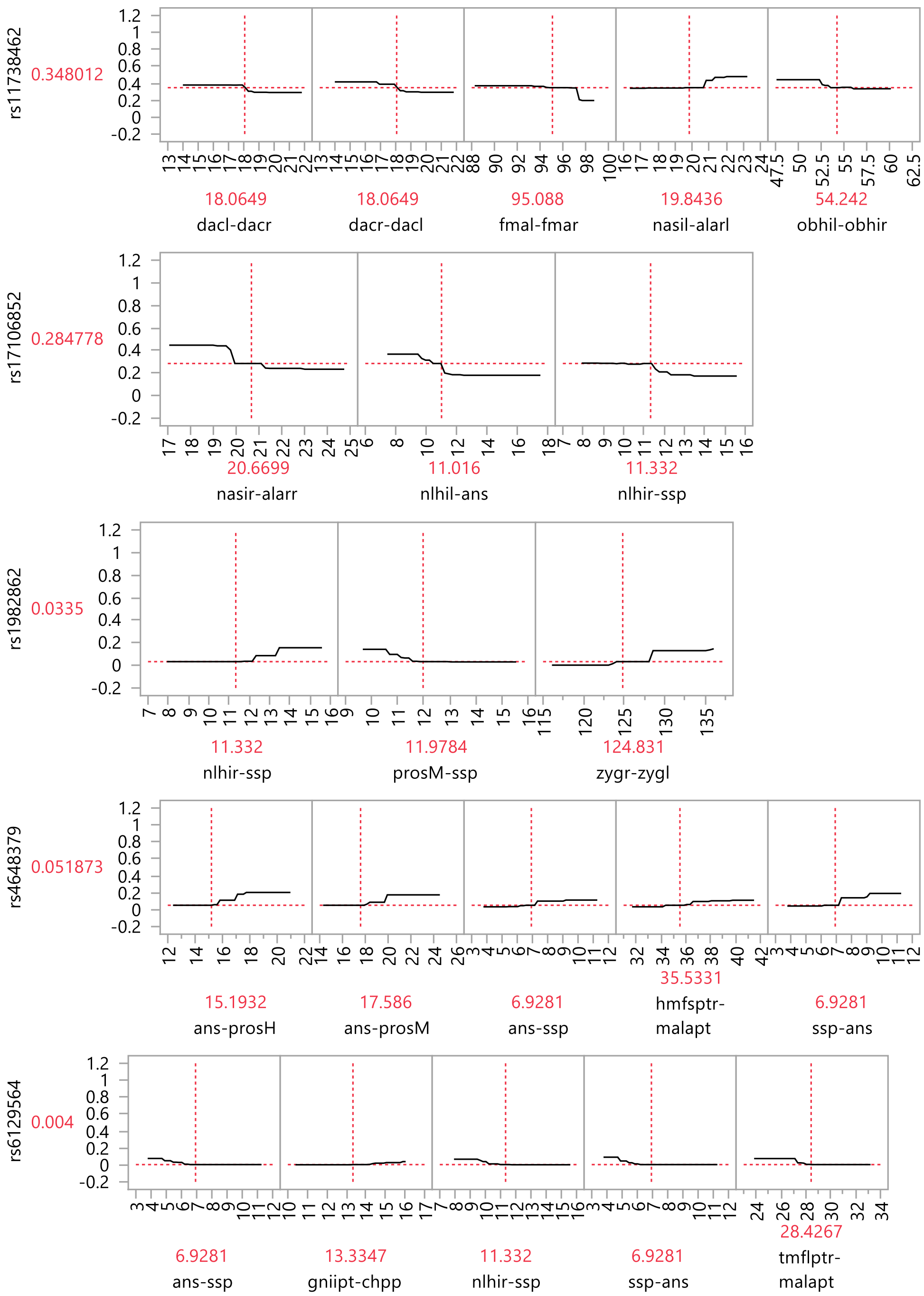

Table 10 Continued

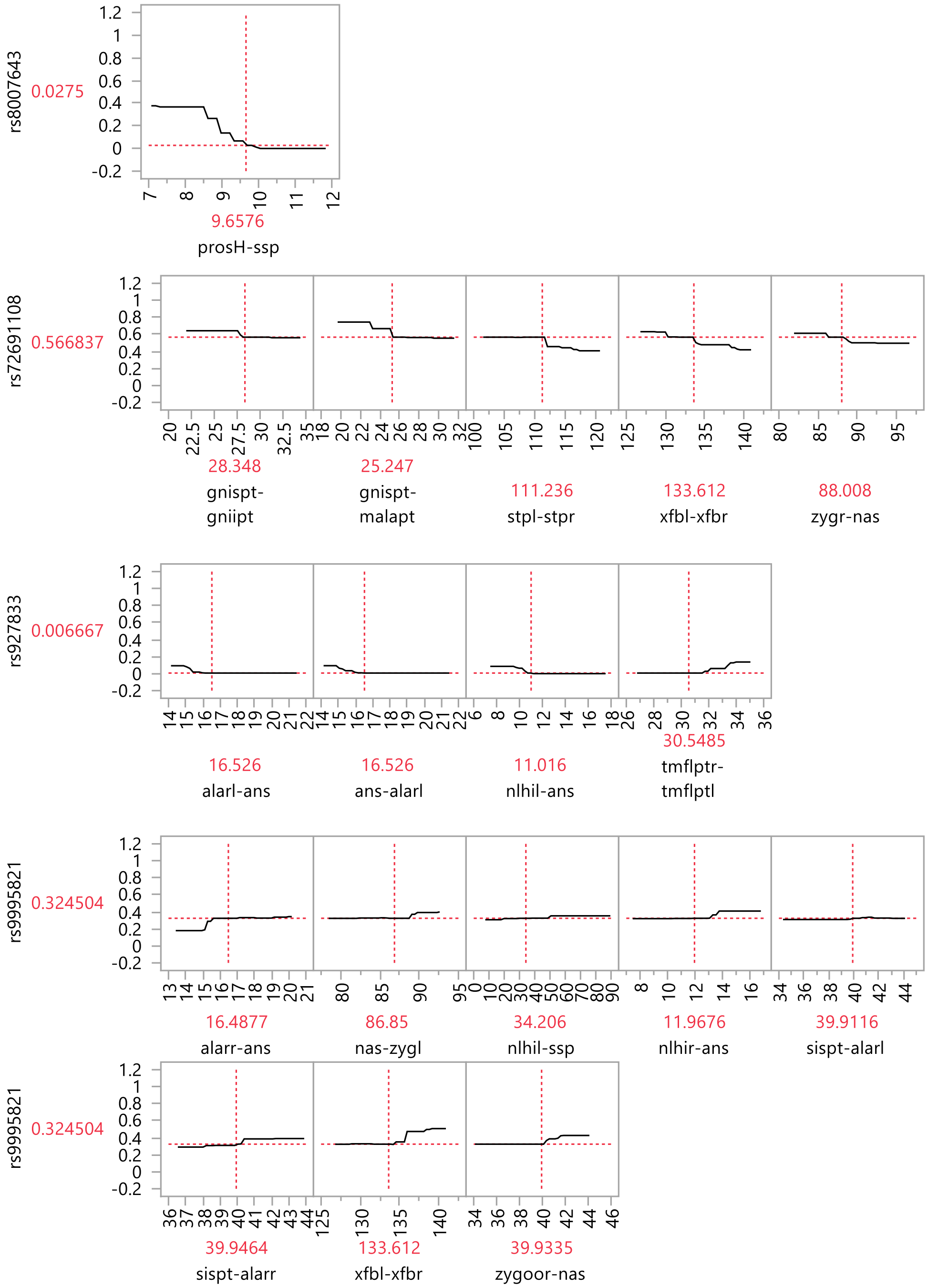

Principal Component Analysis applied to SNPs. PCA was used to shows the variation among the different single nucleotide polymorphisms. The Eigenvalues in Table 11 show the distribution of variation according to the different principal components. The target percent variation for the combined Eigenvalues was chose according to Jolliffe (Jolliffe 2011) and is around 70% -. In order to cover this range, five principal components were taken into consideration. The threshold is highlighted in pink in Table 11, where the cumulative percentage of the first five principal components is 78.137 %. In this case, only PC 1 and 2 were represented in a 2D graph as shown in Figure 18. The distribution of the samples within PC1 and PC2 shows the following patterns, a cluster of around 0% variability of PC1 in samples 1, 2, 4, 6, 9, 10, 11, 13, 16, and 17. There are 4 outliers found on both extremes; samples 3 and 15 are diverting negatively toward negative variation, but samples 12 and 5 are diverging toward positive variations. Sample 14 shows the largest deviation from the cluster for an Eigenvalue of around 4, which makes it an outlier to the group.

Table 11. Eigenvalues of the principal component analysis performed on the 20 targeted SNPs.

Number	Eigenvalue	Percent	Cum Percent
1	2.5857	23.506	23.506
2	2.0022	18.202	41.708
3	1.5836	14.396	56.104
4	1.2260	11.146	67.250
5	1.1976	10.887	78.137
6	0.7442	6.765	84.903
7	0.4891	4.447	89.349
8	0.4113	3.739	93.088
9	0.3565	3.241	96.329
10	0.2130	1.936	98.265
11	0.1908	1.735	100.000

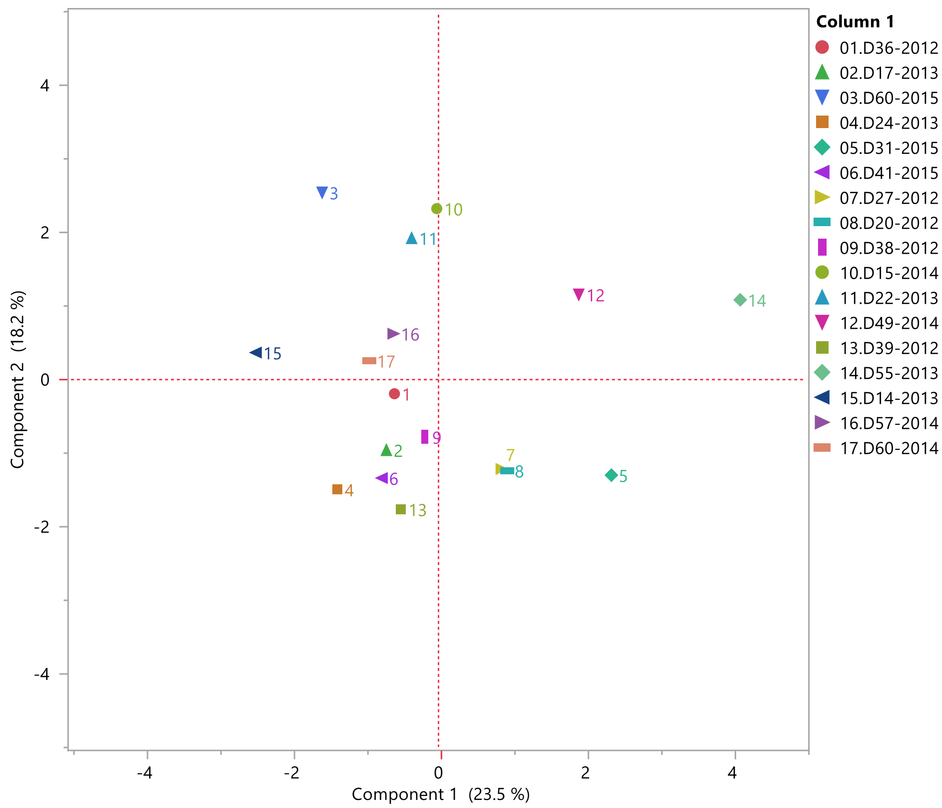

Figure 18. Principal component analysis of the targeted SNPs.

Principal Component Analysis to all Inter-Landmark Distances. The Eigenvalues of this PCA are presented in Table 12. The first six PCA represent 75.77% of the variation. The distribution of the samples does not have any major outliers as shown in Figure 19. Samples 4 and 13 show the extremities of this cluster in PC1, and samples 7 and 10 are the margins in PC2.

Table 12. The eigenvalues of the principal component analysis of all the inter-landmark distances.

Number	Eigenvalue	Percent	Cum Percent
1	19.8063	24.758	24.758
2	15.4547	19.318	44.076
3	8.7692	10.962	55.038
4	6.4710	8.089	63.127
5	5.1868	6.484	69.610
6	4.9306	6.163	75.773
7	3.4053	4.257	80.030
8	3.3445	4.181	84.211
9	3.0668	3.833	88.044
10	2.3329	2.916	90.960

Table 12 Continued

Number	Eigenvalue	Percent	Cum Percent
11	1.7889	2.236	93.196
12	1.6109	2.014	95.210
13	1.2883	1.610	96.820
14	1.1851	1.481	98.302
15	0.7818	0.977	99.279
16	0.5769	0.721	100.000

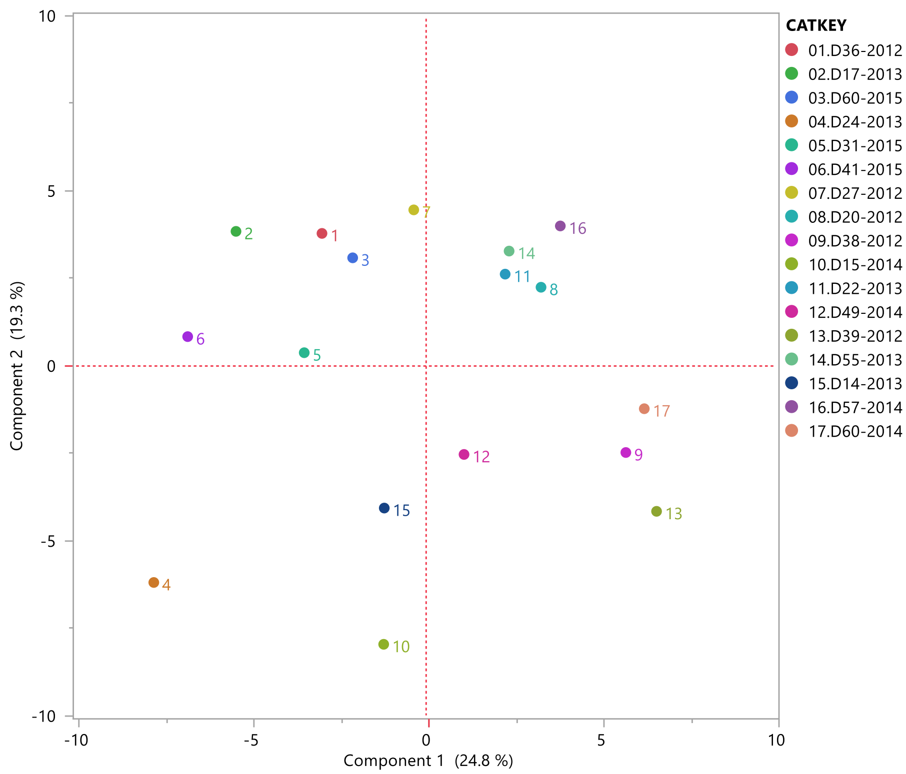

Figure 19. Principal component analysis, showing PCs 1 and 2, for all the inter-landmark distances.

Principal Component Analysis to significant ILDs. The variation of the data is presented in 16 dimensions, and an adequate representation can be achieved by the first five principal components with 76.825% cumulative percentage as shown in Table 13. The principal component 1 and 2 of the inter-landmark distances of interest were plotted, as shown in Figure 20. There is a cluster of samples 1, 2, 3, 5, 6, 7, 11, 14, and 15. The rest are dispersed outside the ellipse. The outliers in three directions are 4, 16, and 17. The rest are dispersed between the rest of the samples.

Table 13. Eigenvalues of the principal component analysis of the significant ILDs.

Number	Eigenvalue	Percent	Cum Percent
1	9.7593	29.574	29.574
2	6.7361	20.412	49.986
3	4.0113	12.156	62.142
4	2.5533	7.737	69.879
5	2.2923	6.946	76.825
6	1.9221	5.825	82.650
7	1.5263	4.625	87.275
8	1.1168	3.384	90.659
9	0.7976	2.417	93.076
10	0.6421	1.946	95.022
11	0.5675	1.720	96.741
12	0.4823	1.461	98.203
13	0.2951	0.894	99.097
14	0.1516	0.459	99.556
15	0.0869	0.263	99.819
16	0.0596	0.181	100.000

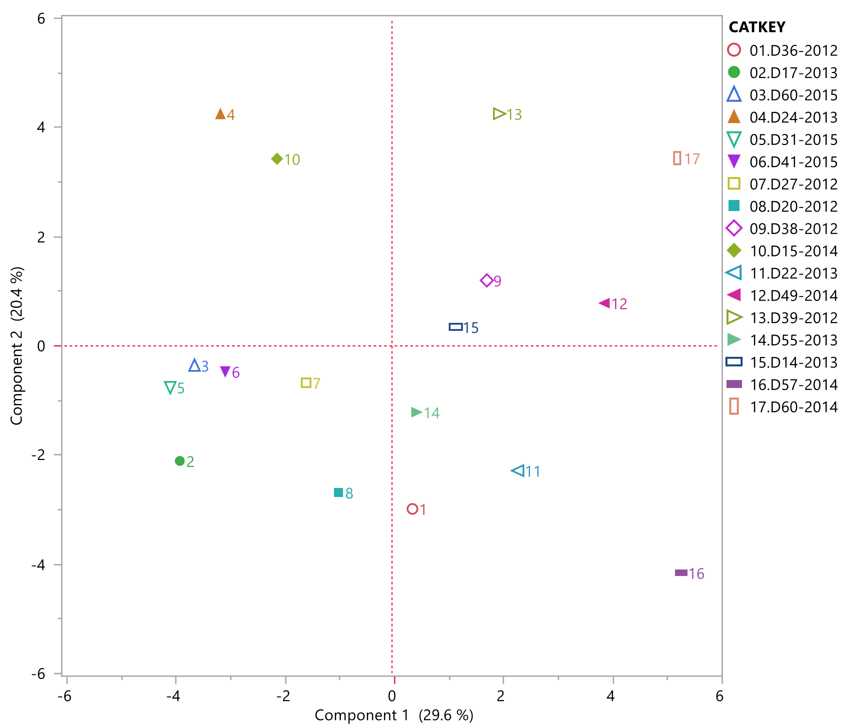

Figure 20. Principal component analysis of the samples using only the significant ILDs.

Procrustes analysis for all individuals with a non-random significance between SNPs and ILDs. This analysis was performed on all individuals. The sum of squares obtained was 0.95 with a symmetric correlation in a symmetric Procrustes analysis with no significance, giving a p-value of 0.759. The high value of the sum of squares suggests that the data points are highly dispersed from the mean as shown in Table 14. They do not show any correlation nor significance.

Table 14. The results of pair-wise Procrustes analysis between ILDs and SNPs.

	ILDs to SNPs Sum of squares	**ILDs to SNPs Correlation in a symmetric Procrustes rotation**	**ILDs to SNPs Significance**	**ILDs to SNPs Permutations**
All Individuals	0.952910462	0.217001241	0.759	999

V. DISCUSSION

Analysis of SNPs and craniometric markers separately

The different analyses performed on each variable group through principal components analysis helped to clarify the nature of the variation for the sampled individuals. The principal component analysis (PCA) performed in MorphoJ for the coordinates of the 99 landmarks showed both a strong agreement among the shapes of the skulls regardless of their size, overlapping of samples regardless of sex. This suggests that for the purposes of this experiment, sex was not a determining factor in examining bilateral correlations. However, the PCA performed on the semi-landmarks obtained for the frontal arc gave different shapes by sex, especially toward the superciliary arch and the supraorbital margin of the frontal bone where the glabella and Supraglabella landmarks are present (White et al. 2012). This morphology is consistent with macroscopic observations that drive cranial sex scoring approaches and reflects an area important to estimating the sex of the individual in discriminant functional analysis (Walker 2008). These findings might also be due to the older ages of the females used in this sample who ranged from 42- 58, as aging is believed to affect the robusticity of the skull (Urban et al. 2016), in turn affecting the prominence of the supraorbital margin. However, the small variation of the distance of rotations (0.03) in Figure 13 are an indication of the homogeneity of the individuals within the sample. This can be attributed to the absence of the influence of size on the craniofacial shape in individuals from the same group (Kimmerle et al. 2008).

At the same time, there was a distinct pattern with the results of the DNA sequencing. The bioinformatics analysis showed a distinct pattern between the presence and absence of SNPs. The 20 SNP targets chosen at the beginning of this research (culled from previous literature on soft tissue facial shapes, e.g., Adhikari et al. 2016b; Claes et al. 2018; Shaffer et al. 2016) showed significance in the whole genome wide association studies. However, 9 out of the 20 SNPs did not make any appearance in this study sample. This absence may indicate that portability of results from population-level studies - such as whole genome association studies - can be variable in their application on smaller sample sizes and at the level of the individual. I chose to include four different SNPs that were found to be of significance in Latin American populations (Adhikari et al. 2016b), with the expectation that they would not be significant in my European American sample. In an interesting outcome, however, the four Latin American SNPs (rs7559271, rs3827760, rs17640804, rs927833) were all absent in the samples with the exception of rs927833, as shown in Table 7. This means that while three out the four SNPs were not present, rs927833 was present in two individuals. One of those two individuals wrote in the ancestry section while filling out the donation paperwork that they were white with Lumbee (Native American) ancestry. The other individual had transitioned from male (at birth) to female, and it is unknown how estrogen hormone treatment can affect genetic marker expression and craniofacial measurements.

These findings can be explained by biodistances between populations and show how geography and population history can be a factor affecting the similarities between genetic markers found among populations (Relethford 2016).

Associations between SNPs and ILDs

The results obtained from the different tests to assess the association between the genetic markers and the craniofacial measurements showed similarities but also differences. The Spearman's rank-order correlation was a tool that helped decrease the pool for analysis by evaluating only the significant correlation between the categorial genetic input and the continuous craniometric data. I only interpreted correlations with a p-value lower than 0.01. The correlation between groups on the individual level gave interesting results where there were associations that were not accounted for in previous literature. These include the significant association between rs6129564 and Anterior nasal spine- Subspinale (ans-ssp), gnathion- chin protrusion (gniipt-chpp), most inferior nasal border R- Subspinale (nlhir-ssp), and TMF lingual point R- pogonion (tmflptr-malapt). In the literature, rs6129564 is correlated with cranial width (Shaffer et al. 2016). In my hypothesis, I assigned two different measurements to this category; stephanion L-stephanion R (stpl-stpr) and Maximum frontal point L- Maximum frontal point R (xfbl-xfbr). However, the results showed that this genetic marker does not affect any of the suggested measurements, but it is associated with different measurements from different functional groups related to the philtrum, chin protrusion, and nose tip. This different association can be an indication of underlying association related to the formation of the visceral portion of the cranium. The development of the human face occurs during week 4 to 7 of the prenatal development. During the 5^{th} and 6^{th} week, the frontonasal process, philtrum, and lateral and medial nasal process (nasal capsule) develop (Chiego 2018). The visceral branchial components including Meckel’s cartilage give rise to several skeletal elements such as the petrous portion of the temporal bone and the mandible

(Retzlaff 1987). This association in development occurs during a period in which environmental factors can affect the development of the embryo, especially during the 5th week. These observations of developmental timing of the cranium may explain the effects on the manifestation of genetic markers and rs6129564, for example. In addition, there are several factors that can affect the exhibition of certain markers which are not only environmental but also related to genetic inheritance that links back to population ancestries (European in this case) (Cole et al. 2017).

Another unique example in those correlations is the association between rs1716852, rs9278332, and most inferior nasal border L – anterior nasal spine (nlhil-ans). In this special case, the two SNPs and the one ILD are interchangeably correlated with each other. This shows that SNPs need not be expected to have only have significant correlations with an ILD, but that they can also have correlations between each other. The association between the SNPs, as genetic mutations, can be interpreted as genomic imprinting where the presence of a genetic marker can either silence or enhance the effect of another marker (Bajrami and Spiroski 2016).

The different significant associations between craniometric and genetic markers had also distinct results in the two-way hierarchical clustering. This test showed how the measurements that are morphologically next to each other are clustered next to each other, such as gnispt-malapt (Infradentale-pogonion) and gnispt-gniipt (Infradentale-gnathion). This is an interesting cluster where those landmarks lay on the midline of the face (Langley et al. 2016). But, there are several variables that do not have this association. This variation in clusters can be related to the variability of certain measurements between individuals of this sample.

Another cluster between two neighbors rs1982862 and alarl-ans (nasal ala breadth L side- Anterior nasal spine) is also correlated according to functional group. Both of these variables are related to the same morphological group Nasal Ala length (L &R). The correlation, however, between those two variables does not match with the insignificant results obtained from Spearman's correlation where the coefficient correlation is 0.45 and the p-value is 0.072 shown in Appendix IV. This closeness between those two variables indicates that there is an overlying relationship between them. Three different articles were able to find a soft tissue correlation between rs1982862 and Pronasale To Left Alare area (Claes et al. 2018; Paternoster et al. 2012b; Shaffer et al. 2016). This association corresponds with the random clustered created between the SNP and nasal ala breadth L side- Anterior nasal spine distance. However, due to the lack of any significant correlation in the non-parametric test, the association may be related to soft-tissue development that was observed in previous literature but not related directly to hard tissue.

The clustering of individuals in the two-way hierarchical analysis corresponds with the distribution of the samples in the PCA of the significant ILDs. Here, the least variable samples are clustered neighboring each other. These results confirm the notion of homogeneity of the individuals within the present sample.

These findings motivated another question: Do the linked inter-landmark distances provide a predictive model for the presence or absence of their associated SNPs? I was able to answer this question through the bootstrap analysis and the predictive profiler statistical assessments associated with the Random Forest Model building. Those tests provide a new approach that can help in the prediction of correlations, the pattern seen in the profile predictor of each ILD's value is distinct where the values have different plateaus according to the relative values of the associated SNPs. This output can be interpreted as an indicator of the categorial nature of the absence and presence of the associated SNPs. This behavior in prediction is very interesting, especially how some of those variables showed values that can be assessed in future research, such as the prediction profiles of rs9278332, rs80076432, and rs61295642. In other words, the prediction profiles have three distinct patterns, as shown in Figure 21. The first pattern in blue represents a homozygosity at this locus with the minor allele giving a higher value of prosthion- Subspinale distance. The second pattern in purple represent the heterozygosity of this locus (presence of the minor and major alleles). The third allele in green represents the homozygosity at this locus of the major allele, where the value in the prediction profile of the rs8007643 is almost 0. Those distinctive patterns are a first statistical representation of a correlation between genetic markers and craniometrics that can be applied in future studies. In the future, after increasing the sample size for this project, the forensic anthropologist can take the measurements from the skull and learn if this specific SNP is present or not.

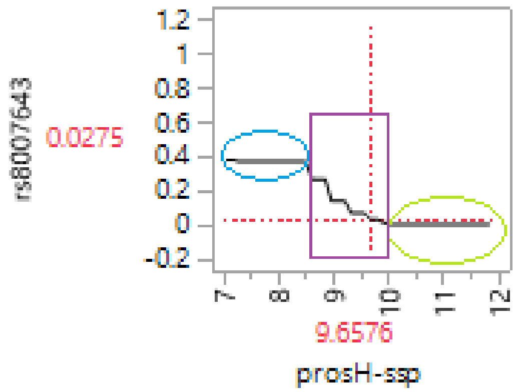

Figure 21. The prediction profile of rs8007643 where the different stages are highlighted. The blue circle corresponds to the presence of the SNP, the green circle corresponds to the absence of the SNP, and the purple rectangle corresponds to the heterozygosity at the alleles at this position.

Unfortunately, the small sample size prevented a validation of this analysis by choosing holdout samples for testing and training Bootstrap Forest models. These predictive measurements cannot be directly used when applying this approach on a larger sample to increase accuracy and decrease generalized error (Shao 1996).

After applying correlations on a one to one basis, I applied the principal component analysis (PCA) and the pairwise Procrustes test to show any group correlations. PCA results have a slightly different pattern in sample distribution between ILDs and SNPs, but the overall consistency is present in both groups of variables. This is consistent with the criteria set forth at the beginning of this analysis to evaluate individuals with the same ancestry, within a defined age range, and absence of facial fractures. The few outliers found in each set of variables is likely a simple representation of human variability within a population (Little et al. 2006), and can be an indication of an individual's unique features that distinguish them from others. But, the correlation on the non-randomness analysis in a symmetric Procrustes test showed no visible correlation on group level because the sum of squares is 0.95 and the correlation is 0.22. If I had only performed a

Procrustes analysis, I would have missed the individual correlations obtained with the Spearman’s test.

All those different tests showed different results that make answering this thesis’ research question a challenge: it cannot be reduced to a simple yes/no answer, in terms of associations between SNPs and ILDs. Yes, there is a correlation between the SNP markers and craniofacial measurements. However, the associations are not linear correlations as suggested in my hypothesis but rather hierarchical and multiple. This may be due to the different measurements used on the skull then the ones on the face with soft tissue as reported previously in the literature (Shaffer et al. 2016), but they correlate to other measurements from other functional groups as shown in the Results chapter. There are some SNPs that did not show any type of correlation in my research, but since they showed correlations in previous soft tissue research, this implies that while those SNPs are related to the soft tissue of the face, they are not related to the craniofacial hard tissue (or they can be influenced by environmental factors).

This raises an important point, which is the validity of conclusions from previous literature on predictive facial genetics to the application of forensic anthropology work. Since there were similarities and differences between the proposed (expected) correlation and the actual correlation, this suggests that genetic-soft tissues approaches (Paternoster et al. 2012b) can be used to help set a starting point for relationship between genetic markers and craniofacial measurements, however they are not enough to show the different variability and associations each marker expresses on the skull. The fact that the correlated SNPs and ILDs had mostly different functional groups than what was expected shows a hierarchical correlation between several morphologies of the face. This multibranch correlation affects the morphological structure of the face in more than just a unilateral relationship between two variables. Some of the most recent literature tackled this issue confirming the necessity of observing the association in a multidimensional approach (Claes et al. 2018; White et al. 2019). This difference in morphological groups between SNPs and ILDs raises an obvious concern and future direction: the necessity for more research in forensic anthropology to tackle more validation studies before using any facial models developed by commercial entities since those prediction does not apply directly to the skull that is available in a forensic case.

Application in the field

Three fields of forensic identity (DNA, anthropology, and art) present a challenge to identify the proper methodology to answer the major research question of concern here. Because this is the first time this subject has been approached using genetic and craniometric data from the same individuals to asses previously established genetic markers within one population, this study's methodology was compiled from different methods from the three fields. I created a cost-effective approach while preserving the quality of the work. I decided to collect my data through a geometric morphometrics platform due to the availability and frequent use in biological anthropology, thereby, linking my approach to conventions within the field while also inspiring similar experiments in the future (Algee-Hewitt and Wheat 2016; Spradley and Jantz 2016). The sequencing of the DNA through next generation technologies with multiplexing was a way to reduce cost and target specific regions of interest in the genome. I was able to use a laboratory in close proximity to my location and work on the process over couple of months. For the articulation of the mandible for reconstructing the face, I applied the same methods used by leading forensic artists in the United States (Taylor 2001), thereby, linking both fields in practice.

The implications of this study can affect each field separately in the long and short terms. The forensic genetic field is currently focusing on either identification using short tandem repeats (STR) markers, depending on different populations and countries (El Andari et al. 2013), or on the new emerging techniques of three dimensional facial reconstruction from DNA (Claes et al. 2014). This thesis project plays a role in recognizing the importance of those facial reconstruction approaches through DNA, but it also acknowledged the importance looking critically at these results, asking what factors can affect the analysis and change our readings of the conclusions drawn by that literature. On the other hand, for forensic facial reconstruction techniques, this study contributes to the better understanding of the difference and association between soft and hard tissue. This can be helpful in decision making for placing soft tissue markers on to a dry skull in sculpture-based facial approximation: it offers the promise of a more accurate approach than that of prevailing techniques, which obtain such measurements through the soft tissue on corpses (Wilkinson 2004b). Additionally, in the future researchers should include not only the emerging techniques in forensic approximation through identification of tissue depth by CT scans (Sakuma et al. 2010) but also incorporate life history factors in order to for assessing the reliability of genetics and environment in shaping the face of an individual.

Finally, this project will be mostly beneficial to forensic anthropology as a growing, multidisciplinary field, with practitioners and researchers engaging equally in skeletal and DNA driven work. Several studies have investigated the relationships between populations over space and time and the microevolutionary processes that effect differences. These authors use genetic and craniometric data from different individuals due to the lack of availability (Hughes et al. 2017; Relethford 2016; Roseman 2004; Spradley 2006). However, this study shows that it is important to also acknowledge how using the data from same individuals can provide more insight to the overall complexity of geneflow and biodistance. As interpreted previously, some of the SNPs found usually in Latin American populations was observed in individuals with a Native American ancestral history. This population history effect on genetic manifestation can now also be connected to the measurement of the face. These results caution researchers against applying soft-tissue driven techniques for assessing the skull simply because they have precedent..

In this pilot study, I was able to obtain preliminary results that can pave the way for more inter-disciplinary approaches that actively connect the three fields of Bioanthropology, Forensic Science and Art. The outcome of this study's integration of the three fields' methods has shown the importance of pursuing larger studies focused on the association between the skull and the genetic markers. While this project is the first test of the skull/soft-tissue and DNA association, its results and my interpretation demonstrate how new, more holistic information can change the course of interpreting prior findings. I argue; therefore, it is no longer acceptable to discuss all the different theories of variation in facial morphology without taking into consideration other factors that can shape our face. This best-practice directive is especially important for forensic anthropology as the face is a major tool used in determining the biological profile of an individual and ultimately providing an identification of the deceased and for the families.

The results obtained from this project can be seen as the missing link: those underlying skeletal data which currently geneticists are not taking into consideration when creating the three-dimensional models of the face from certain genetic markers. Once having established more thoroughly an association between genes, and soft and hard tissues, researchers can create a standard practice procedure: when a skull is found, the measurements are taken by a forensic anthropologist, then applied against prediction profiles to determine the presence or absence of certain SNPs, that can be linked back to the on-going research to create a face from those SNPs. This new pipeline practice will not just be time effective, but it will also be cost-effective. However, to reach this point, more SNPs need to be looked at for their associations with the inter-landmark distances.

VI. CONCLUSION

This pilot study represents the first attempt at integrating the different fields of forensic science and connecting them through an inter-disciplinary approach to the study of genetics and craniometrics for facial approximation purposes. While small in size, analysis of this sample found strong evidence for correlations between individual traits. These results suggest that work can be used to reliably support future forensic anthropology research. They also challenge the easy assumption that genetic associations are sufficiently similar between skull and tissue to warrant the use of the same SNPs in their analysis. I argue, therefore, that more research studies should access each SNP individually because some of the attributed ones, as seen in this study, failed to be expressed on the hard tissue and it may be only related to the soft tissue.

In the future, it will be of interest to increase sample size and add additional SNP markers previously claimed to be informative of face shape in the literature, and to observe the patterns of correlation. The amount of information gathered for the "population" in this way and the possibility of even linking genetic markers to craniometrics on an individual level can help in future studies that seek to understand genetic heritability, environmental effects, and plasticity of the skull. Further, the discrepancy observed between the different population markers can be of help in developing new techniques in forensic facial approximation. When large numbers of unidentified individuals must undergo a Forensic Anthropology laboratory analysis, in the cases of mass disasters and mass graves, time and cost are key considerations for identifying those remains. It is hoped that, with more results available, the marriage of forensic anthropology techniques with the identification of genetic markers relevant to the cranium can lead to drawing a face on each skull to facilitate their identification.

APPENDIX SECTION

Appendix I

Sample_ID	Sample Name	I7_Index_ID	index	I5_Index_ID	index2
1	D20_2012	Full_RP_BC_5	CATCACGT	Dual_P5_BC_1	GACTGACT
2	D15_2014	Full_RP_BC_5	CATCACGT	Dual_P5_BC_2	GCATGCAT
3	D24_2013	Full_RP_BC_5	CATCACGT	Dual_P5_BC_3	ATCGATCG
4	D31_2015	Full_RP_BC_5	CATCACGT	Dual_P5_BC_4	CTAGCTAG
5	D41_2015	Full_RP_BC_5	CATCACGT	Dual_P5_BC_5	GTACGTAC
6	D27_2012	Full_RP_BC_5	CATCACGT	Dual_P5_BC_6	GTCAGTCA
7	D55_2013	Full_RP_BC_5	CATCACGT	Dual_P5_BC_7	ACGTACGT
8	D57_2014	Full_RP_BC_5	CATCACGT	Dual_P5_BC_8	ATGCATGC
9	D14_2013	Full_RP_BC_5	CATCACGT	Dual_P5_BC_9	CTGACTGA
10	D60_2014	Full_RP_BC_5	CATCACGT	Dual_P5_BC_10	AGTCAGCT
11	D38_2012	Full_RP_BC_5	CATCACGT	Dual_P5_BC_11	CAGTCGAC
12	D60_2015	Full_RP_BC_5	CATCACGT	Dual_P5_BC_12	ACGTAGCA
13	D17_2013	Full_RP_BC_5	CATCACGT	Dual_P5_BC_13	GATCGATA
14	D22_2013	Full_RP_BC_5	CATCACGT	Dual_P5_BC_15	CATGTCAG
15	D36_2012	Full_RP_BC_5	CATCACGT	Dual_P5_BC_17	ACTGAGTC
16	D49_2014	Full_RP_BC_5	CATCACGT	Dual_P5_BC_20	TGCATGAG
17	D39_2012	Full_RP_BC_6	TAGTATCG	Dual_P5_BC_1	GACTGACT

SNP	Amplification size	(+) barcode	(+) adapter	Chr	Start	End	Difference	SNP Location	Minor Allele	SNP location2
rs72691108	98	165	234	chr1	119219500	119219597	97	119219552	A=0.1699/851	53
rs4648379	109	176	245	chr1	3344899	3345007	108	3344952	T=0.3700/1853	54
rs12786942	100	167	236	chr11	101523980	101524079	99	101524034	T=0.0669/335	55
rs10862567	100	167	236	chr12	83028523	83028622	99	83028573	T=0.2568/1286	51
rs8007643	100	167	236	chr14	20897588	20897687	99	20897642	T=0.1016/509	55
rs17106852	107	174	243	chr14	37569208	37569314	106	37569263	G=0.0619/310	56
rs7559271	97	164	233	chr2	222203519	222203615	96	222203567	A=0.4659/2333	49
rs3827760	100	167	236	chr2	108897102	108897201	99	108897145	G=0.2356/1180	44
rs6740960	110	177	246	chr2	41954492	41954601	109	41954539	A=0.3177/1591	48
rs6129564	100	167	236	chr20	40275518	40275617	99	40275563	A=0.1673/838	46
rs927833	110	177	246	chr20	22060892	22061001	109	22060939	T=0.2204/1104	48
rs17447439	109	176	245	chr3	189831570	189831678	108	189831634	G=0.0531/266	65
rs1982862	100	167	236	chr3	55030663	55030762	99	55030713	A=0.1512/757	51
rs2977562	100	167	236	chr3	128387370	128387469	99	128387424	G=0.4792/2400	55
rs9995821	108	175	244	chr4	153907156	153907263	107	153907214	C=0.2522/1263	59
rs11738462	99	166	235	chr5	61717903	61718001	98	61717949	A=0.2408/1206	47
rs6555969	97	164	233	chr5	171701409	171701505	96	171701460	T=0.2716/1360	52
rs5880172	99	166	235	chr6	133294463	133294561	98	133294508	C/T insertion	46
rs17640804	100	167	236	chr7	42091738	42091837	99	42091791	C=0.2113/1058	54
rs10238953	105	172	241	chr7	96495615	96495719	104	96495663	G=0.1160/581	49

SNP	Forward + Adapter	Reverse + Adapter
rs72691108	GGAGCTGTCGTTCACTCTCTGGTTGAGGTGCAATGACA	gtgtgctcttccgatctCTAGCGGCTTGGTTGGTACT
rs4648379	GGAGCTGTCGTTCACTCagtgaaatctctgtgtagctcttgt	gtgtgctcttccgatctacatgatcctcctgtgtgca
rs12786942	GGAGCTGTCGTTCACTCTGGCTGTTAATTTAGGAGGCA	gtgtgctcttccgatctTGGGATGTAGGCAGCTGAGT
rs10862567	GGAGCTGTCGTTCACTCtgtgttctatgaatttgggcaagt	gtgtgctcttccgatctcaggcagagcatgtgattttt
rs8007643	GGAGCTGTCGTTCACTCATGGTTTCCAAGGTGCACCA	gtgtgctcttccgatctTCTCCGGCGAATTGAGAAGT
rs17106852	GGAGCTGTCGTTCACTCTCAAAGATGCAAATATTTGACAAAACA	gtgtgctcttccgatctGGTTTTCTCTAGTAATACAGCTAATGG
rs7559271	GGAGCTGTCGTTCACTCTGGAACTCCTAGATCCGAGGT	gtgtgctcttccgatctGCAGAAATGACAACCAAGCCC
rs3827760	GGAGCTGTCGTTCACTCTTGCCTCGAGAAGACTAGCC	gtgtgctcttccgatctCTTCAGGCCGAAGCTCTCG
rs6740960	GGAGCTGTCGTTCACTCTCGATCCTTGTGCCCTTTCT	gtgtgctcttccgatctCTGAAACGAAGCACAATTAAATTAGA
rs6129564	GGAGCTGTCGTTCACTCAGGGCAGAAAGGCATGGAA	gtgtgctcttccgatctCCCCTGTAATGGATGGCCC
rs927833	GGAGCTGTCGTTCACTCTCTTTATGGGTGCTCTTCAGG	gtgtgctcttccgatctGCAGCCACATATAATGCATAATAGT
rs17447439	GGAGCTGTCGTTCACTCggctactagatggtggagttca	gtgtgctcttccgatctAGGAAGGGTAGGAGCTCAAA
rs1982862	GGAGCTGTCGTTCACTCTGAATCTCAGTTCAATGAAGCATT	gtgtgctcttccgatctCCTTGAGTCTGGAAATAGGGTACT
rs2977562	GGAGCTGTCGTTCACTCCACCTTCTTCAAAGTTCAGAAATGA	gtgtgctcttccgatctTCCCAGATCTTTCTTGGCATC
rs9995821	GGAGCTGTCGTTCACTCCCTCTTCCTGCTTATTAGTTATTTTCA	gtgtgctcttccgatctAGGGTATCTGACAATGTAACTCATG
rs11738462	GGAGCTGTCGTTCACTCGTGCCACCTTCCACCTGCTT	gtgtgctcttccgatctTGACAGGAAGAAGGAGCCCA
rs6555969	GGAGCTGTCGTTCACTCTTTCATTACAAAGCCCGGGC	gtgtgctcttccgatctATCCCAACGAGAATCCGTGT
rs5880172	GGAGCTGTCGTTCACTCgtggtcgtcccgcctcag	gtgtgctcttccgatctgaaaTGTATTTCGATGTTGAATGACA
rs17640804	GGAGCTGTCGTTCACTCTGTGGAGGGAAGGAAAACAG	gtgtgctcttccgatctCAGCAATATCCGCTCGCTCG
rs10238953	GGAGCTGTCGTTCACTCTCAGAAGCACTTTTGTTTGGAAGA	gtgtgctcttccgatctTGTCAGGAAATGATCAGTATTGGC

SNP	Amplicon-Read 1	Amplicon-Read 2
rs72691108	TCTGGTTGAGGTGCAATGACAAATTTCTGGTGTGTTCTTTGTAGAGGAACTCGATTGAGGACCAGAGGTCCAGTCACAAGTACCAACCAAGCCGCTAG	CTAGCGGCTTGGTTGGTACTTGTGACTGGACCTCTGGTCCTCAATCGAGTTCCTCTACAAAGAACACACCAGAAATTTGTCATTGCACCTCAACCAGA
rs4648379	AGTGAAATCTCTGTGTAGCTCTTGTTTTCTGTGGGGCCCTTTGCAACCTCCCTCATGCATGAGCAATTCAGGGGTTTGAGGGGTGTATATGCACACAGGAGGATCATG	CATGATCCTCCTGTGTGCATATACACCCCTCAAACCCCTGAATTGCTCATGCATGAGGGAGGTTGCAAAGGGCCCCACAGAAAACAAGAGCTACACAGAGATTTCACT
rs12786942	TGGCTGTTAATTTAGGAGGCATTCCTCTGAGAGGAATAGCCATTGTCTTTGTCAAAGTCAACACAGGATTACCCATACATACTCAGCTGCCTACATCCCA	TGGGATGTAGGCAGCTGAGTATGTATGGGTAATCCTGTGTTGACTTTGACAAAGACAATGGCTATTCCTCTCAGAGGAATGCCTCCTAAATTAACAGCCA
rs10862567	TGTGTTCTATGAATTTGGGCAAGTGCTTAATGGCACGTATCCACCATTACTGTATCAGATGAAATAGTCGCATTGCTCTAAAAATCACATGCTCTGCCTG	CAGGCAGAGCATGTGATTTTTAGAGCAATGCGACTATTTCATCTGATACAGTAATGGTGGATACGTGCCATTAAGCACTTGCCCAAATTCATAGAACACA
rs8007643	ATGGTTTCCAAGGTGCACCAGTAGATGTTACCAAAATGGCACCACCAGCCAGAACCCACATACATTCACCAGGTCAGTGCACTTCTCAATTCGCCGGAGA	TCTCCGGCGAATTGAGAAGTGCACTGACCTGGTGAATGTATGTGGGTTCTGGCTGGTGGTGCCATTTTGGTAACATCTACTGGTGCACCTTGGAAACCAT
rs17106852	TCAAAGATGCAAATATTTGACAAAACATTAGAATAATAAAACACTGAATTTCTTTATTGATCATGAGGAATATTACTTAACCATTAGCTGTATTACTAGAGAAAACC	GGTTTTCTCTAGTAATACAGCTAATGGTTAAGTAATATTCCTCATGATCAATAAAGAAATTCAGTGTTTTATTATTCTAATGTTTTGTCAAATATTTGCATCTTTGA
rs7559271	TGGAACTCCTAGATCCGAGGTTCTATTGCCTGAATTATGAGAGTTATTCTGCAGTTAGCATGAGGGCTTATAGTCAGGGCTTGGTTGTCATTTCTGC	GCAGAAATGACAACCAAGCCCTGACTATAAGCCCTCATGCTAACTGCAGAATAACTCTCATAATTCAGGCAATAGAACCTCGGATCTAGGAGTTCCA
rs3827760	TTGCCTCGAGAAGACTAGCCGAATGCTCAGCTCCACGTACAACTCTGAGAAGGCTGTTGTGAAAACGTGGCGCCACCTCGCCGAGAGCTTCGGCCTGAAG	CTTCAGGCCGAAGCTCTCGGCGAGGTGGCGCCACGTTTTCACAACAGCCTTCTCAGAGTTGTACGTGGAGCTGAGCATTCGGCTAGTCTTCTCGAGGCAA
rs6740960	TCGATCCTTGTGCCCTTTCTTCTGTGAGCTGTAGCACATGGCCTGCTAATTATGAATTAATCCTCTAAAGAGCATGTTCATTATTCTAATTTAATTGTGCTTCGTTTCAG	CTGAAACGAAGCACAATTAAATTAGAATAATGAACATGCTCTTTAGAGGATTAATTCATAATTAGCAGGCCATGTGCTACAGCTCACAGAAGAAAGGGCACAAGGATCGA
rs6129564	AGGGCAGAAAGGCATGGAAAAAAATATTTATATACACATATGTGTGTGTTTGCATATGGGGTGTAGCCTATTATGTATATTGGGCCATCCATTACAGGGG	CCCCTGTAATGGATGGCCCAATATACATAATAGGCTACACCCCATATGCAAACACACACATATGTGTATATAAATATTTTTTTCCATGCCTTTCTGCCCT

rs927833	TCTTTATGGGTGCTCTTCAGGGGTATCTTTTCAGGGTTCTTGGTCAGCTGGTAAGTGTTACAATAATATCTCTTTTGAATATGTAACTATTATGCATTATATGTGGCTGC	GCAGCCACATATAATGCATAATAGTTACATATTCAAAAGAGATATTATTGTAACACTTACCAGCTGACCAAGAACCCTGAAAAGATACCCCTGAAGAGCACCCATAAAGA
rs17447439	GGCTACTAGATGGTGGAGTTCAGACTCTGATTTTCTGGCCAGGTGCTCATTTGATGATAGCAGCATGAAGCTCTTCCCATTCTGCACCGTTTGAGCTCCTACCCTTCCT	AGGAAGGGTAGGAGCTCAAACGGTGCAGAATGGGAAGAGCTTCATGCTGCTATCATCAAATGAGCACCTGGCCAGAAAATCAGAGTCTGAACTCCACCATCTAGTAGCC
rs1982862	TGAATCTCAGTTCAATGAAGCATTTTACTGGGGACAGGGTTTCCCTGATTCTTTTCCTCAGATGCTCAGAGGAAAAAGTACCCTATTTCCAGACTCAAGG	CCTTGAGTCTGGAAATAGGGTACTTTTTCCTCTGAGCATCTGAGGAAAAGAATCAGGGAAACCCTGTCCCCAGTAAAATGCTTCATTGAACTGAGATTCA
rs2977562	CACCTTCTTCAAAGTTCAGAAATGAAGGTGCTGTGTGGCAAGACACAAAGGTGCATGAGTCCAGGCTCGCAAAAGTCGTGATGCCAAGAAAGATCTGGGA	TCCCAGATCTTTCTTGGCATCACGACTTTTGCGAGCCTGGACTCATGCACCTTTGTGTCTTGCCACACAGCACCTTCATTTCTGAACTTTGAAGAAGGTG
rs9995821	CCTCTTCCTGCTTATTAGTTATTTTCATTCATGTGGCTACACTCATATCTGAGCCACATTGAATGAATTTGACTAATAAATTTCATGAGTTACATTGTCAGATACCCT	AGGGTATCTGACAATGTAACTCATGAAATTTATTAGTCAAATTCATTCAATGTGGCTCAGATATGAGTGTAGCCACATGAATGAAAATAACTAATAAGCAGGAAGAGG
rs11738462	GTGCCACCTTCCACCTGCTTCTCCTTCCAGTACTCTCCGGTGCAATGCTTCTTTGTGCCATCCCACTTATGACCAGAAATGGGCTCCTTCTTCCTGTCA	TGACAGGAAGAAGGAGCCCATTTCTGGTCATAAGTGGGATGGCACAAAGAAGCATTGCACCGGAGAGTACTGGAAGGAGAAGCAGGTGGAAGGTGGCAC
rs6555969	TTTCATTACAAAGCCCGGGCCCCATTCCAATCCTCTCATCTGTCCCTCTAATGGGCTCCGACAGATCACTCCACAGTACACGGATTCTCGTTGGGAT	ATCCCAACGAGAATCCGTGTACTGTGGAGTGATCTGTCGGAGCCCATTAGAGGGACAGATGAGAGGATTGGAATGGGGCCCGGGCTTTGTAATGAAA
rs5880172	GTGGTCGTCCCGCCTCAGCCTCCTTAGTAGCTGGTGTGTGTCACCACTCTGCTCAGTCTCTTGCCCTTTGTGTTGTCATTCAACATCGAAATACATTTC	GAAATGTATTTCGATGTTGAATGACAACACAAAGGGCAAGAGACTGAGCAGAGTGGTGACACACACCAGCTACTAAGGAGGCTGAGGCGGGACGACCAC
rs17640804	TGTGGAGGGAAGGAAAACAGTTTGGCCTCACTCACCTCCGGGAAGAATCGTTAAGGAACTGTTTAAATAATAAACTGAGCCGAGCGAGCGGATATTGCTG	CAGCAATATCCGCTCGCTCGGCTCAGTTTATTATTTAAACAGTTCCTTAACGATTCTTCCCGGAGGTGAGTGAGGCCAAACTGTTTTCCTTCCCTCCACA
rs10238953	TCAGAAGCACTTTTGTTTGGAAGAGGGGAAAGGAAGATCGCGGAAACTGGAAAACATCCATGAAATTAGCCCTAAATCATGGCCAATACTGATCATTTCCTGACA	TGTCAGGAAATGATCAGTATTGGCCATGATTTAGGGCTAATTTCATGGATGTTTTCCAGTTTCCGCGATCTTCCTTTCCCCTCTTCCAAACAAAAGTGCTTCTGA

Appendix II

The different SNPs and their correlated Inter-landmark distances:

Functional group	SNP	ILD	ILD visualization
Eye-Nasion- Eye	rs72691108	dacl-dacr zygool-zygoor nas-dacr nas-dacl obhsr-nas obhsr-obhsl obhsl-nas zygool-nas zygoor-nas	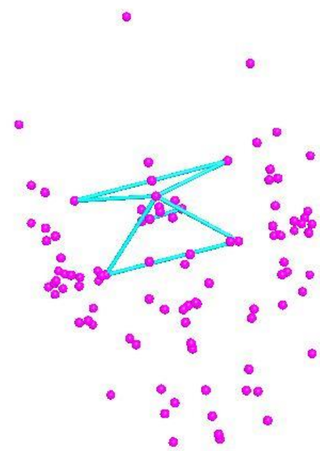
Eye-Nasion- Eye	rs7559271	nas-dacl dacr-nas dacr-dacl wnbl-wnbr nas-wnbl wnbr-nas	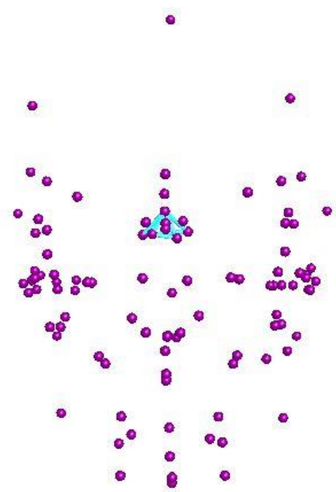

Eye-Nasion- Eye	rs17447439	dacl-dacr obhsl-obhsr fmal-fmar ectl-ectr wmhsr-wmhsl zygool-zygoor obhil-obhir	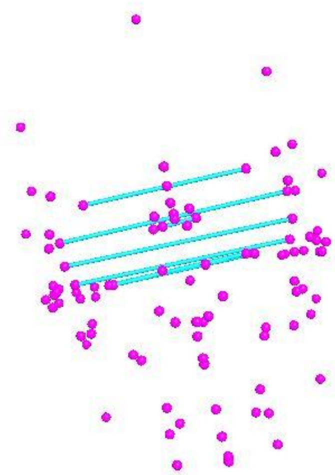
Eye-Nasion- Eye And Zygion-Nasion-Zygion	rs6555969	nas-dacl dacr-nas dacr-dacl zygr-nas nas-zygl zygr-zygl	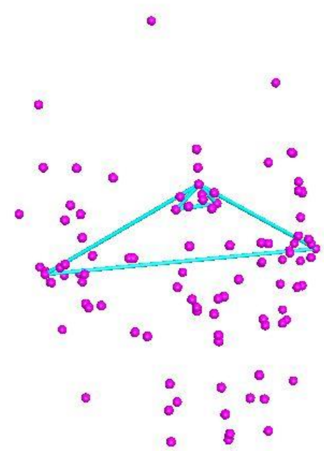
Zygion-Nasion-Zygion	rs12786942	zygr-nas nas-zygl zygr-zygl	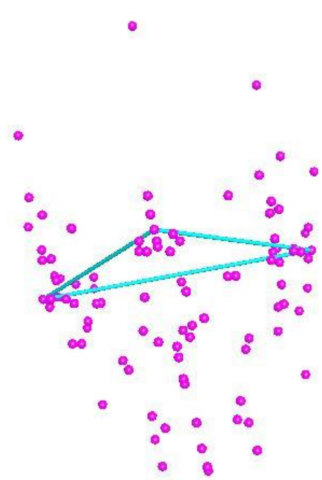

Nasal Ala length (L &R)	rs4648379	sispt-nasil sispt-alarl nasil-alarl alarr-ans alarl-nlhil sispt-nlhil ans-alarl alarr-nlhir sispt-ans nlhil-ans nasir-alarr sispt-alarr sispt-nasir sispt-nlhir nlhir-ans	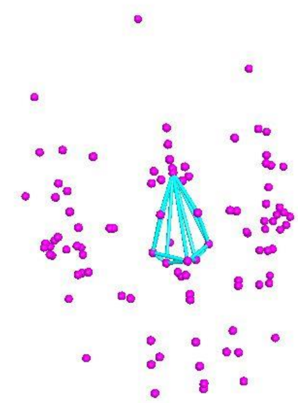
Nasal Ala length (L &R)	rs8007643	sispt-nasil sispt-alarl nasil-alarl alarr-ans alarl-nlhil sispt-nlhil ans-alarl sispt-ans nlhil-ans nasir-alarr sispt-alarr sispt-nasir sispt-nlhir nlhir-ans	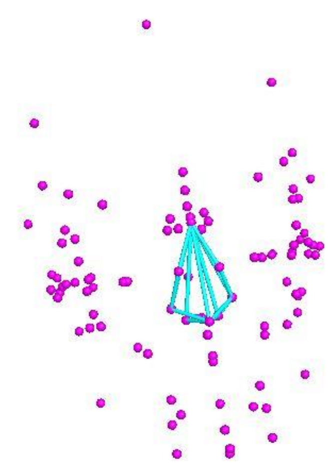
Nasal Ala length (L)	rs1982862	sispt-nasil sispt-alarl nasil-alarl alarl-nlhil sispt-nlhil ans-alarl sispt-ans nlhil-ans	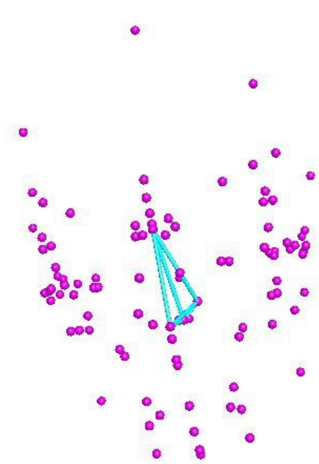

Nasal Ala length (L)	rs11738462	sispt-nasil sispt-alarl nasil-alarl alarl-nlhil sispt-nlhil ans-alarl sispt-ans nlhil-ans	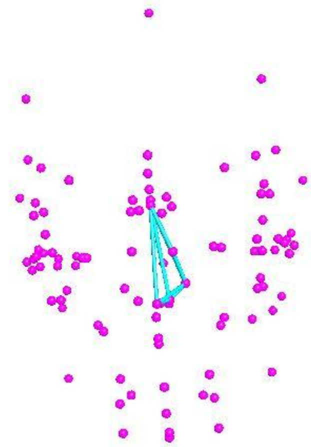
Cranial width	rs17106852	xfbl-xfbr stpl-stpr	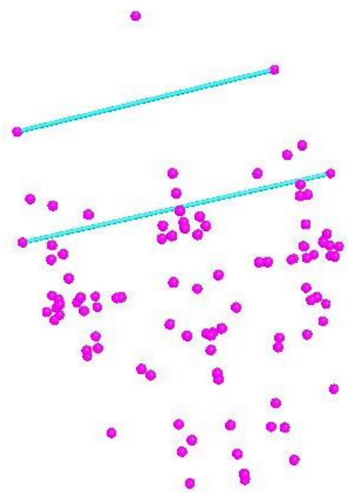
Cranial width	rs6129564	xfbl-xfbr stpl-stpr	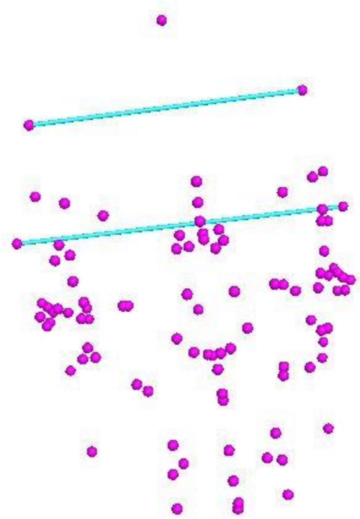

R endocation in space	rs10862567	nassr-nasir dacr-nassr dacr-nasir	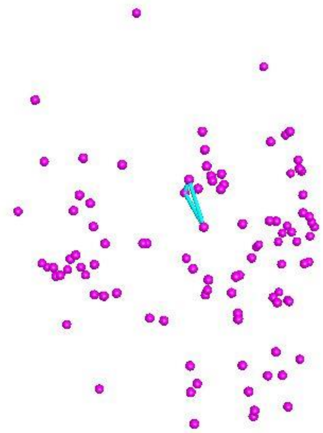
Chin protrusion	rs3827760	prosH-tmfbptr prosH-tmfbptl tmfbptl-tmfbptr prosM-tmfbptr prosM-tmfbptl chpp-hmfiptr hmfiptr-hmfiptl chpp-hmfiptl hmfsptr-chpp hmfsptl-hmfsptr chpp-hmfsptl gnispt-chpp chpp-malapt gnispt-malapt gnispt-gniipt gniipt-chpp tmfbptr-malapt hmfsptr-malapt malapt-hmfsptl tmfbptl-malapt hmfiptl-malapt hmfiptr-malapt tmflptr-tmflptl tmflptr-malapt tmflptl-malapt	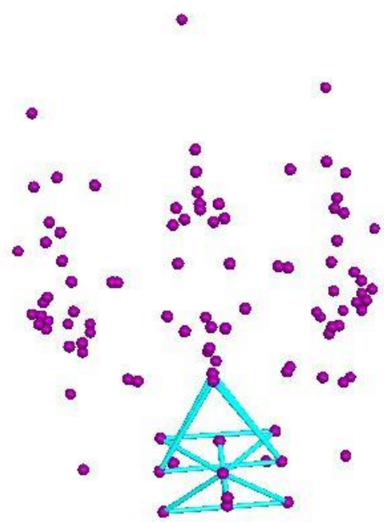

Chin protrusion	rs6740960	prosH-tmfbptr prosH-tmfbptl tmfbptl-tmfbptr prosM-tmfbptr prosM-tmfbptl chpp-hmfiptr hmfiptr-hmfiptl chpp-hmfiptl hmfsptr-chpp hmfsptl-hmfsptr chpp-hmfsptl gnispt-chpp chpp-malapt gnispt-malapt gnispt-gniipt gniipt-chpp tmfbptr-malapt hmfsptr-malapt malapt-hmfsptl tmfbptl-malapt hmfiptl-malapt hmfiptr-malapt tmflptr-tmflptl tmflptr-malapt tmflptl-malapt	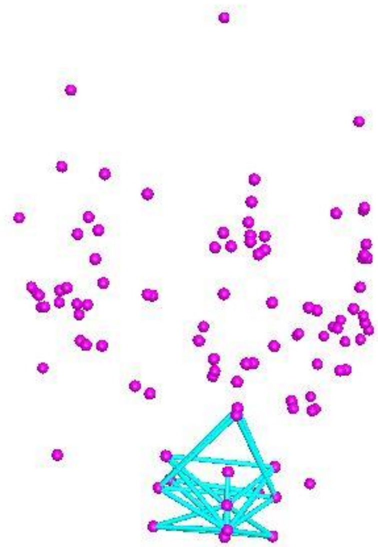
Chin protrusion	rs10238953	prosH-tmfbptr prosH-tmfbptl tmfbptl-tmfbptr prosM-tmfbptr prosM-tmfbptl chpp-hmfiptr hmfiptr-hmfiptl chpp-hmfiptl hmfsptr-chpp hmfsptl-hmfsptr chpp-hmfsptl gnispt-chpp chpp-malapt gnispt-malapt gnispt-gniipt	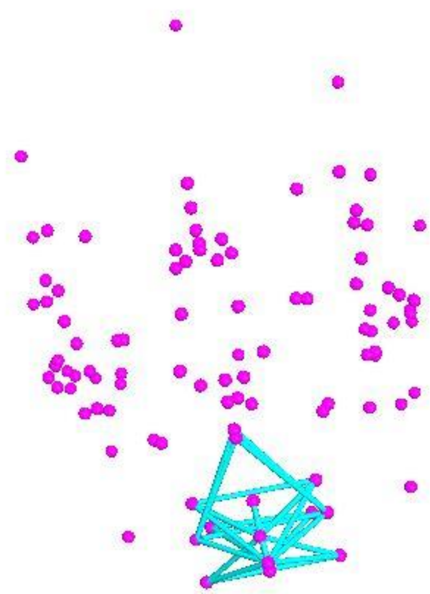

		gniipt-chpp tmfbptr-malapt hmfsptr-malapt malapt-hmfsptl tmfbptl-malapt hmfiptl-malapt hmfiptr-malapt tmflptr-tmflptl tmflptr-malapt tmflptl-malapt	
Nose wing breadth	rs927833	alarl-nlhil alarr-nlhir alarr-alarl nlhil-nlhir	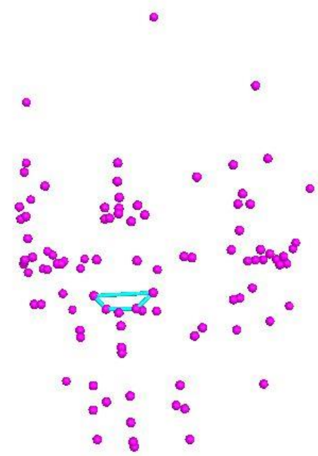
Nose wing breadth	rs17640804	alarl-nlhil alarr-nlhir alarr-alarl nlhil-nlhir	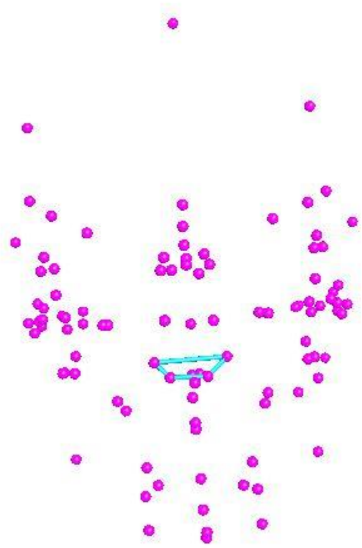

Philitrum width	rs2977562	alarr-ans nlhil-ans nlhir-ans ans-prosH ans-prosM nlhir-nlhil alarl-alarr alarl-ans prosH-ssp prosM-ssp ans-ssp	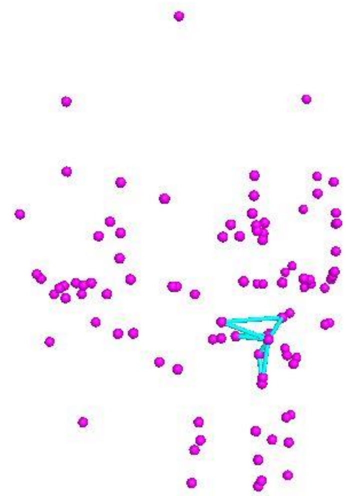
Nose tip	rs9995821	sispt-ans nlhil-ans nlhir-ans nlhir-nlhil nlhir-ssp ssp-ans nlhil-ssp	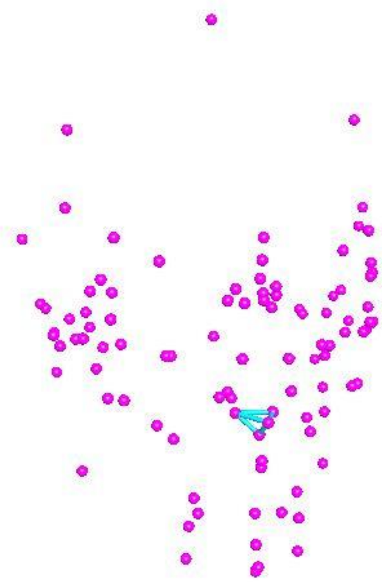

Forehead	rs5880172	Frontal arc	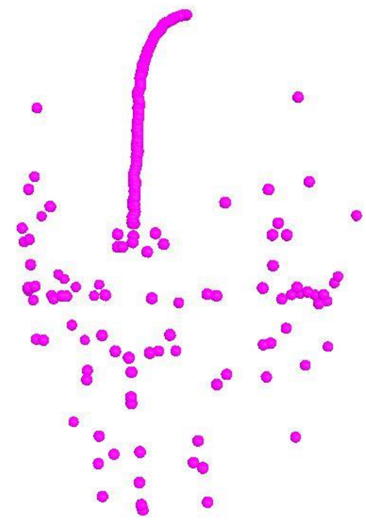

Appendix III

PCA plot/loading matrix/ Eigenvalue for SNPs

	Prin1	Prin2	Prin3	Prin4	Prin5	Prin6	Prin7	Prin8	Prin9	Prin10	Prin11
rs72691108	-0.21690	-0.43911	0.67257	0.02487	-0.31404	0.19376	0.03770	0.37501	-0.10263	0.08876	0.10262
rs4648379	0.18420	-0.26273	-0.81876	0.03815	-0.16661	0.27930	0.18499	0.12598	0.17217	0.00400	0.19928
rs12786942	-0.43871	0.54315	0.04477	-0.28829	0.38268	-0.07062	0.50584	0.10177	-0.08740	0.03287	0.03208
rs8007643	0.70380	0.29783	-0.26740	0.34952	0.12738	-0.13903	-0.01265	0.37169	-0.02798	0.12323	-0.18016
rs17106852	0.73375	-0.26944	0.17351	-0.42947	0.20418	0.01017	0.02455	-0.17195	0.04982	0.31208	0.05122
rs6129564	-0.18808	0.64701	0.13987	-0.38541	-0.46424	0.01873	-0.07435	0.08488	0.37720	0.05015	-0.06703
rs927833	0.75582	-0.02857	0.36646	-0.14372	0.27696	-0.25911	0.00253	0.13013	0.17333	-0.24677	0.14578
rs1982862	-0.36270	0.13179	0.13872	0.18838	0.72047	0.43575	-0.21651	0.06445	0.18690	0.03412	0.01620
rs2977562	0.49189	0.11145	0.41554	0.50953	-0.17978	0.32532	0.33608	-0.20252	0.11214	-0.04113	-0.08330
rs9995821	0.14263	0.83396	0.07799	0.36373	-0.13574	-0.06464	-0.14787	-0.07816	-0.13092	0.09350	0.26331
rs11738462	-0.52728	-0.37331	0.07331	0.48746	0.06932	-0.48666	0.09813	-0.03624	0.26161	0.12814	0.04676

PCA plot/loading matrix/ Eigenvalue for ILDs

	Prin1	Prin2	Prin3	Prin4	Prin5	Prin6	Prin7	Prin8	Prin9	Prin10	Prin11	Prin12	Prin13	Prin14	Prin15	Prin16
dacl-dacr	0.39313	0.67762	-0.40886	0.34953	0.10406	0.01538	-0.00764	-0.04826	-0.00588	-0.04512	0.04035	0.10582	0.20077	0.10602	-0.10131	-0.08234
obhsl-obhsr	0.60663	0.37035	-0.14403	0.16388	0.41786	-0.28814	-0.26388	-0.27818	-0.01548	0.09844	-0.11389	-0.07932	-0.08410	-0.04957	-0.03789	0.04925
fmal-fmar	0.39932	0.77295	-0.04324	0.05755	0.16194	-0.27756	0.05094	0.02015	-0.22690	0.18465	0.07765	-0.01238	-0.18054	0.02678	0.04365	0.06839
ectl-ectr	0.43104	-0.66477	0.05831	0.42532	-0.19957	0.00021	-0.16634	0.30358	0.00059	0.07717	-0.10033	-0.06140	-0.07170	0.03308	-0.03599	-0.03166
wmhsr-wmhsl	0.44322	0.66213	0.11350	0.04296	0.05902	-0.41559	0.26312	0.04431	-0.05151	0.00260	-0.14977	-0.04224	-0.16318	-0.02894	0.14889	0.16280
zygool-zygoor	0.13067	0.77550	0.10042	0.16160	0.06366	-0.39768	0.25451	0.07463	0.09484	0.17546	0.23324	-0.04498	0.00140	0.12706	-0.01946	-0.00667
obhil-obhir	-0.01069	0.73526	0.07103	0.33190	-0.20552	-0.13613	0.08781	0.18456	-0.06619	-0.02353	-0.14991	0.24810	-0.30905	0.18338	0.11580	-0.10012
nas-dacr	0.39626	0.33041	-0.13950	0.51509	0.21316	0.51640	0.17197	0.01090	0.08757	0.19196	-0.13805	0.10166	-0.05328	0.11085	0.09056	-0.09992
nas-dacl	0.51038	0.17902	-0.37666	0.53481	0.31761	0.23101	0.17380	0.03554	0.00705	0.21166	-0.10334	0.15745	-0.08340	0.05963	-0.02899	0.04673
obhsr-nas	0.48596	0.53360	-0.10637	-0.05381	0.24808	0.06869	-0.21735	-0.37880	0.29380	-0.00382	-0.20113	-0.06631	-0.16747	0.15893	-0.14633	-0.04482
obhsr-obhsl	0.60663	0.37035	-0.14403	0.16388	0.41786	-0.28814	-0.26388	-0.27818	-0.01548	0.09844	-0.11389	-0.07932	-0.08410	-0.04957	-0.03789	0.04925
obhsl-nas	0.41422	-0.04180	-0.16340	0.23151	0.52328	-0.51301	-0.31883	-0.08734	-0.11674	0.10136	-0.14890	-0.01468	0.00245	-0.13767	0.17398	0.06767
zygool-nas	0.30774	0.34427	0.07504	0.29175	0.45286	-0.55539	0.29785	-0.06259	-0.06738	0.13502	0.17778	-0.03750	-0.06426	-0.09324	-0.03977	0.14024
zygoor-nas	0.02132	0.49123	0.34715	0.20633	0.21286	-0.05735	0.28424	-0.14087	0.39158	0.31442	0.14928	-0.23989	0.22543	-0.10196	-0.06550	-0.21996
dacr-nas	0.39626	0.33041	-0.13950	0.51509	0.21316	0.51640	0.17197	0.01090	0.08757	0.19196	-0.13805	0.10166	-0.05328	0.11085	0.09056	-0.09992
dacr-dacl	0.39313	0.67762	-0.40886	0.34953	0.10406	0.01538	-0.00764	-0.04826	-0.00588	-0.04512	0.04035	0.10582	0.20077	0.10602	-0.10131	-0.08234
wnbl-wnbr	-0.53545	0.54758	-0.21495	0.23305	0.17377	0.21135	-0.08668	0.04245	-0.12075	-0.00457	0.03642	0.20291	0.33365	-0.07564	0.22357	0.06792
nas-wnbl	-0.39557	0.23414	-0.41637	0.32314	0.24992	0.33191	-0.34609	-0.01085	-0.18857	0.37526	0.08399	-0.06766	0.00915	-0.17396	0.00646	0.00286
wnbr-nas	-0.30617	0.18302	-0.35925	0.27429	0.21538	0.54021	-0.34758	-0.07440	-0.17816	0.36953	0.01673	-0.14878	0.06845	-0.08390	0.03396	-0.01785
sispt-nasil	0.37771	-0.37634	-0.19763	0.43289	0.19925	-0.24438	0.24491	0.37518	0.11268	-0.13240	0.26805	-0.03843	0.12714	-0.25295	0.01995	-0.07063
nasil-alarl	0.17120	-0.61953	0.17367	-0.30329	0.16834	0.47492	0.07627	-0.13053	-0.15620	0.28025	-0.03662	-0.01485	-0.14567	0.22440	0.05516	0.09416
alarr-ans	0.46445	0.28694	0.42805	0.20616	-0.45967	0.09801	-0.15906	0.15805	0.26265	0.15544	0.24494	-0.03918	0.18299	-0.11310	-0.03846	0.05101
alarl-nlhil	0.16915	-0.00481	-0.20145	0.54389	-0.34164	-0.20773	-0.34498	-0.14175	0.49925	0.10648	0.15263	0.09704	-0.06800	-0.03094	0.16692	0.09615
sispt-nlhil	0.49221	-0.74248	-0.02672	0.20156	0.08161	-0.01763	0.24041	0.08966	0.16768	0.13940	-0.04618	0.00873	-0.10691	-0.10280	-0.00140	0.14335
ans-alarl	0.20853	0.07988	0.67234	0.44682	-0.15386	-0.09156	-0.40883	0.27603	0.07671	0.00123	0.01500	0.00805	-0.11303	-0.03134	-0.04233	-0.03648
alarr-nlhir	0.25101	0.04875	-0.47558	0.15560	-0.56336	-0.19369	-0.09278	-0.18032	0.47505	0.12326	0.11410	0.11602	-0.03972	0.03437	-0.11574	0.06861
sispt-ans	0.31754	-0.77197	0.14587	0.33204	-0.06663	-0.13705	0.02158	0.29978	0.05840	0.14077	-0.15055	0.08233	0.02349	-0.04668	-0.05059	0.01360
nlhil-ans	0.38016	0.14368	0.76795	0.05441	0.10268	0.02600	-0.17900	0.30177	-0.13441	-0.04040	-0.09218	-0.13902	-0.11130	-0.03723	-0.19105	0.10003
nasir-alarr	0.18615	-0.68413	0.37932	-0.04144	0.20991	0.44422	-0.15612	-0.07408	0.19490	0.01639	0.13619	0.11784	-0.01911	-0.04882	-0.07722	-0.03238

	Prin1	Prin2	Prin3	Prin4	Prin5	Prin6	Prin7	Prin8	Prin9	Prin10	Prin11	Prin12	Prin13	Prin14	Prin15	Prin16
sispt-alarr	0.32311	-0.61829	0.29457	-0.26203	0.27648	0.22595	0.21836	0.17160	0.16774	0.18253	-0.09652	0.25984	0.07080	-0.07957	-0.05612	0.02206
sispt-nasir	0.39725	-0.21085	-0.22389	0.09865	-0.02949	-0.56936	0.42307	0.35094	-0.08800	0.06304	-0.08730	0.14078	0.24231	0.05252	-0.00225	0.10025
sispt-nlhir	0.48012	-0.71942	0.00980	-0.05466	0.01512	0.10091	0.18662	0.02600	0.30301	0.19175	-0.11384	0.20912	0.04487	-0.01699	-0.08889	0.08631
nlhir-ans	0.53894	0.25032	0.63997	0.02436	-0.10328	0.27335	-0.13444	0.16749	-0.00503	0.02374	0.18763	-0.10832	0.19733	-0.08624	-0.01238	0.10562
sispt-alarl	0.38247	-0.70292	-0.01872	-0.10424	0.23766	0.19466	0.40516	0.15243	0.00938	0.12894	0.10734	0.05388	-0.11431	-0.11548	0.08581	0.04173
zygr-nas	0.56443	0.06192	0.51015	0.01109	0.12104	-0.14962	0.16542	-0.42272	0.15937	-0.11763	-0.28583	-0.00485	0.18717	0.10550	0.07774	0.03089
nas-zygl	0.74343	0.07313	0.32440	0.40632	-0.04957	0.03534	0.19327	-0.10637	0.10997	-0.09765	-0.16597	0.03705	0.19077	0.07287	0.14972	-0.06777
zygr-zygl	0.62045	0.22186	0.58412	0.01242	-0.04823	-0.05331	0.36651	-0.14702	-0.03916	-0.03491	0.02956	-0.15688	-0.02215	-0.08338	0.16598	-0.01137
nassr-nasir	0.52723	-0.40571	-0.32202	0.41819	-0.20238	-0.11700	0.02886	0.34430	-0.22470	-0.04921	0.06576	-0.10429	-0.02873	0.16364	0.07046	-0.06442
dacr-nassr	0.87413	0.00703	0.13944	0.03752	0.02246	0.04587	0.22914	0.04040	0.18628	-0.15331	-0.07691	-0.07612	-0.25508	0.03553	-0.04319	-0.14194
dacr-nasir	0.39617	-0.57713	-0.27306	0.35192	0.01847	-0.11062	-0.02340	0.24733	-0.32104	-0.01872	0.13171	-0.24752	0.10554	0.14739	0.14525	0.03563
xfbl-xfbr	0.39343	0.31996	0.60104	-0.36644	-0.07748	-0.11353	0.13866	-0.26219	-0.00837	0.01739	-0.00827	0.29637	0.22081	0.01611	0.03885	-0.04062
stpl-stpr	0.39087	0.24515	0.21059	-0.10206	0.27333	-0.24621	0.16994	-0.41602	-0.40858	0.00990	0.36787	0.22714	0.04903	0.03109	-0.10417	-0.16403
prosH-tmfbptr	0.77469	-0.09030	-0.17448	0.09383	-0.36560	0.37681	0.12825	-0.12555	-0.00013	-0.01582	0.11251	-0.10160	-0.09524	0.01052	0.08027	-0.07573
prosH-tmfbptl	0.83519	-0.13568	-0.08757	-0.06732	-0.10841	0.20216	-0.06599	-0.36546	-0.13037	0.03762	0.07918	-0.02243	0.07253	-0.16736	-0.10981	0.10392
tmfbptl-tmfbptr	0.47528	0.73694	-0.22006	-0.27639	-0.10318	0.12002	0.00813	0.12241	0.04301	-0.02922	-0.10554	0.07693	-0.07963	-0.13973	-0.08331	-0.11638
prosM-tmfbptr	0.77291	-0.00961	-0.18172	0.08922	-0.34949	0.37692	0.05290	-0.13346	-0.08999	-0.07572	0.13841	-0.13377	-0.08527	-0.06657	0.05174	-0.10698
prosM-tmfbptl	0.79202	-0.04206	-0.13984	-0.04767	-0.15023	0.13955	-0.12632	-0.36363	-0.24018	-0.01126	0.07308	0.00104	0.06799	-0.26103	-0.12641	0.08357
chpp-hmfiptr	0.55645	0.60418	-0.25045	-0.20392	-0.04576	0.18901	0.02891	0.26560	-0.06022	-0.29457	-0.05674	-0.03982	-0.09504	-0.06474	0.01587	-0.05601
hmfiptr-hmfiptl	0.74978	0.29846	-0.18168	-0.18106	-0.08119	-0.30394	-0.08525	0.19261	0.15752	-0.17358	-0.04172	-0.00548	-0.13052	-0.24374	-0.07763	0.02108
chpp-hmfiptl	0.58513	0.17874	-0.47031	-0.32619	0.08285	0.00544	-0.05382	0.34020	-0.08839	-0.11512	0.10814	0.24218	0.15094	0.16100	-0.17635	0.03667
hmfsptr-chpp	0.65048	0.20813	-0.41133	-0.44974	-0.14042	0.12091	0.00415	0.08458	0.07134	0.22311	-0.16022	-0.03549	0.16534	0.04569	0.07498	0.06117
hmfsptl-hmfsptr	0.30949	0.72249	-0.31232	-0.37799	-0.03244	0.18036	0.06341	-0.09083	-0.02607	-0.07246	-0.09894	-0.15168	-0.08979	-0.16387	-0.07321	0.13020
chpp-hmfsptl	0.57392	0.10811	-0.30580	-0.22408	-0.51308	-0.10458	0.01311	0.15108	-0.14049	0.20153	-0.11173	-0.21104	0.10854	0.23987	-0.17015	0.04880
gnispt-chpp	0.63354	-0.55152	-0.07658	-0.01204	-0.21229	-0.24280	0.02084	-0.24588	0.15605	0.12385	-0.03281	-0.24670	0.04994	0.07266	-0.06311	-0.10074
chpp-malapt	0.52518	-0.26553	0.18299	0.39588	-0.00793	0.26723	-0.05705	-0.25575	-0.38005	-0.28103	0.08870	0.18394	-0.11043	-0.14838	0.10848	0.11067
gnispt-malapt	0.73097	-0.54331	0.02282	0.14729	-0.17275	-0.08032	-0.01766	-0.30430	-0.04278	-0.00943	0.01615	-0.12708	-0.00139	0.00140	-0.01284	-0.02424
gnispt-gniipt	0.65841	-0.62179	-0.16899	0.19260	-0.11031	-0.03227	0.12084	-0.21978	-0.03067	-0.05365	0.04398	-0.06207	-0.07698	0.06111	-0.13017	-0.04362
gniipt-chpp	0.21470	-0.22884	-0.25117	0.43259	0.13957	0.39519	0.23420	0.03587	-0.34467	-0.34137	0.14946	0.30938	-0.17258	-0.00620	-0.17802	0.06803
tmfbptr-malapt	0.69222	0.38245	0.04610	-0.51953	0.06390	0.14087	-0.02225	0.09079	-0.08518	0.20362	-0.08741	0.05455	-0.01654	-0.06567	0.07602	0.01267
hmfsptr-malapt	0.84935	-0.07627	-0.20936	-0.30515	-0.15652	0.10968	0.00356	0.02453	-0.12119	0.21326	-0.05255	0.03289	0.08817	0.05042	0.13019	0.08614
malapt-hmfsptl	0.78552	-0.24826	-0.22080	0.07801	-0.40517	-0.01377	-0.06817	-0.06907	-0.22435	0.07886	-0.07208	-0.09331	0.03917	0.13094	-0.03219	0.05053
tmfbptl-malapt	0.75771	0.21734	-0.26704	0.02661	0.01480	0.11936	-0.24083	0.17364	-0.03798	-0.10355	-0.27071	0.06543	0.18037	-0.26095	0.02795	-0.11342
hmfiptl-malapt	0.65037	0.03932	-0.50249	-0.23042	0.16620	-0.09375	-0.12803	0.34709	0.06432	-0.09862	-0.01105	0.21518	0.13595	-0.06497	-0.10008	-0.05995
hmfiptr-malapt	0.38044	0.58796	-0.05128	-0.48020	0.13935	0.02584	0.07011	0.40039	0.00969	-0.08278	-0.02434	-0.14133	-0.16226	-0.14768	0.08746	-0.08791
tmflptr-tmflptl	0.27783	0.03438	-0.15664	-0.42622	-0.49569	-0.23360	0.16080	-0.25234	-0.16405	0.13449	0.41463	0.21229	-0.18683	-0.04458	0.15027	-0.06445
tmflptr-malapt	0.54197	0.28700	0.05480	-0.50354	-0.12425	0.35631	0.02392	0.28064	0.15103	0.08876	0.16327	-0.18283	-0.00096	-0.05091	0.22768	-0.02055
tmflptl-malapt	0.19142	-0.06932	-0.20498	0.16059	-0.41341	-0.02030	-0.26057	-0.27934	0.16931	-0.63418	-0.25967	0.12576	0.12594	0.01359	0.19998	0.05803
alarr-alarl	-0.02075	0.78935	0.11095	0.16625	-0.23921	0.22402	0.01258	0.03840	0.33488	-0.00917	0.25731	0.14209	-0.05284	0.05529	-0.00780	0.15157
nlhil-nlhir	-0.12537	0.67765	0.41011	0.17876	-0.03334	0.34179	0.26073	0.05527	-0.12920	-0.14817	-0.09696	-0.18635	0.08058	0.12576	-0.10985	0.13715
ans-prosH	0.61771	-0.20135	0.09803	-0.25564	0.49574	-0.03448	-0.31705	-0.00189	0.09381	-0.22088	0.21689	-0.04733	-0.00911	0.20947	0.04190	-0.05364
ans-prosM	0.61418	-0.27434	0.12464	-0.28123	0.48394	0.05348	-0.19459	-0.01371	0.23564	-0.15150	0.15917	-0.02730	0.01426	0.25602	0.08274	0.02511
nlhir-nlhil	-0.12537	0.67765	0.41011	0.17876	-0.03334	0.34179	0.26073	0.05527	-0.12920	-0.14817	-0.09696	-0.18635	0.08058	0.12576	-0.10985	0.13715
alarl-alarr	-0.02075	0.78935	0.11095	0.16625	-0.23921	0.22402	0.01258	0.03840	0.33488	-0.00917	0.25731	0.14209	-0.05284	0.05529	-0.00780	0.15157
alarl-ans	0.20853	0.07988	0.67234	0.44682	-0.15386	-0.09156	-0.40883	0.27603	0.07671	0.00123	0.01500	0.00805	-0.11303	-0.03134	-0.04233	-0.03648
prosH-ssp	-0.01813	-0.13447	-0.59397	0.06015	0.48806	0.07611	0.05920	0.03203	0.26008	-0.39673	0.25904	-0.28958	0.00362	0.00545	-0.01390	0.02035
prosM-ssp	0.10391	-0.26866	-0.44088	-0.03683	0.50241	0.21964	0.19244	-0.02165	0.46831	-0.27352	0.13440	-0.20718	0.05526	0.05809	0.05637	0.13570
ans-ssp	0.62803	-0.06176	0.38813	-0.30487	0.28494	-0.03348	-0.42344	0.13839	-0.00064	0.05572	0.11749	0.15543	-0.01744	0.18518	0.03682	0.01970
nlhir-ssp	0.48413	0.14560	0.56701	0.25576	-0.04010	-0.01231	-0.12667	0.06449	-0.46863	-0.13804	0.17003	-0.16110	0.19006	0.06623	0.02753	-0.02713
ssp-ans	0.62803	-0.06176	0.38813	-0.30487	0.28494	-0.03348	-0.42344	0.13839	-0.00064	0.05572	0.11749	0.15543	-0.01744	0.18518	0.03682	0.01970
nlhil-ssp	0.33603	-0.19863	0.79758	0.05213	0.20051	0.13397	0.16938	-0.05686	0.13963	-0.12001	-0.15889	0.09333	0.03761	-0.21172	-0.03690	-0.05699

PCA plot/loading matrix/ Eigenvalue for significant ILD

	Prin1	Prin2	Prin3	Prin4	Prin5	Prin6	Prin7	Prin8	Prin9	Prin10	Prin11	Prin12	Prin13	Prin14	Prin15	Prin16
alarl-ans	0.56173	-0.40538	-0.51815	0.33641	0.04213	-0.29924	0.01165	-0.11723	0.01306	0.01301	0.17614	-0.00636	0.02762	-0.01626	-0.00014	-0.02914
alarr-ans	0.61327	-0.45106	-0.12127	0.02995	0.06442	-0.14151	0.51980	-0.11231	0.17267	0.22334	0.05026	0.04373	-0.01158	0.03423	0.10633	0.03331
ans-alarl	0.56173	-0.40538	-0.51815	0.33641	0.04213	-0.29924	0.01165	-0.11723	0.01306	0.01301	0.17614	-0.00636	0.02762	-0.01626	-0.00014	-0.02914
ans-prosH	0.63044	0.40304	0.34140	0.21163	-0.41174	-0.11419	-0.23363	-0.16400	0.05050	-0.04217	0.03412	0.06272	0.02270	-0.03039	-0.06061	0.01316
ans-prosM	0.64387	0.50637	0.30458	0.19104	-0.38837	0.01110	-0.10795	-0.13141	-0.04592	-0.01826	0.05164	0.06542	0.07931	-0.03590	0.03419	0.04169
ans-ssp	0.80992	0.14728	0.06260	-0.03151	-0.45028	-0.24235	-0.18321	-0.03854	-0.09924	0.07775	0.05712	-0.02757	-0.01640	-0.01934	0.01539	-0.00950
dacl-dacr	0.04344	-0.54200	0.72468	0.30942	0.04965	-0.05544	0.04839	0.07542	-0.10307	0.22078	-0.06896	-0.06343	-0.01934	0.01730	-0.03254	0.00304
dacr-dacl	0.04344	-0.54200	0.72468	0.30942	0.04965	-0.05544	0.04839	0.07542	-0.10307	0.22078	-0.06896	-0.06343	-0.01934	0.01730	-0.03254	0.00304
fmal-fmar	0.24659	-0.66879	0.51681	-0.08285	-0.15014	-0.03822	-0.14211	0.17234	-0.01949	-0.20541	0.16748	-0.21977	-0.00399	0.10619	0.07465	-0.09090
gniipt-chpp	0.00472	0.27823	0.27525	0.36093	0.51266	-0.28178	-0.19404	0.52572	0.09098	0.10351	-0.00949	0.19047	0.02557	0.05997	0.02582	0.00136
gnispt-gniipt	0.39169	0.54243	0.30916	0.04633	0.56261	-0.20729	0.03427	-0.24390	0.01316	-0.03539	0.08769	-0.08255	-0.00404	0.07653	-0.04314	0.10391

	Prin1	Prin2	Prin3	Prin4	Prin5	Prin6	Prin7	Prin8	Prin9	Prin10	Prin11	Prin12	Prin13	Prin14	Prin15	Prin16
gnispt-malapt	0.57204	0.41689	0.22027	-0.04016	0.50344	-0.18416	0.04910	-0.37482	0.02693	-0.05796	-0.00683	-0.09108	0.01458	0.05931	-0.03907	-0.02987
hmfsptr-malapt	0.54826	0.21852	0.52592	-0.36166	0.03936	-0.26608	0.30006	0.02266	-0.21089	-0.02584	-0.11336	-0.11248	-0.09406	0.00749	-0.00700	-0.04227
nasil-alarl	0.30372	0.74833	-0.15396	-0.23876	0.01343	-0.01594	-0.02021	0.26199	-0.07210	-0.00052	-0.15749	-0.22590	0.33776	0.01357	0.04064	0.02465
nasir-alarr	0.45867	0.70486	-0.35551	0.17359	0.01238	0.01031	0.01838	0.06647	0.10052	0.29291	0.01364	0.02680	0.15330	0.05507	-0.05120	-0.07276
nas-zygl	0.74355	-0.17422	0.21738	0.24017	0.43328	0.15119	0.14090	-0.06444	-0.22060	-0.01354	-0.02503	0.06475	0.03730	-0.14671	0.00088	-0.02570
nlhil-ans	0.75424	-0.25837	-0.38608	0.18667	-0.13317	-0.10228	-0.08706	0.17776	0.01920	-0.23414	-0.04851	-0.06816	-0.09904	0.17627	-0.01364	0.09916
nlhil-ssp	0.74402	0.12151	-0.39671	0.15074	0.15527	0.39781	-0.08150	0.12945	-0.04767	-0.00352	0.04099	0.13223	-0.07807	0.07252	-0.09284	-0.06627
nlhir-ans	0.83401	-0.28508	-0.14105	0.07405	-0.09867	-0.04381	0.26767	0.15534	0.20695	0.04985	-0.19472	0.03841	-0.01162	0.03030	0.06659	-0.01231
nlhir-ssp	0.72937	-0.33802	-0.05685	0.11681	0.17497	-0.20393	-0.18790	0.06460	0.27664	-0.15194	-0.29120	-0.04329	-0.02970	-0.19342	0.00656	0.02396
obhil-obhir	-0.04425	-0.82320	0.08727	0.04036	0.08116	-0.12167	-0.05250	0.23763	-0.28938	-0.09652	0.26807	0.14184	0.19561	-0.05139	-0.02498	0.06289
prosH-ssp	-0.34056	0.42220	0.51226	0.54496	-0.19688	0.08981	0.03989	-0.06344	0.23936	-0.14483	0.04596	0.11182	-0.02871	0.00953	-0.01179	-0.00018
prosM-ssp	-0.14257	0.60693	0.43834	0.47327	-0.18644	0.28840	0.19374	-0.02258	0.04533	-0.07530	0.05376	0.11794	0.04286	0.02430	0.11065	0.00047
sispt-alarl	0.30811	0.78999	0.07150	-0.04642	0.22136	0.06346	0.13219	0.29157	0.03449	-0.11096	0.25096	-0.11150	-0.12179	-0.11278	0.03705	-0.01884
sispt-alarr	0.48013	0.69286	-0.20136	-0.06738	-0.00636	0.19095	0.07459	0.25653	-0.19524	0.15546	0.14906	-0.07218	-0.20543	-0.04333	0.01174	0.05034
ssp-ans	0.80992	0.14728	0.06260	-0.03151	-0.45028	-0.24235	-0.18321	-0.03854	-0.09924	0.07775	0.05712	-0.02757	-0.01640	-0.01934	0.01539	-0.00950
stpl-stpr	0.45241	-0.18882	0.41923	-0.26111	0.09009	0.17757	-0.58215	0.09383	0.31640	0.14329	0.04787	-0.06814	-0.01536	-0.00777	-0.02256	-0.00327
tmflptr-malapt	0.48279	-0.01518	0.28358	-0.26642	-0.41514	-0.04553	0.57317	0.22746	0.06764	-0.12858	-0.05378	0.11919	0.05512	0.00136	-0.13914	-0.00095
tmflptr-tmflptl	0.10183	-0.02566	0.34286	-0.79941	0.12981	-0.17555	0.04295	-0.11095	0.25428	0.05891	0.25265	0.18726	0.05506	0.00934	0.01977	0.00325
xfbl-xfbr	0.67779	-0.30193	0.01416	-0.44217	-0.07427	0.36194	-0.15388	0.00444	-0.07280	0.18011	-0.07441	0.21058	-0.05393	0.01311	0.02880	0.04449
zygoor-nas	0.21684	-0.47143	0.02354	0.19108	-0.08012	0.66981	0.19935	-0.04175	0.21464	0.13097	0.16796	-0.30688	0.08129	-0.03104	-0.04530	0.04343
zygr-nas	0.73026	-0.07853	0.10305	0.00456	0.18744	0.46942	-0.14866	-0.25816	-0.26048	-0.07156	-0.12463	0.08585	0.05498	0.05834	0.05682	-0.01219
zygr-zygl	0.79071	-0.25493	0.09393	-0.13624	0.23054	0.33357	0.06922	0.06841	0.10413	-0.29646	0.03974	0.06891	0.05409	0.00080	0.00114	-0.02285

Appendix IV

Variable	by Variable	Spearman ρ	Prob>|ρ|		Variable	by Variable	Spearman ρ	Prob>|ρ|
rs72691108	dacl-dacr	0	1		rs17447439	dacl-dacr	.	.
rs72691108	obhsl-obhsr	-0.1203	0.6456		rs17447439	obhsl-obhsr	.	.
rs72691108	fmal-fmar	-0.0481	0.8545		rs17447439	fmal-fmar	.	.
rs72691108	ectl-ectr	-0.0962	0.7133		rs17447439	ectl-ectr	.	.
rs72691108	wmhsr-wmhsl	0.0241	0.927		rs17447439	wmhsr-wmhsl	.	.
rs72691108	zygool-zygoor	0.1203	0.6456		rs17447439	zygool-zygoor	.	.
rs72691108	obhil-obhir	0.2406	0.3523		rs17447439	obhil-obhir	.	.
rs72691108	nas-dacr	-0.0481	0.8545		rs17447439	nas-dacr	.	.
rs72691108	nas-dacl	-0.2165	0.4039		rs17447439	nas-dacl	.	.
rs72691108	obhsr-nas	-0.0962	0.7133		rs17447439	obhsr-nas	.	.
rs72691108	obhsr-obhsl	-0.1203	0.6456		rs17447439	obhsr-obhsl	.	.
rs72691108	obhsl-nas	0.0481	0.8545		rs17447439	obhsl-nas	.	.
rs72691108	zygool-nas	-0.0481	0.8545		rs17447439	zygool-nas	.	.
rs72691108	zygoor-nas	0	1		rs17447439	zygoor-nas	.	.
rs72691108	dacr-nas	-0.0481	0.8545		rs17447439	dacr-nas	.	.
rs72691108	dacr-dacl	0	1		rs17447439	dacr-dacl	.	.
rs72691108	wnbl-wnbr	0.2646	0.3047		rs17447439	wnbl-wnbr	.	.
rs72691108	nas-wnbl	0.4811	0.0506		rs17447439	nas-wnbl	.	.
rs72691108	wnbr-nas	0.2887	0.2611		rs17447439	wnbr-nas	.	.
rs72691108	sispt-nasil	0.0962	0.7133		rs17447439	sispt-nasil	.	.
rs72691108	nasil-alarl	-0.409	0.1031		rs17447439	nasil-alarl	.	.
rs72691108	alarr-ans	-0.0481	0.8545		rs17447439	alarr-ans	.	.
rs72691108	alarl-nlhil	0.2165	0.4039		rs17447439	alarl-nlhil	.	.
rs72691108	sispt-nlhil	-0.409	0.1031		rs17447439	sispt-nlhil	.	.
rs72691108	ans-alarl	0.0962	0.7133		rs17447439	ans-alarl	.	.
rs72691108	alarr-nlhir	-0.0481	0.8545		rs17447439	alarr-nlhir	.	.
rs72691108	sispt-ans	-0.1203	0.6456		rs17447439	sispt-ans	.	.
rs72691108	nlhil-ans	-0.0481	0.8545		rs17447439	nlhil-ans	.	.
rs72691108	nasir-alarr	-0.2406	0.3523		rs17447439	nasir-alarr	.	.
rs72691108	sispt-alarr	-0.409	0.1031		rs17447439	sispt-alarr	.	.
rs72691108	sispt-nasir	-0.2406	0.3523		rs17447439	sispt-nasir	.	.
rs72691108	sispt-nlhir	-0.409	0.1031		rs17447439	sispt-nlhir	.	.
rs72691108	nlhir-ans	-0.0722	0.7831		rs17447439	nlhir-ans	.	.
rs72691108	sispt-alarl	-0.3127	0.2216		rs17447439	sispt-alarl	.	.
rs72691108	zygr-nas	-0.6495	0.0048		rs17447439	zygr-nas	.	.
rs72691108	nas-zygl	-0.4811	0.0506		rs17447439	nas-zygl	.	.
rs72691108	zygr-zygl	-0.3368	0.1862		rs17447439	zygr-zygl	.	.
rs72691108	nassr-nasir	-0.0241	0.927		rs17447439	nassr-nasir	.	.
rs72691108	dacr-nassr	-0.3849	0.1271		rs17447439	dacr-nassr	.	.
rs72691108	dacr-nasir	-0.1203	0.6456		rs17447439	dacr-nasir	.	.

rs72691108	xfbl-xfbr	-0.5052	0.0386		rs17447439	xfbl-xfbr	.	.
rs72691108	stpl-stpr	-0.6014	0.0107		rs17447439	stpl-stpr	.	.
rs72691108	prosH-tmfbptr	-0.433	0.0825		rs17447439	xfbl-xfbr2	.	.
rs72691108	prosH-tmfbptl	-0.4811	0.0506		rs17447439	prosH-tmfbptr	.	.
rs72691108	tmfbptl-tmfbptr	0.1684	0.5182		rs17447439	prosH-tmfbptl	.	.
rs72691108	prosM-tmfbptr	-0.3368	0.1862		rs17447439	tmfbptl-tmfbptr	.	.
rs72691108	prosM-tmfbptl	-0.3127	0.2216		rs17447439	prosM-tmfbptr	.	.
rs72691108	chpp-hmfiptr	0.0481	0.8545		rs17447439	prosM-tmfbptl	.	.
rs72691108	hmfiptr-hmfiptl	0.1684	0.5182		rs17447439	chpp-hmfiptr	.	.
rs72691108	chpp-hmfiptl	-0.1203	0.6456		rs17447439	hmfiptr-hmfiptl	.	.
rs72691108	hmfsptr-chpp	-0.1925	0.4593		rs17447439	chpp-hmfiptl	.	.
rs72691108	hmfsptl-hmfsptr	0.0722	0.7831		rs17447439	hmfsptr-chpp	.	.
rs72691108	chpp-hmfsptl	-0.1443	0.5805		rs17447439	hmfsptl-hmfsptr	.	.
rs72691108	gnispt-chpp	-0.4811	0.0506		rs17447439	chpp-hmfsptl	.	.
rs72691108	chpp-malapt	-0.3849	0.1271		rs17447439	gnispt-chpp	.	.
rs72691108	gnispt-malapt	-0.5533	0.0212		rs17447439	chpp-malapt	.	.
rs72691108	gnispt-gniipt	-0.6014	0.0107		rs17447439	gnispt-malapt	.	.
rs72691108	gniipt-chpp	-0.2165	0.4039		rs17447439	gnispt-gniipt	.	.
rs72691108	tmfbptr-malapt	-0.2406	0.3523		rs17447439	gniipt-chpp	.	.
rs72691108	hmfsptr-malapt	-0.433	0.0825		rs17447439	tmfbptr-malapt	.	.
rs72691108	malapt-hmfsptl	-0.4571	0.0651		rs17447439	hmfsptr-malapt	.	.
rs72691108	tmfbptl-malapt	-0.0241	0.927		rs17447439	malapt-hmfsptl	.	.
rs72691108	hmfiptl-malapt	-0.0962	0.7133		rs17447439	tmfbptl-malapt	.	.
rs72691108	hmfiptr-malapt	0.0722	0.7831		rs17447439	hmfiptl-malapt	.	.
rs72691108	tmflptr-tmflptl	-0.3849	0.1271		rs17447439	hmfiptr-malapt	.	.
rs72691108	tmflptr-malapt	-0.0241	0.927		rs17447439	tmflptr-tmflptl	.	.
rs72691108	tmflptl-malapt	-0.0962	0.7133		rs17447439	tmflptr-malapt	.	.
rs72691108	alarr-alarl	0.2165	0.4039		rs17447439	tmflptl-malapt	.	.
rs72691108	nlhil-nlhir	0.1684	0.5182		rs17447439	alarr-alarl	.	.
rs72691108	ans-prosH	-0.3127	0.2216		rs17447439	nlhil-nlhir	.	.
rs72691108	ans-prosM	-0.3127	0.2216		rs17447439	ans-prosH	.	.
rs72691108	nlhir-nlhil	0.1684	0.5182		rs17447439	ans-prosM	.	.
rs72691108	alarl-alarr	0.2165	0.4039		rs17447439	nlhir-nlhil	.	.
rs72691108	alarl-ans	0.0962	0.7133		rs17447439	alarl-alarr	.	.
rs72691108	prosH-ssp	0.1443	0.5805		rs17447439	alarl-ans	.	.
rs72691108	prosM-ssp	0.0722	0.7831		rs17447439	prosH-ssp	.	.
rs72691108	ans-ssp	-0.3368	0.1862		rs17447439	prosM-ssp	.	.
rs72691108	nlhir-ssp	-0.2646	0.3047		rs17447439	ans-ssp	.	.
rs72691108	ssp-ans	-0.3368	0.1862		rs17447439	nlhir-ssp	.	.
rs72691108	nlhil-ssp	-0.3368	0.1862		rs17447439	ssp-ans	.	.
rs4648379	dacl-dacr	0.0566	0.8291		rs17447439	nlhil-ssp	.	.
rs4648379	obhsl-obhsr	0.3963	0.1153		rs17447439	rs72691108	.	.
rs4648379	fmal-fmar	-0.0283	0.9141		rs17447439	rs4648379	.	.

rs4648379	ectl-ectr	0.2831	0.2709		rs17447439	rs12786942	.	.
rs4648379	wmhsr-wmhsl	-0.1415	0.5879		rs17447439	rs10862567	.	.
rs4648379	zygool-zygoor	-0.3397	0.1822		rs17447439	rs8007643	.	.
rs4648379	obhil-obhir	-0.1132	0.6652		rs17447439	rs17106852	.	.
rs4648379	nas-dacr	0.1698	0.5146		rs17447439	rs7559271	.	.
rs4648379	nas-dacl	0.2548	0.3237		rs17447439	rs3827760	.	.
rs4648379	obhsr-nas	0.3397	0.1822		rs17447439	rs6740960	.	.
rs4648379	obhsr-obhsl	0.3963	0.1153		rs17447439	rs6129564	.	.
rs4648379	obhsl-nas	0.1981	0.4458		rs17447439	rs927833	.	.
rs4648379	zygool-nas	-0.3114	0.2238		rs1982862	dacl-dacr	-0.1491	0.568
rs4648379	zygoor-nas	-0.4812	0.0505		rs1982862	obhsl-obhsr	-0.0745	0.7762
rs4648379	dacr-nas	0.1698	0.5146		rs1982862	fmal-fmar	0.1118	0.6692
rs4648379	dacr-dacl	0.0566	0.8291		rs1982862	ectl-ectr	0.1863	0.4739
rs4648379	wnbl-wnbr	-0.1415	0.5879		rs1982862	wmhsr-wmhsl	0.1118	0.6692
rs4648379	nas-wnbl	0.1132	0.6652		rs1982862	zygool-zygoor	0.1118	0.6692
rs4648379	wnbr-nas	0.2548	0.3237		rs1982862	obhil-obhir	0.0745	0.7762
rs4648379	sispt-nasil	-0.2265	0.3821		rs1982862	nas-dacr	-0.2609	0.3119
rs4648379	nasil-alarl	0.4246	0.0894		rs1982862	nas-dacl	-0.2981	0.2451
rs4648379	alarr-ans	-0.1132	0.6652		rs1982862	obhsr-nas	-0.1118	0.6692
rs4648379	alarl-nlhil	0.0849	0.7459		rs1982862	obhsr-obhsl	-0.0745	0.7762
rs4648379	sispt-nlhil	0.1981	0.4458		rs1982862	obhsl-nas	-0.1863	0.4739
rs4648379	ans-alarl	0.0849	0.7459		rs1982862	zygool-nas	0.1491	0.568
rs4648379	alarr-nlhir	0.0566	0.8291		rs1982862	zygoor-nas	0.2609	0.3119
rs4648379	sispt-ans	0.2265	0.3821		rs1982862	dacr-nas	-0.2609	0.3119
rs4648379	nlhil-ans	0.1415	0.5879		rs1982862	dacr-dacl	-0.1491	0.568
rs4648379	nasir-alarr	0.2831	0.2709		rs1982862	wnbl-wnbr	-0.4472	0.0719
rs4648379	sispt-alarr	0.1415	0.5879		rs1982862	nas-wnbl	-0.2609	0.3119
rs4648379	sispt-nasir	-0.2265	0.3821		rs1982862	wnbr-nas	-0.2609	0.3119
rs4648379	sispt-nlhir	0.1698	0.5146		rs1982862	sispt-nasil	0.0745	0.7762
rs4648379	nlhir-ans	-0.0849	0.7459		rs1982862	nasil-alarl	-0.0745	0.7762
rs4648379	sispt-alarl	0.1698	0.5146		rs1982862	alarr-ans	0.4472	0.0719
rs4648379	zygr-nas	0.0283	0.9141		rs1982862	alarl-nlhil	0.1118	0.6692
rs4648379	nas-zygl	0.0566	0.8291		rs1982862	sispt-nlhil	0.0745	0.7762
rs4648379	zygr-zygl	0	1		rs1982862	ans-alarl	0.4472	0.0719
rs4648379	nassr-nasir	0.1698	0.5146		rs1982862	alarr-nlhir	-0.0745	0.7762
rs4648379	dacr-nassr	0.2548	0.3237		rs1982862	sispt-ans	0.1118	0.6692
rs4648379	dacr-nasir	0.1698	0.5146		rs1982862	nlhil-ans	0.4099	0.1022
rs4648379	xfbl-xfbr	-0.0283	0.9141		rs1982862	nasir-alarr	0.1491	0.568
rs4648379	stpl-stpr	0.1415	0.5879		rs1982862	sispt-alarr	-0.1118	0.6692
rs4648379	xfbl-xfbr2	-0.0283	0.9141		rs1982862	sispt-nasir	-0.1863	0.4739
rs4648379	prosH-tmfbptr	0.2548	0.3237		rs1982862	sispt-nlhir	-0.1491	0.568
rs4648379	prosH-tmfbptl	0.3963	0.1153		rs1982862	nlhir-ans	0.3354	0.1881
rs4648379	tmfbptl-tmfbptr	0.1698	0.5146		rs1982862	sispt-alarl	-0.1491	0.568

rs4648379	prosM-tmfbptr	0.3397	0.1822		rs1982862	zygr-nas	0.2981	0.2451
rs4648379	prosM-tmfbptl	0.3114	0.2238		rs1982862	nas-zygl	0.2609	0.3119
rs4648379	chpp-hmfiptr	0.2548	0.3237		rs1982862	zygr-zygl	0.4845	0.0487
rs4648379	hmfiptr-hmfiptl	0.1981	0.4458		rs1982862	nassr-nasir	0.1863	0.4739
rs4648379	chpp-hmfiptl	0.3963	0.1153		rs1982862	dacr-nassr	0.2236	0.3883
rs4648379	hmfsptr-chpp	0.368	0.1461		rs1982862	dacr-nasir	-0.0373	0.8871
rs4648379	hmfsptl-hmfsptr	0.0849	0.7459		rs1982862	xfbl-xfbr	0.2609	0.3119
rs4648379	chpp-hmfsptl	0.3397	0.1822		rs1982862	stpl-stpr	0.3727	0.1407
rs4648379	gnispt-chpp	0.2831	0.2709		rs1982862	xfbl-xfbr2	0.2609	0.3119
rs4648379	chpp-malapt	0.3114	0.2238		rs1982862	prosH-tmfbptr	0.0745	0.7762
rs4648379	gnispt-malapt	0.3397	0.1822		rs1982862	prosH-tmfbptl	0.2236	0.3883
rs4648379	gnispt-gniipt	0.3963	0.1153		rs1982862	tmfbptl-tmfbptr	0	1
rs4648379	gniipt-chpp	0.1981	0.4458		rs1982862	prosM-tmfbptr	0.2981	0.2451
rs4648379	tmfbptr-malapt	0.368	0.1461		rs1982862	prosM-tmfbptl	0.2609	0.3119
rs4648379	hmfsptr-malapt	0.5095	0.0367		rs1982862	chpp-hmfiptr	0	1
rs4648379	malapt-hmfsptl	0.3963	0.1153		rs1982862	hmfiptr-hmfiptl	0.0745	0.7762
rs4648379	tmfbptl-malapt	0.3963	0.1153		rs1982862	chpp-hmfiptl	-0.3354	0.1881
rs4648379	hmfiptl-malapt	0.4812	0.0505		rs1982862	hmfsptr-chpp	-0.4099	0.1022
rs4648379	hmfiptr-malapt	0.0566	0.8291		rs1982862	hmfsptl-hmfsptr	-0.1491	0.568
rs4648379	tmflptr-tmflptl	0.1415	0.5879		rs1982862	chpp-hmfsptl	0	1
rs4648379	tmflptr-malapt	0.1981	0.4458		rs1982862	gnispt-chpp	0.1491	0.568
rs4648379	tmflptl-malapt	0.3114	0.2238		rs1982862	chpp-malapt	0.3727	0.1407
rs4648379	alarr-alarl	-0.1698	0.5146		rs1982862	gnispt-malapt	0.2981	0.2451
rs4648379	nlhil-nlhir	-0.3114	0.2238		rs1982862	gnispt-gniipt	0.1491	0.568
rs4648379	ans-prosH	0.6228	0.0076		rs1982862	gniipt-chpp	0.1118	0.6692
rs4648379	ans-prosM	0.6228	0.0076		rs1982862	tmfbptr-malapt	-0.1491	0.568
rs4648379	nlhir-nlhil	-0.3114	0.2238		rs1982862	hmfsptr-malapt	-0.1863	0.4739
rs4648379	alarl-alarr	-0.1698	0.5146		rs1982862	malapt-hmfsptl	0.1863	0.4739
rs4648379	alarl-ans	0.0849	0.7459		rs1982862	tmfbptl-malapt	-0.1118	0.6692
rs4648379	prosH-ssp	0.0283	0.9141		rs1982862	hmfiptl-malapt	-0.2609	0.3119
rs4648379	prosM-ssp	0.0283	0.9141		rs1982862	hmfiptr-malapt	0.0373	0.8871
rs4648379	ans-ssp	0.5944	0.0118		rs1982862	tmflptr-tmflptl	0.1118	0.6692
rs4648379	nlhir-ssp	0.0849	0.7459		rs1982862	tmflptr-malapt	-0.0745	0.7762
rs4648379	ssp-ans	0.5944	0.0118		rs1982862	tmflptl-malapt	-0.1118	0.6692
rs4648379	nlhil-ssp	-0.1698	0.5146		rs1982862	alarr-alarl	0.1491	0.568
rs4648379	rs72691108	-0.3105	0.2251		rs1982862	nlhil-nlhir	0.2236	0.3883
rs12786942	dacl-dacr	0	1		rs1982862	ans-prosH	0.0745	0.7762
rs12786942	obhsl-obhsr	-0.063	0.8102		rs1982862	ans-prosM	-0.0373	0.8871
rs12786942	fmal-fmar	0.378	0.1347		rs1982862	nlhir-nlhil	0.2236	0.3883
rs12786942	ectl-ectr	-0.063	0.8102		rs1982862	alarl-alarr	0.1491	0.568
rs12786942	wmhsr-wmhsl	0.0945	0.7183		rs1982862	alarl-ans	0.4472	0.0719
rs12786942	zygool-zygoor	0.315	0.2182		rs1982862	prosH-ssp	-0.3727	0.1407
rs12786942	obhil-obhir	0.0945	0.7183		rs1982862	prosM-ssp	-0.4845	0.0487

rs12786942	nas-dacr	0.2205	0.3951		rs1982862	ans-ssp	0.1118	0.6692
rs12786942	nas-dacl	0.252	0.3292		rs1982862	nlhir-ssp	0.5217	0.0317
rs12786942	obhsr-nas	-0.0945	0.7183		rs1982862	ssp-ans	0.1118	0.6692
rs12786942	obhsr-obhsl	-0.063	0.8102		rs1982862	nlhil-ssp	0.4099	0.1022
rs12786942	obhsl-nas	-0.2835	0.2702		rs1982862	rs72691108	-0.0215	0.9347
rs12786942	zygool-nas	0.378	0.1347		rs1982862	rs4648379	-0.2025	0.4356
rs12786942	zygoor-nas	0.189	0.4676		rs1982862	rs12786942	0.3099	0.2261
rs12786942	dacr-nas	0.2205	0.3951		rs1982862	rs10862567	.	.
rs12786942	dacr-dacl	0	1		rs1982862	rs8007643	-0.1333	0.6099
rs12786942	wnbl-wnbr	-0.0315	0.9045		rs1982862	rs17106852	-0.2025	0.4356
rs12786942	nas-wnbl	-0.063	0.8102		rs1982862	rs7559271	.	.
rs12786942	wnbr-nas	0.0315	0.9045		rs1982862	rs3827760	.	.
rs12786942	sispt-nasil	-0.126	0.6299		rs1982862	rs6740960	.	.
rs12786942	nasil-alarl	0.126	0.6299		rs1982862	rs6129564	-0.1333	0.6099
rs12786942	alarr-ans	0.126	0.6299		rs1982862	rs927833	-0.1333	0.6099
rs12786942	alarl-nlhil	-0.063	0.8102		rs1982862	rs17447439	.	.
rs12786942	sispt-nlhil	0.2205	0.3951		rs2977562	dacl-dacr	-0.0732	0.7801
rs12786942	ans-alarl	0	1		rs2977562	obhsl-obhsr	-0.3172	0.2148
rs12786942	alarr-nlhir	0.0315	0.9045		rs2977562	fmal-fmar	-0.0732	0.7801
rs12786942	sispt-ans	-0.0315	0.9045		rs2977562	ectl-ectr	0.3416	0.1797
rs12786942	nlhil-ans	0.189	0.4676		rs2977562	wmhsr-wmhsl	0.122	0.6409
rs12786942	nasir-alarr	-0.063	0.8102		rs2977562	zygool-zygoor	0.0732	0.7801
rs12786942	sispt-alarr	0.063	0.8102		rs2977562	obhil-obhir	0.4148	0.0978
rs12786942	sispt-nasir	0.189	0.4676		rs2977562	nas-dacr	0.2684	0.2976
rs12786942	sispt-nlhir	0.0945	0.7183		rs2977562	nas-dacl	0.0488	0.8525
rs12786942	nlhir-ans	0.063	0.8102		rs2977562	obhsr-nas	-0.0976	0.7094
rs12786942	sispt-alarl	0.1575	0.5461		rs2977562	obhsr-obhsl	-0.3172	0.2148
rs12786942	zygr-nas	0.063	0.8102		rs2977562	obhsl-nas	-0.122	0.6409
rs12786942	nas-zygl	0.0315	0.9045		rs2977562	zygool-nas	-0.1464	0.5751
rs12786942	zygr-zygl	0.126	0.6299		rs2977562	zygoor-nas	0.1464	0.5751
rs12786942	nassr-nasir	0.189	0.4676		rs2977562	dacr-nas	0.2684	0.2976
rs12786942	dacr-nassr	-0.0315	0.9045		rs2977562	dacr-dacl	-0.0732	0.7801
rs12786942	dacr-nasir	0.0315	0.9045		rs2977562	wnbl-wnbr	0.0244	0.9259
rs12786942	xfbl-xfbr	0.0315	0.9045		rs2977562	nas-wnbl	0.0244	0.9259
rs12786942	stpl-stpr	0.2835	0.2702		rs2977562	wnbr-nas	-0.0244	0.9259
rs12786942	xfbl-xfbr2	0.0315	0.9045		rs2977562	sispt-nasil	0.0244	0.9259
rs12786942	prosH-tmfbptr	0.126	0.6299		rs2977562	nasil-alarl	-0.122	0.6409
rs12786942	prosH-tmfbptl	0.0945	0.7183		rs2977562	alarr-ans	0.4636	0.0609
rs12786942	tmfbptl-tmfbptr	-0.063	0.8102		rs2977562	alarl-nlhil	0.3904	0.1214
rs12786942	prosM-tmfbptr	0	1		rs2977562	sispt-nlhil	0.0244	0.9259
rs12786942	prosM-tmfbptl	0	1		rs2977562	ans-alarl	0.4392	0.0778
rs12786942	chpp-hmfiptr	-0.189	0.4676		rs2977562	alarr-nlhir	0.2684	0.2976
rs12786942	hmfiptr-hmfiptl	-0.3465	0.1731		rs2977562	sispt-ans	0.2196	0.3971

rs12786942	chpp-hmfiptl	-0.063	0.8102		rs2977562	nlhil-ans	0.0488	0.8525
rs12786942	hmfsptr-chpp	-0.126	0.6299		rs2977562	nasir-alarr	-0.0488	0.8525
rs12786942	hmfsptl-hmfsptr	0.0315	0.9045		rs2977562	sispt-alarr	0.0244	0.9259
rs12786942	chpp-hmfsptl	0.189	0.4676		rs2977562	sispt-nasir	0.0488	0.8525
rs12786942	gnispt-chpp	0	1		rs2977562	sispt-nlhir	0.0976	0.7094
rs12786942	chpp-malapt	0.063	0.8102		rs2977562	nlhir-ans	0.3172	0.2148
rs12786942	gnispt-malapt	0.063	0.8102		rs2977562	sispt-alarl	-0.1464	0.5751
rs12786942	gnispt-gniipt	0.126	0.6299		rs2977562	zygr-nas	0.0976	0.7094
rs12786942	gniipt-chpp	0.252	0.3292		rs2977562	nas-zygl	0.366	0.1486
rs12786942	tmfbptr-malapt	-0.0945	0.7183		rs2977562	zygr-zygl	0.244	0.3453
rs12786942	hmfsptr-malapt	0.063	0.8102		rs2977562	nassr-nasir	0.1464	0.5751
rs12786942	malapt-hmfsptl	0.126	0.6299		rs2977562	dacr-nassr	0.2196	0.3971
rs12786942	tmfbptl-malapt	-0.2835	0.2702		rs2977562	dacr-nasir	0.0244	0.9259
rs12786942	hmfiptl-malapt	-0.3465	0.1731		rs2977562	xfbl-xfbr	0.0488	0.8525
rs12786942	hmfiptr-malapt	-0.189	0.4676		rs2977562	stpl-stpr	-0.4148	0.0978
rs12786942	tmflptr-tmflptl	0.1575	0.5461		rs2977562	xfbl-xfbr2	0.0488	0.8525
rs12786942	tmflptr-malapt	-0.252	0.3292		rs2977562	prosH-tmfbptr	0.2196	0.3971
rs12786942	tmflptl-malapt	-0.4725	0.0555		rs2977562	prosH-tmfbptl	-0.0244	0.9259
rs12786942	alarr-alarl	0.252	0.3292		rs2977562	tmfbptl-tmfbptr	0.0976	0.7094
rs12786942	nlhil-nlhir	0.315	0.2182		rs2977562	prosM-tmfbptr	0.1464	0.5751
rs12786942	ans-prosH	-0.378	0.1347		rs2977562	prosM-tmfbptl	-0.122	0.6409
rs12786942	ans-prosM	-0.315	0.2182		rs2977562	chpp-hmfiptr	0.0976	0.7094
rs12786942	nlhir-nlhil	0.315	0.2182		rs2977562	hmfiptr-hmfiptl	0.122	0.6409
rs12786942	alarl-alarr	0.252	0.3292		rs2977562	chpp-hmfiptl	-0.1952	0.4528
rs12786942	alarl-ans	0	1		rs2977562	hmfsptr-chpp	0.122	0.6409
rs12786942	prosH-ssp	-0.2205	0.3951		rs2977562	hmfsptl-hmfsptr	-0.122	0.6409
rs12786942	prosM-ssp	-0.2835	0.2702		rs2977562	chpp-hmfsptl	0.122	0.6409
rs12786942	ans-ssp	-0.189	0.4676		rs2977562	gnispt-chpp	0.0244	0.9259
rs12786942	nlhir-ssp	0.126	0.6299		rs2977562	chpp-malapt	0.0732	0.7801
rs12786942	ssp-ans	-0.189	0.4676		rs2977562	gnispt-malapt	0.0732	0.7801
rs12786942	nlhil-ssp	0.126	0.6299		rs2977562	gnispt-gniipt	0	1
rs12786942	rs72691108	-0.1818	0.4848		rs2977562	gniipt-chpp	-0.1952	0.4528
rs12786942	rs4648379	-0.2568	0.3198		rs2977562	tmfbptr-malapt	0.1708	0.5122
rs10862567	dacl-dacr	.	.		rs2977562	hmfsptr-malapt	0.122	0.6409
rs10862567	obhsl-obhsr	.	.		rs2977562	malapt-hmfsptl	0.1952	0.4528
rs10862567	fmal-fmar	.	.		rs2977562	tmfbptl-malapt	0.1708	0.5122
rs10862567	ectl-ectr	.	.		rs2977562	hmfiptl-malapt	0	1
rs10862567	wmhsr-wmhsl	.	.		rs2977562	hmfiptr-malapt	0.1464	0.5751
rs10862567	zygool-zygoor	.	.		rs2977562	tmflptr-tmflptl	0.0244	0.9259
rs10862567	obhil-obhir	.	.		rs2977562	tmflptr-malapt	0.244	0.3453
rs10862567	nas-dacr	.	.		rs2977562	tmflptl-malapt	0.244	0.3453
rs10862567	nas-dacl	.	.		rs2977562	alarr-alarl	0.1708	0.5122
rs10862567	obhsr-nas	.	.		rs2977562	nlhil-nlhir	0	1

rs10862567	obhsr-obhsl	.	.		rs2977562	ans-prosH	-0.2928	0.2541
rs10862567	obhsl-nas	.	.		rs2977562	ans-prosM	-0.1464	0.5751
rs10862567	zygool-nas	.	.		rs2977562	nlhir-nlhil	0	1
rs10862567	zygoor-nas	.	.		rs2977562	alarl-alarr	0.1708	0.5122
rs10862567	dacr-nas	.	.		rs2977562	alarl-ans	0.4392	0.0778
rs10862567	dacr-dacl	.	.		rs2977562	prosH-ssp	-0.4636	0.0609
rs10862567	wnbl-wnbr	.	.		rs2977562	prosM-ssp	-0.244	0.3453
rs10862567	nas-wnbl	.	.		rs2977562	ans-ssp	-0.0732	0.7801
rs10862567	wnbr-nas	.	.		rs2977562	nlhir-ssp	0.0976	0.7094
rs10862567	sispt-nasil	.	.		rs2977562	ssp-ans	-0.0732	0.7801
rs10862567	nasil-alarl	.	.		rs2977562	nlhil-ssp	0.1464	0.5751
rs10862567	alarr-ans	.	.		rs2977562	rs72691108	0.169	0.5166
rs10862567	alarl-nlhil	.	.		rs2977562	rs4648379	-0.0994	0.7041
rs10862567	sispt-nlhil	.	.		rs2977562	rs12786942	-0.2398	0.354
rs10862567	ans-alarl	.	.		rs2977562	rs10862567	.	.
rs10862567	alarr-nlhir	.	.		rs2977562	rs8007643	0.3055	0.2331
rs10862567	sispt-ans	.	.		rs2977562	rs17106852	0.1823	0.4837
rs10862567	nlhil-ans	.	.		rs2977562	rs7559271	.	.
rs10862567	nasir-alarr	.	.		rs2977562	rs3827760	.	.
rs10862567	sispt-alarr	.	.		rs2977562	rs6740960	.	.
rs10862567	sispt-nasir	.	.		rs2977562	rs6129564	-0.0655	0.8029
rs10862567	sispt-nlhir	.	.		rs2977562	rs927833	0.3055	0.2331
rs10862567	nlhir-ans	.	.		rs2977562	rs17447439	.	.
rs10862567	sispt-alarl	.	.		rs2977562	rs1982862	-0.0655	0.8029
rs10862567	zygr-nas	.	.		rs9995821	dacl-dacr	0.1925	0.4593
rs10862567	nas-zygl	.	.		rs9995821	obhsl-obhsr	-0.0722	0.7831
rs10862567	zygr-zygl	.	.		rs9995821	fmal-fmar	0.2406	0.3523
rs10862567	nassr-nasir	.	.		rs9995821	ectl-ectr	-0.0722	0.7831
rs10862567	dacr-nassr	.	.		rs9995821	wmhsr-wmhsl	0.2165	0.4039
rs10862567	dacr-nasir	.	.		rs9995821	zygool-zygoor	0.3127	0.2216
rs10862567	xfbl-xfbr	.	.		rs9995821	obhil-obhir	0.1925	0.4593
rs10862567	stpl-stpr	.	.		rs9995821	nas-dacr	0.2406	0.3523
rs10862567	xfbl-xfbr2	.	.		rs9995821	nas-dacl	0.2406	0.3523
rs10862567	prosH-tmfbptr	.	.		rs9995821	obhsr-nas	0.1203	0.6456
rs10862567	prosH-tmfbptl	.	.		rs9995821	obhsr-obhsl	-0.0722	0.7831
rs10862567	tmfbptl-tmfbptr	.	.		rs9995821	obhsl-nas	-0.0241	0.927
rs10862567	prosM-tmfbptr	.	.		rs9995821	zygool-nas	0.3127	0.2216
rs10862567	prosM-tmfbptl	.	.		rs9995821	zygoor-nas	0.5052	0.0386
rs10862567	chpp-hmfiptr	.	.		rs9995821	dacr-nas	0.2406	0.3523
rs10862567	hmfiptr-hmfiptl	.	.		rs9995821	dacr-dacl	0.1925	0.4593
rs10862567	chpp-hmfiptl	.	.		rs9995821	wnbl-wnbr	0.0241	0.927
rs10862567	hmfsptr-chpp	.	.		rs9995821	nas-wnbl	-0.3608	0.1548
rs10862567	hmfsptl-hmfsptr	.	.		rs9995821	wnbr-nas	-0.3608	0.1548

rs10862567	chpp-hmfsptl	.	.		rs9995821	sispt-nasil	0.1925	0.4593
rs10862567	gnispt-chpp	.	.		rs9995821	nasil-alarl	-0.0241	0.927
rs10862567	chpp-malapt	.	.		rs9995821	alarr-ans	0.5052	0.0386
rs10862567	gnispt-malapt	.	.		rs9995821	alarl-nlhil	0	1
rs10862567	gnispt-gniipt	.	.		rs9995821	sispt-nlhil	0.1443	0.5805
rs10862567	gniipt-chpp	.	.		rs9995821	ans-alarl	0.1203	0.6456
rs10862567	tmfbptr-malapt	.	.		rs9995821	alarr-nlhir	0.0481	0.8545
rs10862567	hmfsptr-malapt	.	.		rs9995821	sispt-ans	0.0481	0.8545
rs10862567	malapt-hmfsptl	.	.		rs9995821	nlhil-ans	0.2406	0.3523
rs10862567	tmfbptl-malapt	.	.		rs9995821	nasir-alarr	0.2406	0.3523
rs10862567	hmfiptl-malapt	.	.		rs9995821	sispt-alarr	0.5052	0.0386
rs10862567	hmfiptr-malapt	.	.		rs9995821	sispt-nasir	0.2646	0.3047
rs10862567	tmflptr-tmflptl	.	.		rs9995821	sispt-nlhir	0.3849	0.1271
rs10862567	tmflptr-malapt	.	.		rs9995821	nlhir-ans	0.5292	0.0289
rs10862567	tmflptl-malapt	.	.		rs9995821	sispt-alarl	0.1684	0.5182
rs10862567	alarr-alarl	.	.		rs9995821	zygr-nas	0.4571	0.0651
rs10862567	nlhil-nlhir	.	.		rs9995821	nas-zygl	0.5052	0.0386
rs10862567	ans-prosH	.	.		rs9995821	zygr-zygl	0.3127	0.2216
rs10862567	ans-prosM	.	.		rs9995821	nassr-nasir	-0.2887	0.2611
rs10862567	nlhir-nlhil	.	.		rs9995821	dacr-nassr	0.3127	0.2216
rs10862567	alarl-alarr	.	.		rs9995821	dacr-nasir	-0.3127	0.2216
rs10862567	alarl-ans	.	.		rs9995821	xfbl-xfbr	0.6014	0.0107
rs10862567	prosH-ssp	.	.		rs9995821	stpl-stpr	0.2406	0.3523
rs10862567	prosM-ssp	.	.		rs9995821	xfbl-xfbr2	0.6014	0.0107
rs10862567	ans-ssp	.	.		rs9995821	prosH-tmfbptr	0	1
rs10862567	nlhir-ssp	.	.		rs9995821	prosH-tmfbptl	0.1684	0.5182
rs10862567	ssp-ans	.	.		rs9995821	tmfbptl-tmfbptr	0.0722	0.7831
rs10862567	nlhil-ssp	.	.		rs9995821	prosM-tmfbptr	-0.0241	0.927
rs10862567	rs72691108	.	.		rs9995821	prosM-tmfbptl	0.0241	0.927
rs10862567	rs4648379	.	.		rs9995821	chpp-hmfiptr	0.0722	0.7831
rs10862567	rs12786942	.	.		rs9995821	hmfiptr-hmfiptl	0	1
rs8007643	dacl-dacr	0.0745	0.7762		rs9995821	chpp-hmfiptl	0.0962	0.7133
rs8007643	obhsl-obhsr	-0.0745	0.7762		rs9995821	hmfsptr-chpp	0.0722	0.7831
rs8007643	fmal-fmar	-0.1863	0.4739		rs9995821	hmfsptl-hmfsptr	0.0241	0.927
rs8007643	ectl-ectr	-0.0373	0.8871		rs9995821	chpp-hmfsptl	-0.2646	0.3047
rs8007643	wmhsr-wmhsl	-0.2609	0.3119		rs9995821	gnispt-chpp	-0.1443	0.5805
rs8007643	zygool-zygoor	-0.1491	0.568		rs9995821	chpp-malapt	0.1203	0.6456
rs8007643	obhil-obhir	-0.0745	0.7762		rs9995821	gnispt-malapt	-0.0722	0.7831
rs8007643	nas-dacr	0.1118	0.6692		rs9995821	gnispt-gniipt	0.0241	0.927
rs8007643	nas-dacl	-0.1118	0.6692		rs9995821	gniipt-chpp	0.0481	0.8545
rs8007643	obhsr-nas	0.2236	0.3883		rs9995821	tmfbptr-malapt	0.3127	0.2216
rs8007643	obhsr-obhsl	-0.0745	0.7762		rs9995821	hmfsptr-malapt	0.1203	0.6456
rs8007643	obhsl-nas	-0.1491	0.568		rs9995821	malapt-hmfsptl	-0.0481	0.8545

rs8007643	zygool-nas	-0.3727	0.1407		rs9995821	tmfbptl-malapt	0.0962	0.7133
rs8007643	zygoor-nas	0.2609	0.3119		rs9995821	hmfiptl-malapt	0.0722	0.7831
rs8007643	dacr-nas	0.1118	0.6692		rs9995821	hmfiptr-malapt	0.2165	0.4039
rs8007643	dacr-dacl	0.0745	0.7762		rs9995821	tmflptr-tmflptl	0.0481	0.8545
rs8007643	wnbl-wnbr	0.1491	0.568		rs9995821	tmflptr-malapt	0.1925	0.4593
rs8007643	nas-wnbl	0.0745	0.7762		rs9995821	tmflptl-malapt	-0.1684	0.5182
rs8007643	wnbr-nas	0.2609	0.3119		rs9995821	alarr-alarl	0.3849	0.1271
rs8007643	sispt-nasil	-0.3354	0.1881		rs9995821	nlhil-nlhir	0.1443	0.5805
rs8007643	nasil-alarl	0.1863	0.4739		rs9995821	ans-prosH	0.0241	0.927
rs8007643	alarr-ans	0.2981	0.2451		rs9995821	ans-prosM	0.1203	0.6456
rs8007643	alarl-nlhil	-0.0373	0.8871		rs9995821	nlhir-nlhil	0.1443	0.5805
rs8007643	sispt-nlhil	-0.0373	0.8871		rs9995821	alarl-alarr	0.3849	0.1271
rs8007643	ans-alarl	-0.0373	0.8871		rs9995821	alarl-ans	0.1203	0.6456
rs8007643	alarr-nlhir	0.1118	0.6692		rs9995821	prosH-ssp	-0.3127	0.2216
rs8007643	sispt-ans	0.0373	0.8871		rs9995821	prosM-ssp	-0.1443	0.5805
rs8007643	nlhil-ans	0	1		rs9995821	ans-ssp	0.1925	0.4593
rs8007643	nasir-alarr	0.2236	0.3883		rs9995821	nlhir-ssp	0.0481	0.8545
rs8007643	sispt-alarr	0.3354	0.1881		rs9995821	ssp-ans	0.1925	0.4593
rs8007643	sispt-nasir	-0.1491	0.568		rs9995821	nlhil-ssp	0.5774	0.0152
rs8007643	sispt-nlhir	0.3354	0.1881		rs9995821	rs72691108	-0.2917	0.256
rs8007643	nlhir-ans	0.2609	0.3119		rs9995821	rs4648379	-0.2451	0.343
rs8007643	sispt-alarl	-0.0373	0.8871		rs9995821	rs12786942	0.1818	0.4848
rs8007643	zygr-nas	0.2609	0.3119		rs9995821	rs10862567	.	.
rs8007643	nas-zygl	0.1863	0.4739		rs9995821	rs8007643	0.3873	0.1246
rs8007643	zygr-zygl	0.0745	0.7762		rs9995821	rs17106852	-0.2451	0.343
rs8007643	nassr-nasir	-0.3727	0.1407		rs9995821	rs7559271	.	.
rs8007643	dacr-nassr	0.0373	0.8871		rs9995821	rs3827760	.	.
rs8007643	dacr-nasir	-0.3354	0.1881		rs9995821	rs6740960	.	.
rs8007643	xfbl-xfbr	0.4472	0.0719		rs9995821	rs6129564	0.3873	0.1246
rs8007643	stpl-stpr	0.1118	0.6692		rs9995821	rs927833	0.0215	0.9347
rs8007643	xfbl-xfbr2	0.4472	0.0719		rs9995821	rs17447439	.	.
rs8007643	prosH-tmfbptr	0.1118	0.6692		rs9995821	rs1982862	0.0215	0.9347
rs8007643	prosH-tmfbptl	0.2981	0.2451		rs9995821	rs2977562	0.3099	0.2261
rs8007643	tmfbptl-tmfbptr	0.1491	0.568		rs11738462	dacl-dacr	-0.5528	0.0214
rs8007643	prosM-tmfbptr	0.1118	0.6692		rs11738462	obhsl-obhsr	-0.3266	0.2007
rs8007643	prosM-tmfbptl	0.2236	0.3883		rs11738462	fmal-fmar	-0.5276	0.0295
rs8007643	chpp-hmfiptr	0.0373	0.8871		rs11738462	ectl-ectr	0.1256	0.6309
rs8007643	hmfiptr-hmfiptl	-0.1118	0.6692		rs11738462	wmhsr-wmhsl	-0.3518	0.1662
rs8007643	chpp-hmfiptl	0.1118	0.6692		rs11738462	zygool-zygoor	-0.2764	0.2829
rs8007643	hmfsptr-chpp	0.3354	0.1881		rs11738462	obhil-obhir	-0.5025	0.0398
rs8007643	hmfsptl-hmfsptr	0.0745	0.7762		rs11738462	nas-dacr	-0.2261	0.3828
rs8007643	chpp-hmfsptl	0.2236	0.3883		rs11738462	nas-dacl	-0.3015	0.2396
rs8007643	gnispt-chpp	0.1118	0.6692		rs11738462	obhsr-nas	-0.2764	0.2829

rs8007643	chpp-malapt	-0.1118	0.6692		rs11738462	obhsr-obhsl	-0.3266	0.2007
rs8007643	gnispt-malapt	0.0373	0.8871		rs11738462	obhsl-nas	-0.3015	0.2396
rs8007643	gnispt-gniipt	0.0373	0.8871		rs11738462	zygool-nas	-0.2764	0.2829
rs8007643	gniipt-chpp	-0.3354	0.1881		rs11738462	zygoor-nas	-0.0251	0.9237
rs8007643	tmfbptr-malapt	0.3727	0.1407		rs11738462	dacr-nas	-0.2261	0.3828
rs8007643	hmfsptr-malapt	0.3354	0.1881		rs11738462	dacr-dacl	-0.5528	0.0214
rs8007643	malapt-hmfsptl	0.1491	0.568		rs11738462	wnbl-wnbr	-0.2513	0.3307
rs8007643	tmfbptl-malapt	0.2236	0.3883		rs11738462	nas-wnbl	0	1
rs8007643	hmfiptl-malapt	0.1863	0.4739		rs11738462	wnbr-nas	0	1
rs8007643	hmfiptr-malapt	0.0373	0.8871		rs11738462	sispt-nasil	0.0754	0.7737
rs8007643	tmflptr-tmflptl	0.1118	0.6692		rs11738462	nasil-alarl	0.5025	0.0398
rs8007643	tmflptr-malapt	0.1118	0.6692		rs11738462	alarr-ans	0.0503	0.8481
rs8007643	tmflptl-malapt	0.0373	0.8871		rs11738462	alarl-nlhil	0	1
rs8007643	alarr-alarl	0.0373	0.8871		rs11738462	sispt-nlhil	0.1508	0.5636
rs8007643	nlhil-nlhir	-0.0745	0.7762		rs11738462	ans-alarl	0.1759	0.4995
rs8007643	ans-prosH	0.0373	0.8871		rs11738462	alarr-nlhir	-0.201	0.4392
rs8007643	ans-prosM	0.0745	0.7762		rs11738462	sispt-ans	0.0754	0.7737
rs8007643	nlhir-nlhil	-0.0745	0.7762		rs11738462	nlhil-ans	0.3015	0.2396
rs8007643	alarl-alarr	0.0373	0.8871		rs11738462	nasir-alarr	0.4774	0.0526
rs8007643	alarl-ans	-0.0373	0.8871		rs11738462	sispt-alarr	0.1759	0.4995
rs8007643	prosH-ssp	-0.4845	0.0487		rs11738462	sispt-nasir	-0.3266	0.2007
rs8007643	prosM-ssp	-0.3354	0.1881		rs11738462	sispt-nlhir	0.0754	0.7737
rs8007643	ans-ssp	0.2236	0.3883		rs11738462	nlhir-ans	0.2764	0.2829
rs8007643	nlhir-ssp	0	1		rs11738462	sispt-alarl	0.2513	0.3307
rs8007643	ssp-ans	0.2236	0.3883		rs11738462	zygr-nas	-0.2261	0.3828
rs8007643	nlhil-ssp	0.2236	0.3883		rs11738462	nas-zygl	-0.2513	0.3307
rs8007643	rs72691108	-0.3873	0.1246		rs11738462	zygr-zygl	0.1256	0.6309
rs8007643	rs4648379	0.2279	0.3791		rs11738462	nassr-nasir	-0.1256	0.6309
rs8007643	rs12786942	-0.169	0.5166		rs11738462	dacr-nassr	-0.1759	0.4995
rs8007643	rs10862567	.	.		rs11738462	dacr-nasir	0.3015	0.2396
rs17106852	dacl-dacr	0.368	0.1461		rs11738462	xfbl-xfbr	-0.1508	0.5636
rs17106852	obhsl-obhsr	0.1698	0.5146		rs11738462	stpl-stpr	-0.1759	0.4995
rs17106852	fmal-fmar	0.2265	0.3821		rs11738462	xfbl-xfbr2	-0.1508	0.5636
rs17106852	ectl-ectr	-0.2831	0.2709		rs11738462	prosH-tmfbptr	-0.1005	0.7011
rs17106852	wmhsr-wmhsl	0.2831	0.2709		rs11738462	prosH-tmfbptl	-0.0251	0.9237
rs17106852	zygool-zygoor	0.3397	0.1822		rs11738462	tmfbptl-tmfbptr	-0.4523	0.0683
rs17106852	obhil-obhir	0.368	0.1461		rs11738462	prosM-tmfbptr	-0.1005	0.7011
rs17106852	nas-dacr	0.1698	0.5146		rs11738462	prosM-tmfbptl	-0.0754	0.7737
rs17106852	nas-dacl	0.0566	0.8291		rs11738462	chpp-hmfiptr	-0.3015	0.2396
rs17106852	obhsr-nas	0.3114	0.2238		rs11738462	hmfiptr-hmfiptl	-0.2513	0.3307
rs17106852	obhsr-obhsl	0.1698	0.5146		rs11738462	chpp-hmfiptl	-0.1759	0.4995
rs17106852	obhsl-nas	0	1		rs11738462	hmfsptr-chpp	-0.3015	0.2396
rs17106852	zygool-nas	0.0566	0.8291		rs11738462	hmfsptl-hmfsptr	-0.2513	0.3307

rs17106852	zygoor-nas	0.2548	0.3237		rs11738462	chpp-hmfsptl	-0.3015	0.2396
rs17106852	dacr-nas	0.1698	0.5146		rs11738462	gnispt-chpp	0.0754	0.7737
rs17106852	dacr-dacl	0.368	0.1461		rs11738462	chpp-malapt	0	1
rs17106852	wnbl-wnbr	0.1981	0.4458		rs11738462	gnispt-malapt	0.0251	0.9237
rs17106852	nas-wnbl	0.1415	0.5879		rs11738462	gnispt-gniipt	-0.0503	0.8481
rs17106852	wnbr-nas	0.1981	0.4458		rs11738462	gniipt-chpp	-0.0754	0.7737
rs17106852	sispt-nasil	-0.1132	0.6652		rs11738462	tmfbptr-malapt	-0.1759	0.4995
rs17106852	nasil-alarl	-0.4246	0.0894		rs11738462	hmfsptr-malapt	-0.2261	0.3828
rs17106852	alarr-ans	-0.0566	0.8291		rs11738462	malapt-hmfsptl	-0.2261	0.3828
rs17106852	alarl-nlhil	0.1415	0.5879		rs11738462	tmfbptl-malapt	-0.3769	0.1359
rs17106852	sispt-nlhil	-0.3397	0.1822		rs11738462	hmfiptl-malapt	-0.3015	0.2396
rs17106852	ans-alarl	-0.3963	0.1153		rs11738462	hmfiptr-malapt	-0.0754	0.7737
rs17106852	alarr-nlhir	0.368	0.1461		rs11738462	tmflptr-tmflptl	-0.0251	0.9237
rs17106852	sispt-ans	-0.3397	0.1822		rs11738462	tmflptr-malapt	0.2261	0.3828
rs17106852	nlhil-ans	-0.5378	0.026		rs11738462	tmflptl-malapt	-0.2764	0.2829
rs17106852	nasir-alarr	-0.5944	0.0118		rs11738462	alarr-alarl	-0.1759	0.4995
rs17106852	sispt-alarr	-0.3963	0.1153		rs11738462	nlhil-nlhir	-0.1256	0.6309
rs17106852	sispt-nasir	0.0566	0.8291		rs11738462	ans-prosH	0.1759	0.4995
rs17106852	sispt-nlhir	-0.2265	0.3821		rs11738462	ans-prosM	0.2513	0.3307
rs17106852	nlhir-ans	-0.2548	0.3237		rs11738462	nlhir-nlhil	-0.1256	0.6309
rs17106852	sispt-alarl	-0.3963	0.1153		rs11738462	alarl-alarr	-0.1759	0.4995
rs17106852	zygr-nas	-0.1415	0.5879		rs11738462	alarl-ans	0.1759	0.4995
rs17106852	nas-zygl	-0.0566	0.8291		rs11738462	prosH-ssp	0.2513	0.3307
rs17106852	zygr-zygl	0.0283	0.9141		rs11738462	prosM-ssp	0.3518	0.1662
rs17106852	nassr-nasir	0.0283	0.9141		rs11738462	ans-ssp	0.1508	0.5636
rs17106852	dacr-nassr	0.1698	0.5146		rs11738462	nlhir-ssp	0.1256	0.6309
rs17106852	dacr-nasir	-0.1981	0.4458		rs11738462	ssp-ans	0.1508	0.5636
rs17106852	xfbl-xfbr	-0.0849	0.7459		rs11738462	nlhil-ssp	0.2513	0.3307
rs17106852	stpl-stpr	0.0283	0.9141		rs11738462	rs72691108	0.2031	0.4343
rs17106852	xfbl-xfbr2	-0.0849	0.7459		rs11738462	rs4648379	-0.1195	0.6478
rs17106852	prosH-tmfbptr	0.2265	0.3821		rs11738462	rs12786942	-0.019	0.9423
rs17106852	prosH-tmfbptl	-0.0849	0.7459		rs11738462	rs10862567	.	.
rs17106852	tmfbptl-tmfbptr	0.4812	0.0505		rs11738462	rs8007643	-0.2697	0.2952
rs17106852	prosM-tmfbptr	0.2265	0.3821		rs11738462	rs17106852	-0.4097	0.1025
rs17106852	prosM-tmfbptl	-0.0849	0.7459		rs11738462	rs7559271	.	.
rs17106852	chpp-hmfiptr	0.3397	0.1822		rs11738462	rs3827760	.	.
rs17106852	hmfiptr-hmfiptl	0.2548	0.3237		rs11738462	rs6740960	.	.
rs17106852	chpp-hmfiptl	0.2265	0.3821		rs11738462	rs6129564	-0.2697	0.2952
rs17106852	hmfsptr-chpp	0.3963	0.1153		rs11738462	rs927833	-0.2697	0.2952
rs17106852	hmfsptl-hmfsptr	0.3397	0.1822		rs11738462	rs17447439	.	.
rs17106852	chpp-hmfsptl	0.4529	0.0679		rs11738462	rs1982862	0.1124	0.6677
rs17106852	gnispt-chpp	0.1415	0.5879		rs11738462	rs2977562	-0.1324	0.6124
rs17106852	chpp-malapt	-0.4246	0.0894		rs11738462	rs9995821	-0.2031	0.4343

rs17106852	gnispt-malapt	-0.0849	0.7459		rs6555969	dacl-dacr	.	.
rs17106852	gnispt-gniipt	-0.0566	0.8291		rs6555969	obhsl-obhsr	.	.
rs17106852	gniipt-chpp	-0.3114	0.2238		rs6555969	fmal-fmar	.	.
rs17106852	tmfbptr-malapt	0.1415	0.5879		rs6555969	ectl-ectr	.	.
rs17106852	hmfsptr-malapt	0.2548	0.3237		rs6555969	wmhsr-wmhsl	.	.
rs17106852	malapt-hmfsptl	0.1132	0.6652		rs6555969	zygool-zygoor	.	.
rs17106852	tmfbptl-malapt	0.1415	0.5879		rs6555969	obhil-obhir	.	.
rs17106852	hmfiptl-malapt	0.3114	0.2238		rs6555969	nas-dacr	.	.
rs17106852	hmfiptr-malapt	0.3397	0.1822		rs6555969	nas-dacl	.	.
rs17106852	tmflptr-tmflptl	0.2548	0.3237		rs6555969	obhsr-nas	.	.
rs17106852	tmflptr-malapt	0.1981	0.4458		rs6555969	obhsr-obhsl	.	.
rs17106852	tmflptl-malapt	0.1698	0.5146		rs6555969	obhsl-nas	.	.
rs17106852	alarr-alarl	0.1132	0.6652		rs6555969	zygool-nas	.	.
rs17106852	nlhil-nlhir	-0.0283	0.9141		rs6555969	zygoor-nas	.	.
rs17106852	ans-prosH	-0.1132	0.6652		rs6555969	dacr-nas	.	.
rs17106852	ans-prosM	-0.1981	0.4458		rs6555969	dacr-dacl	.	.
rs17106852	nlhir-nlhil	-0.0283	0.9141		rs6555969	wnbl-wnbr	.	.
rs17106852	alarl-alarr	0.1132	0.6652		rs6555969	nas-wnbl	.	.
rs17106852	alarl-ans	-0.3963	0.1153		rs6555969	wnbr-nas	.	.
rs17106852	prosH-ssp	0.1415	0.5879		rs6555969	sispt-nasil	.	.
rs17106852	prosM-ssp	0.0566	0.8291		rs6555969	nasil-alarl	.	.
rs17106852	ans-ssp	-0.1981	0.4458		rs6555969	alarr-ans	.	.
rs17106852	nlhir-ssp	-0.2548	0.3237		rs6555969	alarl-nlhil	.	.
rs17106852	ssp-ans	-0.1981	0.4458		rs6555969	sispt-nlhil	.	.
rs17106852	nlhil-ssp	-0.5944	0.0118		rs6555969	ans-alarl	.	.
rs17106852	rs72691108	-0.0327	0.9009		rs6555969	alarr-nlhir	.	.
rs17106852	rs4648379	0.0192	0.9416		rs6555969	sispt-ans	.	.
rs17106852	rs12786942	-0.2568	0.3198		rs6555969	nlhil-ans	.	.
rs17106852	rs10862567	.	.		rs6555969	nasir-alarr	.	.
rs17106852	rs8007643	0.2279	0.3791		rs6555969	sispt-alarr	.	.
rs7559271	dacl-dacr	.	.		rs6555969	sispt-nasir	.	.
rs7559271	obhsl-obhsr	.	.		rs6555969	sispt-nlhir	.	.
rs7559271	fmal-fmar	.	.		rs6555969	nlhir-ans	.	.
rs7559271	ectl-ectr	.	.		rs6555969	sispt-alarl	.	.
rs7559271	wmhsr-wmhsl	.	.		rs6555969	zygr-nas	.	.
rs7559271	zygool-zygoor	.	.		rs6555969	nas-zygl	.	.
rs7559271	obhil-obhir	.	.		rs6555969	zygr-zygl	.	.
rs7559271	nas-dacr	.	.		rs6555969	nassr-nasir	.	.
rs7559271	nas-dacl	.	.		rs6555969	dacr-nassr	.	.
rs7559271	obhsr-nas	.	.		rs6555969	dacr-nasir	.	.
rs7559271	obhsr-obhsl	.	.		rs6555969	xfbl-xfbr	.	.
rs7559271	obhsl-nas	.	.		rs6555969	stpl-stpr	.	.
rs7559271	zygool-nas	.	.		rs6555969	xfbl-xfbr2	.	.

rs7559271	zygoor-nas	.	.		rs6555969	prosH-tmfbptr	.	.
rs7559271	dacr-nas	.	.		rs6555969	prosH-tmfbptl	.	.
rs7559271	dacr-dacl	.	.		rs6555969	tmfbptl-tmfbptr	.	.
rs7559271	wnbl-wnbr	.	.		rs6555969	prosM-tmfbptr	.	.
rs7559271	nas-wnbl	.	.		rs6555969	prosM-tmfbptl	.	.
rs7559271	wnbr-nas	.	.		rs6555969	chpp-hmfiptr	.	.
rs7559271	sispt-nasil	.	.		rs6555969	hmfiptr-hmfiptl	.	.
rs7559271	nasil-alarl	.	.		rs6555969	chpp-hmfiptl	.	.
rs7559271	alarr-ans	.	.		rs6555969	hmfsptr-chpp	.	.
rs7559271	alarl-nlhil	.	.		rs6555969	hmfsptl-hmfsptr	.	.
rs7559271	sispt-nlhil	.	.		rs6555969	chpp-hmfsptl	.	.
rs7559271	ans-alarl	.	.		rs6555969	gnispt-chpp	.	.
rs7559271	alarr-nlhir	.	.		rs6555969	chpp-malapt	.	.
rs7559271	sispt-ans	.	.		rs6555969	gnispt-malapt	.	.
rs7559271	nlhil-ans	.	.		rs6555969	gnispt-gniipt	.	.
rs7559271	nasir-alarr	.	.		rs6555969	gniipt-chpp	.	.
rs7559271	sispt-alarr	.	.		rs6555969	tmfbptr-malapt	.	.
rs7559271	sispt-nasir	.	.		rs6555969	hmfsptr-malapt	.	.
rs7559271	sispt-nlhir	.	.		rs6555969	malapt-hmfsptl	.	.
rs7559271	nlhir-ans	.	.		rs6555969	tmfbptl-malapt	.	.
rs7559271	sispt-alarl	.	.		rs6555969	hmfiptl-malapt	.	.
rs7559271	zygr-nas	.	.		rs6555969	hmfiptr-malapt	.	.
rs7559271	nas-zygl	.	.		rs6555969	tmflptr-tmflptl	.	.
rs7559271	zygr-zygl	.	.		rs6555969	tmflptr-malapt	.	.
rs7559271	nassr-nasir	.	.		rs6555969	tmflptl-malapt	.	.
rs7559271	dacr-nassr	.	.		rs6555969	alarr-alarl	.	.
rs7559271	dacr-nasir	.	.		rs6555969	nlhil-nlhir	.	.
rs7559271	xfbl-xfbr	.	.		rs6555969	ans-prosH	.	.
rs7559271	stpl-stpr	.	.		rs6555969	ans-prosM	.	.
rs7559271	xfbl-xfbr2	.	.		rs6555969	nlhir-nlhil	.	.
rs7559271	prosH-tmfbptr	.	.		rs6555969	alarl-alarr	.	.
rs7559271	prosH-tmfbptl	.	.		rs6555969	alarl-ans	.	.
rs7559271	tmfbptl-tmfbptr	.	.		rs6555969	prosH-ssp	.	.
rs7559271	prosM-tmfbptr	.	.		rs6555969	prosM-ssp	.	.
rs7559271	prosM-tmfbptl	.	.		rs6555969	ans-ssp	.	.
rs7559271	chpp-hmfiptr	.	.		rs6555969	nlhir-ssp	.	.
rs7559271	hmfiptr-hmfiptl	.	.		rs6555969	ssp-ans	.	.
rs7559271	chpp-hmfiptl	.	.		rs6555969	nlhil-ssp	.	.
rs7559271	hmfsptr-chpp	.	.		rs6555969	rs72691108	.	.
rs7559271	hmfsptl-hmfsptr	.	.		rs6555969	rs4648379	.	.
rs7559271	chpp-hmfsptl	.	.		rs6555969	rs12786942	.	.
rs7559271	gnispt-chpp	.	.		rs6555969	rs10862567	.	.
rs7559271	chpp-malapt	.	.		rs6555969	rs8007643	.	.

rs7559271	gnispt-malapt	.	.		rs6555969	rs17106852	.	.
rs7559271	gnispt-gniipt	.	.		rs6555969	rs7559271	.	.
rs7559271	gniipt-chpp	.	.		rs6555969	rs3827760	.	.
rs7559271	tmfbptr-malapt	.	.		rs6555969	rs6740960	.	.
rs7559271	hmfsptr-malapt	.	.		rs6555969	rs6129564	.	.
rs7559271	malapt-hmfsptl	.	.		rs6555969	rs927833	.	.
rs7559271	tmfbptl-malapt	.	.		rs6555969	rs17447439	.	.
rs7559271	hmfiptl-malapt	.	.		rs6555969	rs1982862	.	.
rs7559271	hmfiptr-malapt	.	.		rs6555969	rs2977562	.	.
rs7559271	tmflptr-tmflptl	.	.		rs6555969	rs9995821	.	.
rs7559271	tmflptr-malapt	.	.		rs6555969	rs11738462	.	.
rs7559271	tmflptl-malapt	.	.		rs5880172	dacl-dacr	.	.
rs7559271	alarr-alarl	.	.		rs5880172	obhsl-obhsr	.	.
rs7559271	nlhil-nlhir	.	.		rs5880172	fmal-fmar	.	.
rs7559271	ans-prosH	.	.		rs5880172	ectl-ectr	.	.
rs7559271	ans-prosM	.	.		rs5880172	wmhsr-wmhsl	.	.
rs7559271	nlhir-nlhil	.	.		rs5880172	zygool-zygoor	.	.
rs7559271	alarl-alarr	.	.		rs5880172	obhil-obhir	.	.
rs7559271	alarl-ans	.	.		rs5880172	nas-dacr	.	.
rs7559271	prosH-ssp	.	.		rs5880172	nas-dacl	.	.
rs7559271	prosM-ssp	.	.		rs5880172	obhsr-nas	.	.
rs7559271	ans-ssp	.	.		rs5880172	obhsr-obhsl	.	.
rs7559271	nlhir-ssp	.	.		rs5880172	obhsl-nas	.	.
rs7559271	ssp-ans	.	.		rs5880172	zygool-nas	.	.
rs7559271	nlhil-ssp	.	.		rs5880172	zygoor-nas	.	.
rs7559271	rs72691108	.	.		rs5880172	dacr-nas	.	.
rs7559271	rs4648379	.	.		rs5880172	dacr-dacl	.	.
rs7559271	rs12786942	.	.		rs5880172	wnbl-wnbr	.	.
rs7559271	rs10862567	.	.		rs5880172	nas-wnbl	.	.
rs7559271	rs8007643	.	.		rs5880172	wnbr-nas	.	.
rs7559271	rs17106852	.	.		rs5880172	sispt-nasil	.	.
rs3827760	dacl-dacr	.	.		rs5880172	nasil-alarl	.	.
rs3827760	obhsl-obhsr	.	.		rs5880172	alarr-ans	.	.
rs3827760	fmal-fmar	.	.		rs5880172	alarl-nlhil	.	.
rs3827760	ectl-ectr	.	.		rs5880172	sispt-nlhil	.	.
rs3827760	wmhsr-wmhsl	.	.		rs5880172	ans-alarl	.	.
rs3827760	zygool-zygoor	.	.		rs5880172	alarr-nlhir	.	.
rs3827760	obhil-obhir	.	.		rs5880172	sispt-ans	.	.
rs3827760	nas-dacr	.	.		rs5880172	nlhil-ans	.	.
rs3827760	nas-dacl	.	.		rs5880172	nasir-alarr	.	.
rs3827760	obhsr-nas	.	.		rs5880172	sispt-alarr	.	.
rs3827760	obhsr-obhsl	.	.		rs5880172	sispt-nasir	.	.
rs3827760	obhsl-nas	.	.		rs5880172	sispt-nlhir	.	.

rs3827760	zygool-nas	.	.		rs5880172	nlhir-ans	.	.
rs3827760	zygoor-nas	.	.		rs5880172	sispt-alarl	.	.
rs3827760	dacr-nas	.	.		rs5880172	zygr-nas	.	.
rs3827760	dacr-dacl	.	.		rs5880172	nas-zygl	.	.
rs3827760	wnbl-wnbr	.	.		rs5880172	zygr-zygl	.	.
rs3827760	nas-wnbl	.	.		rs5880172	nassr-nasir	.	.
rs3827760	wnbr-nas	.	.		rs5880172	dacr-nassr	.	.
rs3827760	sispt-nasil	.	.		rs5880172	dacr-nasir	.	.
rs3827760	nasil-alarl	.	.		rs5880172	xfbl-xfbr	.	.
rs3827760	alarr-ans	.	.		rs5880172	stpl-stpr	.	.
rs3827760	alarl-nlhil	.	.		rs5880172	xfbl-xfbr2	.	.
rs3827760	sispt-nlhil	.	.		rs5880172	prosH-tmfbptr	.	.
rs3827760	ans-alarl	.	.		rs5880172	prosH-tmfbptl	.	.
rs3827760	alarr-nlhir	.	.		rs5880172	tmfbptl-tmfbptr	.	.
rs3827760	sispt-ans	.	.		rs5880172	prosM-tmfbptr	.	.
rs3827760	nlhil-ans	.	.		rs5880172	prosM-tmfbptl	.	.
rs3827760	nasir-alarr	.	.		rs5880172	chpp-hmfiptr	.	.
rs3827760	sispt-alarr	.	.		rs5880172	hmfiptr-hmfiptl	.	.
rs3827760	sispt-nasir	.	.		rs5880172	chpp-hmfiptl	.	.
rs3827760	sispt-nlhir	.	.		rs5880172	hmfsptr-chpp	.	.
rs3827760	nlhir-ans	.	.		rs5880172	hmfsptl-hmfsptr	.	.
rs3827760	sispt-alarl	.	.		rs5880172	chpp-hmfsptl	.	.
rs3827760	zygr-nas	.	.		rs5880172	gnispt-chpp	.	.
rs3827760	nas-zygl	.	.		rs5880172	chpp-malapt	.	.
rs3827760	zygr-zygl	.	.		rs5880172	gnispt-malapt	.	.
rs3827760	nassr-nasir	.	.		rs5880172	gnispt-gniipt	.	.
rs3827760	dacr-nassr	.	.		rs5880172	gniipt-chpp	.	.
rs3827760	dacr-nasir	.	.		rs5880172	tmfbptr-malapt	.	.
rs3827760	xfbl-xfbr	.	.		rs5880172	hmfsptr-malapt	.	.
rs3827760	stpl-stpr	.	.		rs5880172	malapt-hmfsptl	.	.
rs3827760	xfbl-xfbr2	.	.		rs5880172	tmfbptl-malapt	.	.
rs3827760	prosH-tmfbptr	.	.		rs5880172	hmfiptl-malapt	.	.
rs3827760	prosH-tmfbptl	.	.		rs5880172	hmfiptr-malapt	.	.
rs3827760	tmfbptl-tmfbptr	.	.		rs5880172	tmflptr-tmflptl	.	.
rs3827760	prosM-tmfbptr	.	.		rs5880172	tmflptr-malapt	.	.
rs3827760	prosM-tmfbptl	.	.		rs5880172	tmflptl-malapt	.	.
rs3827760	chpp-hmfiptr	.	.		rs5880172	alarr-alarl	.	.
rs3827760	hmfiptr-hmfiptl	.	.		rs5880172	nlhil-nlhir	.	.
rs3827760	chpp-hmfiptl	.	.		rs5880172	ans-prosH	.	.
rs3827760	hmfsptr-chpp	.	.		rs5880172	ans-prosM	.	.
rs3827760	hmfsptl-hmfsptr	.	.		rs5880172	nlhir-nlhil	.	.
rs3827760	chpp-hmfsptl	.	.		rs5880172	alarl-alarr	.	.
rs3827760	gnispt-chpp	.	.		rs5880172	alarl-ans	.	.

rs3827760	chpp-malapt	.	.		rs5880172	prosH-ssp	.	.
rs3827760	gnispt-malapt	.	.		rs5880172	prosM-ssp	.	.
rs3827760	gnispt-gniipt	.	.		rs5880172	ans-ssp	.	.
rs3827760	gniipt-chpp	.	.		rs5880172	nlhir-ssp	.	.
rs3827760	tmfbptr-malapt	.	.		rs5880172	ssp-ans	.	.
rs3827760	hmfsptr-malapt	.	.		rs5880172	nlhil-ssp	.	.
rs3827760	malapt-hmfsptl	.	.		rs5880172	rs72691108	.	.
rs3827760	tmfbptl-malapt	.	.		rs5880172	rs4648379	.	.
rs3827760	hmfiptl-malapt	.	.		rs5880172	rs12786942	.	.
rs3827760	hmfiptr-malapt	.	.		rs5880172	rs10862567	.	.
rs3827760	tmflptr-tmflptl	.	.		rs5880172	rs8007643	.	.
rs3827760	tmflptr-malapt	.	.		rs5880172	rs17106852	.	.
rs3827760	tmflptl-malapt	.	.		rs5880172	rs7559271	.	.
rs3827760	alarr-alarl	.	.		rs5880172	rs3827760	.	.
rs3827760	nlhil-nlhir	.	.		rs5880172	rs6740960	.	.
rs3827760	ans-prosH	.	.		rs5880172	rs6129564	.	.
rs3827760	ans-prosM	.	.		rs5880172	rs927833	.	.
rs3827760	nlhir-nlhil	.	.		rs5880172	rs17447439	.	.
rs3827760	alarl-alarr	.	.		rs5880172	rs1982862	.	.
rs3827760	alarl-ans	.	.		rs5880172	rs2977562	.	.
rs3827760	prosH-ssp	.	.		rs5880172	rs9995821	.	.
rs3827760	prosM-ssp	.	.		rs5880172	rs11738462	.	.
rs3827760	ans-ssp	.	.		rs5880172	rs6555969	.	.
rs3827760	nlhir-ssp	.	.		rs17640804	dacl-dacr	.	.
rs3827760	ssp-ans	.	.		rs17640804	obhsl-obhsr	.	.
rs3827760	nlhil-ssp	.	.		rs17640804	fmal-fmar	.	.
rs3827760	rs72691108	.	.		rs17640804	ectl-ectr	.	.
rs3827760	rs4648379	.	.		rs17640804	wmhsr-wmhsl	.	.
rs3827760	rs12786942	.	.		rs17640804	zygool-zygoor	.	.
rs3827760	rs10862567	.	.		rs17640804	obhil-obhir	.	.
rs3827760	rs8007643	.	.		rs17640804	nas-dacr	.	.
rs3827760	rs17106852	.	.		rs17640804	nas-dacl	.	.
rs3827760	rs7559271	.	.		rs17640804	obhsr-nas	.	.
rs6740960	dacl-dacr	.	.		rs17640804	obhsr-obhsl	.	.
rs6740960	obhsl-obhsr	.	.		rs17640804	obhsl-nas	.	.
rs6740960	fmal-fmar	.	.		rs17640804	zygool-nas	.	.
rs6740960	ectl-ectr	.	.		rs17640804	zygoor-nas	.	.
rs6740960	wmhsr-wmhsl	.	.		rs17640804	dacr-nas	.	.
rs6740960	zygool-zygoor	.	.		rs17640804	dacr-dacl	.	.
rs6740960	obhil-obhir	.	.		rs17640804	wnbl-wnbr	.	.
rs6740960	nas-dacr	.	.		rs17640804	nas-wnbl	.	.
rs6740960	nas-dacl	.	.		rs17640804	wnbr-nas	.	.
rs6740960	obhsr-nas	.	.		rs17640804	sispt-nasil	.	.

rs6740960	obhsr-obhsl	.	.		rs17640804	nasil-alarl	.	.
rs6740960	obhsl-nas	.	.		rs17640804	alarr-ans	.	.
rs6740960	zygool-nas	.	.		rs17640804	alarl-nlhil	.	.
rs6740960	zygoor-nas	.	.		rs17640804	sispt-nlhil	.	.
rs6740960	dacr-nas	.	.		rs17640804	ans-alarl	.	.
rs6740960	dacr-dacl	.	.		rs17640804	alarr-nlhir	.	.
rs6740960	wnbl-wnbr	.	.		rs17640804	sispt-ans	.	.
rs6740960	nas-wnbl	.	.		rs17640804	nlhil-ans	.	.
rs6740960	wnbr-nas	.	.		rs17640804	nasir-alarr	.	.
rs6740960	sispt-nasil	.	.		rs17640804	sispt-alarr	.	.
rs6740960	nasil-alarl	.	.		rs17640804	sispt-nasir	.	.
rs6740960	alarr-ans	.	.		rs17640804	sispt-nlhir	.	.
rs6740960	alarl-nlhil	.	.		rs17640804	nlhir-ans	.	.
rs6740960	sispt-nlhil	.	.		rs17640804	sispt-alarl	.	.
rs6740960	ans-alarl	.	.		rs17640804	zygr-nas	.	.
rs6740960	alarr-nlhir	.	.		rs17640804	nas-zygl	.	.
rs6740960	sispt-ans	.	.		rs17640804	zygr-zygl	.	.
rs6740960	nlhil-ans	.	.		rs17640804	nassr-nasir	.	.
rs6740960	nasir-alarr	.	.		rs17640804	dacr-nassr	.	.
rs6740960	sispt-alarr	.	.		rs17640804	dacr-nasir	.	.
rs6740960	sispt-nasir	.	.		rs17640804	xfbl-xfbr	.	.
rs6740960	sispt-nlhir	.	.		rs17640804	stpl-stpr	.	.
rs6740960	nlhir-ans	.	.		rs17640804	xfbl-xfbr2	.	.
rs6740960	sispt-alarl	.	.		rs17640804	prosH-tmfbptr	.	.
rs6740960	zygr-nas	.	.		rs17640804	prosH-tmfbptl	.	.
rs6740960	nas-zygl	.	.		rs17640804	tmfbptl-tmfbptr	.	.
rs6740960	zygr-zygl	.	.		rs17640804	prosM-tmfbptr	.	.
rs6740960	nassr-nasir	.	.		rs17640804	prosM-tmfbptl	.	.
rs6740960	dacr-nassr	.	.		rs17640804	chpp-hmfiptr	.	.
rs6740960	dacr-nasir	.	.		rs17640804	hmfiptr-hmfiptl	.	.
rs6740960	xfbl-xfbr	.	.		rs17640804	chpp-hmfiptl	.	.
rs6740960	stpl-stpr	.	.		rs17640804	hmfsptr-chpp	.	.
rs6740960	xfbl-xfbr2	.	.		rs17640804	hmfsptl-hmfsptr	.	.
rs6740960	prosH-tmfbptr	.	.		rs17640804	chpp-hmfsptl	.	.
rs6740960	prosH-tmfbptl	.	.		rs17640804	gnispt-chpp	.	.
rs6740960	tmfbptl-tmfbptr	.	.		rs17640804	chpp-malapt	.	.
rs6740960	prosM-tmfbptr	.	.		rs17640804	gnispt-malapt	.	.
rs6740960	prosM-tmfbptl	.	.		rs17640804	gnispt-gniipt	.	.
rs6740960	chpp-hmfiptr	.	.		rs17640804	gniipt-chpp	.	.
rs6740960	hmfiptr-hmfiptl	.	.		rs17640804	tmfbptr-malapt	.	.
rs6740960	chpp-hmfiptl	.	.		rs17640804	hmfsptr-malapt	.	.
rs6740960	hmfsptr-chpp	.	.		rs17640804	malapt-hmfsptl	.	.
rs6740960	hmfsptl-hmfsptr	.	.		rs17640804	tmfbptl-malapt	.	.

rs6740960	chpp-hmfsptl	.	.		rs17640804	hmfiptl-malapt	.	.
rs6740960	gnispt-chpp	.	.		rs17640804	hmfiptr-malapt	.	.
rs6740960	chpp-malapt	.	.		rs17640804	tmflptr-tmflptl	.	.
rs6740960	gnispt-malapt	.	.		rs17640804	tmflptr-malapt	.	.
rs6740960	gnispt-gniipt	.	.		rs17640804	tmflptl-malapt	.	.
rs6740960	gniipt-chpp	.	.		rs17640804	alarr-alarl	.	.
rs6740960	tmfbptr-malapt	.	.		rs17640804	nlhil-nlhir	.	.
rs6740960	hmfsptr-malapt	.	.		rs17640804	ans-prosH	.	.
rs6740960	malapt-hmfsptl	.	.		rs17640804	ans-prosM	.	.
rs6740960	tmfbptl-malapt	.	.		rs17640804	nlhir-nlhil	.	.
rs6740960	hmfiptl-malapt	.	.		rs17640804	alarl-alarr	.	.
rs6740960	hmfiptr-malapt	.	.		rs17640804	alarl-ans	.	.
rs6740960	tmflptr-tmflptl	.	.		rs17640804	prosH-ssp	.	.
rs6740960	tmflptr-malapt	.	.		rs17640804	prosM-ssp	.	.
rs6740960	tmflptl-malapt	.	.		rs17640804	ans-ssp	.	.
rs6740960	alarr-alarl	.	.		rs17640804	nlhir-ssp	.	.
rs6740960	nlhil-nlhir	.	.		rs17640804	ssp-ans	.	.
rs6740960	ans-prosH	.	.		rs17640804	nlhil-ssp	.	.
rs6740960	ans-prosM	.	.		rs17640804	rs72691108	.	.
rs6740960	nlhir-nlhil	.	.		rs17640804	rs4648379	.	.
rs6740960	alarl-alarr	.	.		rs17640804	rs12786942	.	.
rs6740960	alarl-ans	.	.		rs17640804	rs10862567	.	.
rs6740960	prosH-ssp	.	.		rs17640804	rs8007643	.	.
rs6740960	prosM-ssp	.	.		rs17640804	rs17106852	.	.
rs6740960	ans-ssp	.	.		rs17640804	rs7559271	.	.
rs6740960	nlhir-ssp	.	.		rs17640804	rs3827760	.	.
rs6740960	ssp-ans	.	.		rs17640804	rs6740960	.	.
rs6740960	nlhil-ssp	.	.		rs17640804	rs6129564	.	.
rs6740960	rs72691108	.	.		rs17640804	rs927833	.	.
rs6740960	rs4648379	.	.		rs17640804	rs17447439	.	.
rs6740960	rs12786942	.	.		rs17640804	rs1982862	.	.
rs6740960	rs10862567	.	.		rs17640804	rs2977562	.	.
rs6740960	rs8007643	.	.		rs17640804	rs9995821	.	.
rs6740960	rs17106852	.	.		rs17640804	rs11738462	.	.
rs6740960	rs7559271	.	.		rs17640804	rs6555969	.	.
rs6740960	rs3827760	.	.		rs17640804	rs5880172	.	.
rs6129564	dacl-dacr	0.1118	0.6692		rs10238953	dacl-dacr	.	.
rs6129564	obhsl-obhsr	-0.1491	0.568		rs10238953	obhsl-obhsr	.	.
rs6129564	fmal-fmar	0	1		rs10238953	fmal-fmar	.	.
rs6129564	ectl-ectr	0.0745	0.7762		rs10238953	ectl-ectr	.	.
rs6129564	wmhsr-wmhsl	-0.2609	0.3119		rs10238953	wmhsr-wmhsl	.	.
rs6129564	zygool-zygoor	-0.0745	0.7762		rs10238953	zygool-zygoor	.	.
rs6129564	obhil-obhir	-0.0745	0.7762		rs10238953	obhil-obhir	.	.

rs6129564	nas-dacr	0.2236	0.3883		rs10238953	nas-dacr	.	.
rs6129564	nas-dacl	0.3354	0.1881		rs10238953	nas-dacl	.	.
rs6129564	obhsr-nas	-0.1863	0.4739		rs10238953	obhsr-nas	.	.
rs6129564	obhsr-obhsl	-0.1491	0.568		rs10238953	obhsr-obhsl	.	.
rs6129564	obhsl-nas	0.1118	0.6692		rs10238953	obhsl-nas	.	.
rs6129564	zygool-nas	0.1863	0.4739		rs10238953	zygool-nas	.	.
rs6129564	zygoor-nas	-0.0745	0.7762		rs10238953	zygoor-nas	.	.
rs6129564	dacr-nas	0.2236	0.3883		rs10238953	dacr-nas	.	.
rs6129564	dacr-dacl	0.1118	0.6692		rs10238953	dacr-dacl	.	.
rs6129564	wnbl-wnbr	0.1118	0.6692		rs10238953	wnbl-wnbr	.	.
rs6129564	nas-wnbl	0	1		rs10238953	nas-wnbl	.	.
rs6129564	wnbr-nas	-0.0373	0.8871		rs10238953	wnbr-nas	.	.
rs6129564	sispt-nasil	0.4099	0.1022		rs10238953	sispt-nasil	.	.
rs6129564	nasil-alarl	-0.1118	0.6692		rs10238953	nasil-alarl	.	.
rs6129564	alarr-ans	-0.1118	0.6692		rs10238953	alarr-ans	.	.
rs6129564	alarl-nlhil	0.2609	0.3119		rs10238953	alarl-nlhil	.	.
rs6129564	sispt-nlhil	0.2981	0.2451		rs10238953	sispt-nlhil	.	.
rs6129564	ans-alarl	-0.2609	0.3119		rs10238953	ans-alarl	.	.
rs6129564	alarr-nlhir	0.3727	0.1407		rs10238953	alarr-nlhir	.	.
rs6129564	sispt-ans	0.1863	0.4739		rs10238953	sispt-ans	.	.
rs6129564	nlhil-ans	-0.4472	0.0719		rs10238953	nlhil-ans	.	.
rs6129564	nasir-alarr	0.1863	0.4739		rs10238953	nasir-alarr	.	.
rs6129564	sispt-alarr	0.2236	0.3883		rs10238953	sispt-alarr	.	.
rs6129564	sispt-nasir	0.2981	0.2451		rs10238953	sispt-nasir	.	.
rs6129564	sispt-nlhir	0.3354	0.1881		rs10238953	sispt-nlhir	.	.
rs6129564	nlhir-ans	-0.3727	0.1407		rs10238953	nlhir-ans	.	.
rs6129564	sispt-alarl	0.3354	0.1881		rs10238953	sispt-alarl	.	.
rs6129564	zygr-nas	-0.1491	0.568		rs10238953	zygr-nas	.	.
rs6129564	nas-zygl	-0.0373	0.8871		rs10238953	nas-zygl	.	.
rs6129564	zygr-zygl	-0.4472	0.0719		rs10238953	zygr-zygl	.	.
rs6129564	nassr-nasir	0.1491	0.568		rs10238953	nassr-nasir	.	.
rs6129564	dacr-nassr	-0.1118	0.6692		rs10238953	dacr-nassr	.	.
rs6129564	dacr-nasir	0.0373	0.8871		rs10238953	dacr-nasir	.	.
rs6129564	xfbl-xfbr	-0.2981	0.2451		rs10238953	xfbl-xfbr	.	.
rs6129564	stpl-stpr	-0.1118	0.6692		rs10238953	stpl-stpr	.	.
rs6129564	xfbl-xfbr2	-0.2981	0.2451		rs10238953	xfbl-xfbr2	.	.
rs6129564	prosH-tmfbptr	-0.0373	0.8871		rs10238953	prosH-tmfbptr	.	.
rs6129564	prosH-tmfbptl	-0.1118	0.6692		rs10238953	prosH-tmfbptl	.	.
rs6129564	tmfbptl-tmfbptr	-0.1491	0.568		rs10238953	tmfbptl-tmfbptr	.	.
rs6129564	prosM-tmfbptr	-0.1491	0.568		rs10238953	prosM-tmfbptr	.	.
rs6129564	prosM-tmfbptl	-0.1118	0.6692		rs10238953	prosM-tmfbptl	.	.
rs6129564	chpp-hmfiptr	-0.2609	0.3119		rs10238953	chpp-hmfiptr	.	.
rs6129564	hmfiptr-hmfiptl	-0.2236	0.3883		rs10238953	hmfiptr-hmfiptl	.	.

rs6129564	chpp-hmfiptl	0	1		rs10238953	chpp-hmfiptl	.	.
rs6129564	hmfsptr-chpp	-0.2236	0.3883		rs10238953	hmfsptr-chpp	.	.
rs6129564	hmfsptl-hmfsptr	-0.1491	0.568		rs10238953	hmfsptl-hmfsptr	.	.
rs6129564	chpp-hmfsptl	-0.3354	0.1881		rs10238953	chpp-hmfsptl	.	.
rs6129564	gnispt-chpp	-0.1118	0.6692		rs10238953	gnispt-chpp	.	.
rs6129564	chpp-malapt	0.1491	0.568		rs10238953	chpp-malapt	.	.
rs6129564	gnispt-malapt	-0.0373	0.8871		rs10238953	gnispt-malapt	.	.
rs6129564	gnispt-gniipt	0.1863	0.4739		rs10238953	gnispt-gniipt	.	.
rs6129564	gniipt-chpp	0.559	0.0197		rs10238953	gniipt-chpp	.	.
rs6129564	tmfbptr-malapt	-0.3354	0.1881		rs10238953	tmfbptr-malapt	.	.
rs6129564	hmfsptr-malapt	-0.2236	0.3883		rs10238953	hmfsptr-malapt	.	.
rs6129564	malapt-hmfsptl	-0.1118	0.6692		rs10238953	malapt-hmfsptl	.	.
rs6129564	tmfbptl-malapt	-0.1118	0.6692		rs10238953	tmfbptl-malapt	.	.
rs6129564	hmfiptl-malapt	0.0745	0.7762		rs10238953	hmfiptl-malapt	.	.
rs6129564	hmfiptr-malapt	-0.3354	0.1881		rs10238953	hmfiptr-malapt	.	.
rs6129564	tmflptr-tmflptl	-0.0745	0.7762		rs10238953	tmflptr-tmflptl	.	.
rs6129564	tmflptr-malapt	-0.4845	0.0487		rs10238953	tmflptr-malapt	.	.
rs6129564	tmflptl-malapt	0	1		rs10238953	tmflptl-malapt	.	.
rs6129564	alarr-alarl	0.0745	0.7762		rs10238953	alarr-alarl	.	.
rs6129564	nlhil-nlhir	-0.1491	0.568		rs10238953	nlhil-nlhir	.	.
rs6129564	ans-prosH	-0.2609	0.3119		rs10238953	ans-prosH	.	.
rs6129564	ans-prosM	-0.2236	0.3883		rs10238953	ans-prosM	.	.
rs6129564	nlhir-nlhil	-0.1491	0.568		rs10238953	nlhir-nlhil	.	.
rs6129564	alarl-alarr	0.0745	0.7762		rs10238953	alarl-alarr	.	.
rs6129564	alarl-ans	-0.2609	0.3119		rs10238953	alarl-ans	.	.
rs6129564	prosH-ssp	0.2609	0.3119		rs10238953	prosH-ssp	.	.
rs6129564	prosM-ssp	0.3354	0.1881		rs10238953	prosM-ssp	.	.
rs6129564	ans-ssp	-0.4845	0.0487		rs10238953	ans-ssp	.	.
rs6129564	nlhir-ssp	-0.4845	0.0487		rs10238953	nlhir-ssp	.	.
rs6129564	ssp-ans	-0.4845	0.0487		rs10238953	ssp-ans	.	.
rs6129564	nlhil-ssp	0	1		rs10238953	nlhil-ssp	.	.
rs6129564	rs72691108	-0.0215	0.9347		rs10238953	rs72691108	.	.
rs6129564	rs4648379	-0.2025	0.4356		rs10238953	rs4648379	.	.
rs6129564	rs12786942	0.3099	0.2261		rs10238953	rs12786942	.	.
rs6129564	rs10862567	.	.		rs10238953	rs10862567	.	.
rs6129564	rs8007643	-0.1333	0.6099		rs10238953	rs8007643	.	.
rs6129564	rs17106852	-0.2025	0.4356		rs10238953	rs17106852	.	.
rs6129564	rs7559271	.	.		rs10238953	rs7559271	.	.
rs6129564	rs3827760	.	.		rs10238953	rs3827760	.	.
rs6129564	rs6740960	.	.		rs10238953	rs6740960	.	.
rs927833	dacl-dacr	-0.0373	0.8871		rs10238953	rs6129564	.	.
rs927833	obhsl-obhsr	-0.2236	0.3883		rs10238953	rs927833	.	.
rs927833	fmal-fmar	0.0745	0.7762		rs10238953	rs17447439	.	.

rs927833	ectl-ectr	-0.3354	0.1881		rs10238953	rs1982862	.	.
rs927833	wmhsr-wmhsl	0.1491	0.568		rs10238953	rs2977562	.	.
rs927833	zygool-zygoor	0.0745	0.7762		rs10238953	rs9995821	.	.
rs927833	obhil-obhir	0.1118	0.6692		rs10238953	rs11738462	.	.
rs927833	nas-dacr	-0.1863	0.4739		rs10238953	rs6555969	.	.
rs927833	nas-dacl	-0.2609	0.3119		rs10238953	rs5880172	.	.
rs927833	obhsr-nas	-0.0745	0.7762		rs10238953	rs17640804	.	.
rs927833	obhsr-obhsl	-0.2236	0.3883		rs927833	chpp-hmfiptl	0.0373	0.8871
rs927833	obhsl-nas	-0.1118	0.6692		rs927833	hmfsptr-chpp	0.3727	0.1407
rs927833	zygool-nas	-0.1118	0.6692		rs927833	hmfsptl-hmfsptr	0.2981	0.2451
rs927833	zygoor-nas	0.1863	0.4739		rs927833	chpp-hmfsptl	0.3354	0.1881
rs927833	dacr-nas	-0.1863	0.4739		rs927833	gnispt-chpp	0.0373	0.8871
rs927833	dacr-dacl	-0.0373	0.8871		rs927833	chpp-malapt	-0.3727	0.1407
rs927833	wnbl-wnbr	0.0745	0.7762		rs927833	gnispt-malapt	-0.1491	0.568
rs927833	nas-wnbl	0.0373	0.8871		rs927833	gnispt-gniipt	-0.1863	0.4739
rs927833	wnbr-nas	0	1		rs927833	gniipt-chpp	-0.4472	0.0719
rs927833	sispt-nasil	-0.1491	0.568		rs927833	tmfbptr-malapt	0.3354	0.1881
rs927833	nasil-alarl	-0.2236	0.3883		rs927833	hmfsptr-malapt	0.2609	0.3119
rs927833	alarr-ans	-0.0373	0.8871		rs927833	malapt-hmfsptl	0	1
rs927833	alarl-nlhil	-0.0745	0.7762		rs927833	tmfbptl-malapt	0	1
rs927833	sispt-nlhil	-0.2236	0.3883		rs927833	hmfiptl-malapt	0.1118	0.6692
rs927833	ans-alarl	-0.5217	0.0317		rs927833	hmfiptr-malapt	0.4099	0.1022
rs927833	alarr-nlhir	0.1863	0.4739		rs927833	tmflptr-tmflptl	0.559	0.0197
rs927833	sispt-ans	-0.2981	0.2451		rs927833	tmflptr-malapt	0.1863	0.4739
rs927833	nlhil-ans	-0.4845	0.0487		rs927833	tmflptl-malapt	-0.1118	0.6692
rs927833	nasir-alarr	-0.3727	0.1407		rs927833	alarr-alarl	-0.0745	0.7762
rs927833	sispt-alarr	-0.0373	0.8871		rs927833	nlhil-nlhir	-0.2236	0.3883
rs927833	sispt-nasir	0.1491	0.568		rs927833	ans-prosH	-0.3727	0.1407
rs927833	sispt-nlhir	0	1		rs927833	ans-prosM	-0.4099	0.1022
rs927833	nlhir-ans	-0.1118	0.6692		rs927833	nlhir-nlhil	-0.2236	0.3883
rs927833	sispt-alarl	-0.1118	0.6692		rs927833	alarl-alarr	-0.0745	0.7762
rs927833	zygr-nas	-0.1491	0.568		rs927833	alarl-ans	-0.5217	0.0317
rs927833	nas-zygl	-0.1863	0.4739		rs927833	prosH-ssp	-0.2981	0.2451
rs927833	zygr-zygl	0.0373	0.8871		rs927833	prosM-ssp	-0.2236	0.3883
rs927833	nassr-nasir	-0.1491	0.568		rs927833	ans-ssp	-0.2236	0.3883
rs927833	dacr-nassr	-0.0373	0.8871		rs927833	nlhir-ssp	-0.3354	0.1881
rs927833	dacr-nasir	-0.2981	0.2451		rs927833	ssp-ans	-0.2236	0.3883
rs927833	xfbl-xfbr	0.2236	0.3883		rs927833	nlhil-ssp	-0.2981	0.2451
rs927833	stpl-stpr	0.0745	0.7762		rs927833	rs72691108	-0.0215	0.9347
rs927833	xfbl-xfbr2	0.2236	0.3883		rs927833	rs4648379	-0.2025	0.4356
rs927833	prosH-tmfbptr	0.0745	0.7762		rs927833	rs12786942	-0.169	0.5166
rs927833	prosH-tmfbptl	-0.0373	0.8871		rs927833	rs10862567	.	.
rs927833	tmfbptl-tmfbptr	0.2981	0.2451		rs927833	rs8007643	0.4333	0.0823

rs927833	prosM-tmfbptr	0.0745	0.7762		rs927833	rs17106852	0.6583	0.0041
rs927833	prosM-tmfbptl	0	1		rs927833	rs7559271	.	.
rs927833	chpp-hmfiptr	0.1491	0.568		rs927833	rs3827760	.	.
rs927833	hmfiptr-hmfiptl	0.1863	0.4739		rs927833	rs6740960	.	.
					rs927833	rs6129564	-0.1333	0.6099

LITERATURE CITED

Adhikari K, Fuentes-Guajardo M, Quinto-Sanchez M, Mendoza-Revilla J, Camilo Chacon-Duque J, Acuna-Alonzo V, Jaramillo C, Arias W, Lozano RB, and Perez GM. 2016a. A genome-wide association scan implicates DCHS2, RUNX2, GLI3, PAX1 and EDAR in human facial variation. Nat Commun 7.

Adhikari K, Fuentes-Guajardo M, Quinto-Sanchez M, Mendoza-Revilla J, Camilo Chacon-Duque J, Acuna-Alonzo V, Jaramillo C, Arias W, Lozano RB, Perez GM et al. . 2016b. A genome-wide association scan implicates DCHS2, RUNX2, GLI3, PAX1 and EDAR in human facial variation. Nat Commun 7:11616.

Algee-Hewitt BFB. 2016. Population inference from contemporary American craniometrics. American Journal of Physical Anthropology 160(4):604-624.

Algee-Hewitt BFB. 2017a. Geographic substructure in craniometric estimates of admixture for contemporary American populations. American Journal of Physical Anthropology 164(2):260-280.

Algee-Hewitt BFB. 2017b. Temporal trends in craniometric estimates of admixture for a modern American sample. American Journal of Physical Anthropology 163(4):729-740.

Algee-Hewitt BFB, and Wheat AD. 2016. The reality of virtual anthropology: Comparing digitizer and laser scan data collection methods for the quantitative assessment of the cranium. American Journal of Physical Anthropology 160(1):148-155.

Altes KB. 2016. Feature proportion accuracy of hand-drawn facial approximation. Science & Justice 56(6):443-452.

Alvarez-Cubero MJ, Saiz M, Martínez-García B, Sayalero SM, Entrala C, Lorente JA, and Martinez-Gonzalez LJ. 2017. Next generation sequencing: an application in forensic sciences? Annals of Human Biology 44(7):581-592.

Anderson MJ, and Willis TJ. 2003. Canonical Analysis of Principal Coordinates: A Useful Method of Constrained Ordination for Ecology. Ecology 84(2):511-525.

Bajrami E, and Spiroski M. 2016. Genomic Imprinting. Open access Macedonian journal of medical sciences 4(1):181-184.

Bookstein FL. 1997. Landmark methods for forms without landmarks: Morphometrics of group differences in outline shape. Medical Image Analysis 1(3):225-243.

Bryc K, Durand Eric Y, Macpherson JM, Reich D, and Mountain Joanna L. 2015. The Genetic Ancestry of African Americans, Latinos, and European Americans across the United States. The American Journal of Human Genetics 96(1):37-53.

Budowle B, and van Daal A. 2008. Forensically relevant SNP classes. Biotechniques 44(5):603-608, 610.

Buschang PH, and Hinton RJ. 2005. A Gradient of Potential for Modifying Craniofacial Growth. Seminars in Orthodontics 11(4):219-226.

Cha S, Lim JE, Park AY, Do J-H, Lee SW, Shin C, Cho NH, Kang J-O, Nam JM, Kim J-S et al. . 2018. Identification of five novel genetic loci related to facial morphology by genome-wide association studies. BMC Genomics 19(1):481.

Cheverud JM. 1988. A Comparison of Genetic and Phenotypic Correlations. Evolution 42(5):958-968.

Chiego DJ. 2018. essentials of Oral Histology and embryology: A clinical Approach: Elsevier Health Sciences.

Cho YS, Go MJ, Kim YJ, Heo JY, Oh JH, Ban HJ, Yoon D, Lee MH, Kim DJ, and Park M. 2009. A large-scale genome-wide association study of Asian populations uncovers genetic factors influencing eight quantitative traits. Nat Genet 41.

Claes P, Liberton DK, Daniels K, Rosana KM, Quillen EE, Pearson LN, McEvoy B, Bauchet M, Zaidi AA, Yao W et al. . 2014. Modeling 3D facial shape from DNA. PLoS Genet 10(3):e1004224.

Claes P, Roosenboom J, White JD, Swigut T, Sero D, Li J, Lee MK, Zaidi A, Mattern BC, Liebowitz C et al. . 2018. Genome-wide mapping of global-to-local genetic effects on human facial shape. Nature Genetics.

Cole JB, Manyama M, Larson JR, Liberton DK, Ferrara TM, Riccardi SL, Li M, Mio W, Klein OD, Santorico SA et al. . 2017. Human Facial Shape and Size Heritability and Genetic Correlations. Genetics 205(2):967-978.

Deloukas P, Schuler GD, Gyapay G, Beasley EM, Soderlund C, Rodriguez T, xe, P., Hui L, Matise TC et al. . 1998. A Physical Map of 30,000 Human Genes. Science 282(5389):744-746.

Desjardins P, and Conklin D. 2010. NanoDrop microvolume quantitation of nucleic acids. Journal of visualized experiments : JoVE(45):2565.

Dougherty D, and Robbins A. 1997. sed & awk: UNIX Power Tools: " O'Reilly Media, Inc.".

El Andari A, Othman H, Taroni F, and Mansour I. 2013. Population genetic data for 23 STR markers from Lebanon. Forensic Sci Int Genet 7(4):e108-113.

Ellonen P. 2013. DNA library preparation. FINLAND: FIMM.

Evison MP, Iwamura ESM, Guimarães MA, and Schofield D. 2016. Forensic Facial Reconstruction and Its Contribution to Identification in Missing Person Cases. In: Morewitz SJ, and Sturdy Colls C, editors. Handbook of Missing Persons. Cham: Springer International Publishing. p 427-441.

Fowler J, Cohen L, and Jarvis P. 2013. Practical statistics for field biology: John Wiley & Sons.

Gerasimov MM. 1971. face finder.

Gupta S, Gupta V, Vij H, Vij R, and Tyagi N. 2015. Forensic Facial Reconstruction: The Final Frontier. Journal of Clinical & Diagnostic Research 9(9):26-28.

Guyomarc'h P, Dutailly B, Charton J, Santos F, Desbarats P, and Coqueugniot H. 2014. Anthropological facial approximation in three dimensions (AFA3D): computer-assisted estimation of the facial morphology using geometric morphometrics. J Forensic Sci 59(6):1502-1516.

Hallgrímsson B, Lieberman DE, Liu W, Ford-Hutchinson AF, and Jirik FR. 2007. Epigenetic interactions and the structure of phenotypic variation in the cranium. Evolution & Development 9(1):76-91.

Healthcare G. 2010. Reliable extraction of DNA from Whatman™ FTA™ cards. Application Note 28:9822.

Hessey AL. 2014. Sex estimation from the greater sciatic notch of the human pelvis: a geometric morphometric approach. San Marcos,Texas: Texas State University. 53 p.

His W. 1895. Anatomische Forschungen über Johann Sebastian Bach's Gebeine und Antlitz, nebst Bemerkungen über dessen Bilder, von Wilhelm His: S. Hirzel.

Howells W. 1973. Cranial Variation in Man: A Study by Multivariate Analysis of Patterns of Difference among Recent Human Populations. Papers of the Peabody Museum 67. Harvard University, Cambridge: Peabody Museum p235-236.

Hudson TJ, Stein LD, Gerety SS, Ma J, Castle AB, Silva J, Slonim DK, Baptista R, Kruglyak L, Xu S-H et al. . 1995. An STS-Based Map of the Human Genome. Science 270(5244):1945-1954.

Hughes CE, Algee-Hewitt BFB, Reineke R, Clausing E, and Anderson BE. 2017. Temporal Patterns of Mexican Migrant Genetic Ancestry: Implications for Identification. American Anthropologist 119(2):193-208.

Jantz RL, and Ousley SD. 2005. FORDISC 3: computerized forensic discriminant functions. Version 3:292.

Jolliffe I. 2011. Principal component analysis: Springer.

Kapp-Simon KA, Simon DJ, and Kristovich S. 1992. Self-perception, social skills, adjustment, and inhibition in young adolescents with craniofacial anomalies. Cleft Palate Craniofac J 29.

Kimmerle EH, Ross A, and Slice D. 2008. Sexual Dimorphism in America: Geometric Morphometric Analysis of the Craniofacial Region*. Journal of Forensic Sciences 53(1):54-57.

Klingenberg CP. 2011. MorphoJ: An integrated software package for geometric morphometrics. Molecular Ecology Resources 11(2):353-357.

Kranioti EF, García-Donas JG, Can IO, and Ekizoglu O. 2018. Ancestry estimation of three Mediterranean populations based on cranial metrics. Forensic Science International 286:265.e261-265.e268.

Langley NR, Lee Meadows Jantz, Stephen D. Ousley, and Jantz. RL. 2016. Data Collection Procedures for Forensic Skeletal Material 2.0. . University of Tennessee.

Langmead B, and Salzberg SL. 2012. Fast gapped-read alignment with Bowtie 2. Nature Methods 9(4):357-359.

Lao O, Liu F, Wollstein A, and Kayser M. 2014. GAGA: A New Algorithm for Genomic Inference of Geographic Ancestry Reveals Fine Level Population Substructure in Europeans. PLOS Computational Biology 10(2):e1003480.

Lee WJ, Wilkinson CM, Hwang HS, and Lee SM. 2015. Correlation between average tissue depth data and quantitative accuracy of forensic craniofacial reconstructions measured by geometric surface comparison method. J Forensic Sci 60(3):572-580.

Li H. 2011. A statistical framework for SNP calling, mutation discovery, association mapping and population genetical parameter estimation from sequencing data. Bioinformatics 27(21):2987-2993.

Little BB, Buschang PH, Reyes MEP, Tan SK, and Malina RM. 2006. Craniofacial dimensions in children in rural Oaxaca, Southern Mexico: Secular change, 1968–2000. American Journal of Physical Anthropology 131(1):127-136.

Liu F, van der Lijn F, Schurmann C, Zhu G, Chakravarty MM, Hysi PG, Wollstein A, Lao O, de Bruijne M, Ikram MA et al. . 2012. A Genome-Wide Association Study Identifies Five Loci Influencing Facial Morphology in Europeans. PLOS Genetics 8(9):e1002932.

Liu F, van Duijn K, Vingerling JR, Hofman A, Uitterlinden AG, Janssens AC, and Kayser M. 2009. Eye color and the prediction of complex phenotypes from genotypes. Curr Biol 19(5):R192-193.

Liu X, Han S, Wang Z, Gelernter J, and Yang B-Z. 2013. Variant Callers for Next-Generation Sequencing Data: A Comparison Study. PLOS ONE 8(9):e75619.

Maroñas O, Söchtig J, Ruiz Y, Phillips C, Carracedo Á, and Lareu MV. 2015. The genetics of skin, hair, and eye color variation and its relevance to forensic pigmentation predictive tests. Forensic science review 27(1):13-40.

Martin M. 2011. Cutadapt removes adapter sequences from high-throughput sequencing reads. 2011 17(1):3.

McKinney W. 2012. Python for data analysis: Data wrangling with Pandas, NumPy, and IPython: " O'Reilly Media, Inc.".

Mielke JH, Konigsberg LW, and Relethford J. 2011. Human Biological Variation: Oxford University Press.

Mitchell PD, Boston C, Chamberlain AT, Chaplin S, Chauhan V, Evans J, Fowler L, Powers N, Walker D, Webb H et al. . 2011. The study of anatomy in England from 1700 to the early 20th century. Journal of anatomy 219(2):91-99.

Mossey PA, Arngrimsson R, McColl J, Vintiner GM, and Connor JM. 1998. Prediction of liability to orofacial clefting using genetic and craniofacial data from parents. Journal of Medical Genetics(5):371.

NanoLabs P. 2016. Parabon Snapshot Workflow investigation. In: NanoLabs P, editor.

O'Higgins P, and Jones N. 2006. Morphologika 2.5. Tools for shape analysis.–Hull York Medical School, University of York.

Ousley S. 2004. 3Skull Computer Program. Version 2:111.

Paternoster L, Zhurov AI, Toma AM, Kemp JP, St Pourcain B, Timpson NJ, McMahon G, McArdle W, Ring SM, and Smith GD. 2012a. Genome-wide association study of three-dimensional facial morphology identifies a variant in PAX3 associated with nasion position. Am J Hum Genet 90.

Paternoster L, Zhurov AI, Toma AM, Kemp JP, St Pourcain B, Timpson NJ, McMahon G, McArdle W, Ring SM, Smith GD et al. . 2012b. Genome-wide association study of three-dimensional facial morphology identifies a variant in PAX3 associated with nasion position. Am J Hum Genet 90(3):478-485.

Peng S, Tan J, Hu S, Zhou H, Guo J, Jin L, and Tang K. 2013. Detecting Genetic Association of Common Human Facial Morphological Variation Using High Density 3D Image Registration. PLOS Computational Biology 9(12):e1003375.

Phips A, and Larry H. 1996. Clustering and classification: World Scientific.

Raaum R. 2006. Resample.exe. NYCEP Morphometrics Group.

Reijnders MRF, Miller KA, Alvi M, Goos JAC, Lees MM, de Burca A, Henderson A, Kraus A, Mikat B, de Vries BBA et al. . 2018. De Novo and Inherited Loss-of-Function Variants in TLK2: Clinical and Genotype-Phenotype Evaluation of a Distinct Neurodevelopmental Disorder. The American Journal of Human Genetics 102(6):1195-1203.

Relethford JH. 2016. Biological Distances and Population Genetics in Bioarchaeology. Biological Distance Analysis. p 23-33.

Relethford JH, Crawford MH, and Blangero J. 1997. Genetic Drift and Gene Flow in Post-Famine Ireland. Human Biology 69(4):443-465.

Retzlaff EW. 1987. Embryological Development of the Cranium. In: Retzlaff EW, and Mitchell FL, editors. The Cranium and Its Sutures: Anatomy, Physiology, Clinical Applications and Annotated Bibliography of Research in the Cranial Field. Berlin, Heidelberg: Springer Berlin Heidelberg. p 1-4.

Roseman CC. 2004. Detecting interregionally diversifying natural selection on modern human cranial form by using matched molecular and morphometric data. Proceedings of the National Academy of Sciences of the United States of America 101(35):12824-12829.

Sakuma A, Ishii M, Yamamoto S, Shimofusa R, Kobayashi K, Motani H, Hayakawa M, Yajima D, Takeichi H, and Iwase H. 2010. Application of postmortem 3D-CT facial reconstruction for personal identification. J Forensic Sci 55(6):1624-1629.

Sall J, Lehman A, Stephens ML, and Creighton L. 2012. JMP start statistics: a guide to statistics and data analysis using JMP: Sas Institute.

Sambrook J, and Russell DW. 2001. Molecular cloning : a laboratory manual: Cold Spring Harbor, N.Y. : Cold Spring Harbor Laboratory Press, c2001.3rd ed.

Sassoumi V. 1958. New method of identifying disaster victims. Journal of the Franklin Institute 266(2):147-148.

Shaffer JR, Orlova E, Lee MK, Leslie EJ, Raffensperger ZD, Heike CL, Cunningham ML, Hecht JT, Kau CH, Nidey NL et al. . 2016. Genome-Wide Association Study Reveals Multiple Loci Influencing Normal Human Facial Morphology. PLoS Genet 12(8):e1006149.

Shao J. 1996. Bootstrap Model Selection. Journal of the American Statistical Association 91(434):655-665.

Sherwood RJ, Duren DL, Demerath EW, Czerwinski SA, Siervogel RM, and Towne B. 2008. Quantitative genetics of modern human cranial variation. Journal of Human Evolution 54(6):909-914.

Sholts SB, Warmlander SK, Flores LM, Miller KW, and Walker PL. 2010. Variation in the measurement of cranial volume and surface area using 3D laser scanning technology. J Forensic Sci 55(4):871-876.

Slice DE. 2005. Modern morphometrics in physical anthropology: New York : Kluwer Academic/Plenum Publishers, ©2005.

Slice DE. 2013. Morpheus et al. Tallahassee, Florida, U.S.A.: Department of Scientific Computing, The Florida State University.

Spradley M, and Jantz RL. 2016. Ancestry Estimation in Forensic Anthropology: Geometric Morphometric versus Standard and Nonstandard Interlandmark Distances. Journal of Forensic Sciences (Wiley-Blackwell) 61(4):892-897.

Spradley MK. 2006. Biological anthropological aspects of the African diaspora; geographic origins, secular trends, and plastic versus genetic influences utilizing craniometric data. Tennessee: University of Tennessee.

Spradley MK. 2016. Metric Methods for the Biological Profile in Forensic Anthropology: Sex, Ancestry, and Stature. Academic Forensic Pathology 6(3):391-399.

Stewart EA, McKusick KB, Aggarwal A, Bajorek E, Brady S, Chu A, Fang N, Hadley D, Harris M, and Hussain S. 1997. An STS-based radiation hybrid map of the human genome. Genome research 7(5):422-433.

Taylor KT. 2001. Forensic art and illustration: Boca Raton, Fla. : CRC Press, c2001.

Toomey D. 2016. Learning Jupyter: Packt Publishing Ltd.

Ulahannan D, Kovac MB, Mulholland PJ, Cazier JB, and Tomlinson I. 2013. Technical and implementation issues in using next-generation sequencing of cancers in clinical practice. British Journal Of Cancer 109:827.

Untergasser A, Cutcutache I, Koressaar T, Ye J, Faircloth BC, Remm M, and Rozen SG. 2012. Primer3—new capabilities and interfaces. Nucleic acids research 40(15):e115-e115.

Urban JE, Weaver AA, Lillie EM, Maldjian JA, Whitlow CT, and Stitzel JD. 2016. Evaluation of morphological changes in the adult skull with age and sex. Journal of anatomy 229(6):838-846.

Veljan D. 2000. The 2500-year-old Pythagorean theorem. Mathematics Magazine 73(4):259-272.

Walker PL. 2008. Sexing skulls using discriminant function analysis of visually assessed traits. American Journal of Physical Anthropology 136(1):39-50.

Walsh S, Chaitanya L, Clarisse L, Wirken L, Draus-Barini J, Kovatsi L, Maeda H, Ishikawa T, Sijen T, de Knijff P et al. . 2014. Developmental validation of the HIrisPlex system: DNA-based eye and hair colour prediction for forensic and anthropological usage. Forensic Sci Int Genet 9:150-161.

Wang C, Szpiech ZA, Degnan JH, Jakobsson M, Pemberton TJ, Hardy JA, Singleton AB, and Rosenberg NA. 2010. Comparing spatial maps of human population-genetic variation using Procrustes analysis. Statistical applications in genetics and molecular biology 9(1):13-13.

Webster M, and Sheets HD. 2010. A practical introduction to landmark-based geometric morphometrics. The Paleontological Society Papers 16:163-188.

Welcker H. 1883. Schiller's Schädel und Todtenmaske: nebst Mittheilungen über Schädel und Todtenmaske Kant's. Mit einem Titelbilde, 6 Lithographirten Tafeln und 29 in den Text Eingedruckten Holzstichen: Friedrich Vieweg und Sohn.

White JD, Roosenboom J, Indencleef K, Mohammed J, Li J, Ortega-Castrillon A, Swigut T, Lee MK, Gonzalez-Zarzar T, Zaidi AA et al. . 2019. Meta-analysis identifies 48 SNPs with multiple independent effects on human facial features. 88th Annual Meeting of the American-Association-of-Physical-Anthropologists (AAPA). Cleveland, OH.

White TD, Black MT, and Folkens PA. 2012. Human osteology: Amsterdam ; Boston : Elsevier/Academic Press, ©2012.
3rd ed.

Wilkinson C. 2004a. Forensic Facial Reconstruction. Cambridge: Cambridge University Press.

Wilkinson C. 2004b. The history of facial reconstruction. In: Wilkinson C, editor. Forensic Facial Reconstruction. Cambridge: Cambridge University Press. p 39-68.

Wilkinson C, and Rynn C. 2012. Craniofacial Identification. Cambridge, UNITED KINGDOM: Cambridge University Press.

Wright S. 1943. Isolation by Distance. Genetics 28(2):114-138.